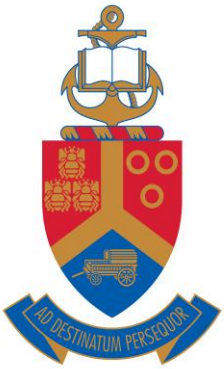

UNIVERSITEIT VAN PRETORIA
UNIVERSITY OF PRETORIA
YUNIBESITHI YA PRETORIA

Mechanical and hydraulic properties of residual dolomite and wad found in the Malmani Subgroup in South Africa

By

Duan Swart

1431 2868

Submitted in fulfilment of the requirements for the degree

MSc Engineering Geology

In the Faculty of Natural and Agricultural Sciences

University of Pretoria

June 2019

DECLARATION OF ORIGINALITY / DECLARATION ON PLAGIARISM

The ***Department of Geology (University of Pretoria)*** places great emphasis upon integrity and ethical conduct in the preparation of all written work submitted for academic evaluation. While academic staff teaches you about referencing techniques and how to avoid plagiarism, you too have a responsibility in this regard. If you are at any stage uncertain as to what is required, you should speak to your lecturer before any written work is submitted.

You are guilty of plagiarism if you copy something from another author's work (e.g. a book, an article or a website) without acknowledging the source and pass it off as your own. In effect, you are stealing something that belongs to someone else. This is not only the case when you copy work word-for-word (verbatim), but also when you submit someone else's work in a slightly altered form (paraphrase) or use a line of argument without acknowledging it. You are not allowed to use work previously produced by another student. You are also not allowed to let anybody copy your work with the intention of passing if off as his/her work.

Students who commit plagiarism will not be given any credit for plagiarised work. The matter may also be referred to the Disciplinary Committee (Students) for a ruling. Plagiarism is regarded as a serious contravention of the University's rules and can lead to expulsion from the University.

The declaration which follows must accompany all written work submitted while you are a student of the ***Department of Geology (University of Pretoria)***. No written work will be accepted unless the declaration has been completed and attached.

I, the undersigned, declare that:

1. I understand what plagiarism is and am aware of the University's policy in this regard.
2. I declare that this assignment (e.g. essay, report, project, assignment, dissertation, thesis, etc) is my own original work. Where other people's work has been used (either from a printed source, Internet or any other source), this has been properly acknowledged and referenced in accordance with Departmental requirements.
3. I have not used work previously produced by another student or any other person to hand in as my own.
4. I have not allowed, and will not allow, anyone to copy my work with the intention of passing it off as his or her own work.

   I, Duan Swart, declare that the thesis/dissertation, which I hereby submit for the degree MSc Engineering Geology at the University if Pretoria, is my own work and has not been previously been submitted by me for a degree at this or any other tertiary institution.

Full names of student:	Duan Swart
Student number:	14312868
Date submitted:	2019
Topic of work:	Mechanical and hydraulic properties of residual dolomite and wad found in the Malmani Subgroup in South Africa
Signature:	
Supervisors:	Prof Jan Louis van Rooy, Matthys Dippenaar, Department of Geology

Table of Contents

.

Figures List

Tables List

Abstract

Dolomitic land is known for subsidence and sinkhole formation, making development such as housing unsafe, especially when wad is found. Wad and residual dolomite are usually found at the bedrock-soil interface and in grykes, in an unsaturated, non- to highly-reworked, state. These are critical areas for ground stability of a dolomite site (Buttrick, 1986). This research aims to better understand the geotechnical properties and hydrological behaviour of unsaturated wad and residual dolomite in relation to the grading, fabric and geochemical composition and the microstructure of the particles of the material, and how the reworking processes alter these characteristic properties. The fabric of the residuum is inherent to the structure of the parent rock, which is determined by the stress history of the rock. The fabric influences the unsaturated behavioural characteristics and water holding capacity of the material. The high and variable liquid limits is dependent on the overall fine grading, and the nanoparticle structure and large reactive surfaces exhibited by the metal oxides in the material. The residuum is typically non-dispersive, possess a low density, when not reworked, that can be below that of water, mostly grades in the silt fraction and has hydraulic conductivities in the order of $1x10^{-6}$ m/s. The mobilisation potential is dependent on the presence of the fabric, variance of sorting of the material's grain sizes and the disparity of the degree of saturation above and below the wetting front moving through the material. The material is considered reworked when mechanical processes destroy the structured or non-structured inherent fabric and foreign material is introduced into the soil matrix. The factors influencing the consequential broad potential behavioural and characteristic properties of the material are the type and degree of reworking and the environment of reworking.

1. Introduction

The already densely populated and urbanised Gauteng province is under constant pressure to develop land for housing to accommodate for the influx of people into, and the homeless that already reside in the 'Place of Gold'. The need for developable land is thus an essential resource for the future of Gauteng, some of which has been deemed undevelopable due to the presence of subsurface dolomite formations and wad. Oosthuizen & Richardson (2011) stated, "25% of Gauteng, parts of Mpumalanga, Limpopo, North West and Northern Cape provinces, are underlain by dolomite". The dolomite residuum located in Gauteng province has a negative connotation due to the formation of sinkholes and subsidence that in the past fifty years has led to the loss of more than 38 lives and more than R1 billion for damage to infrastructure (Buttrick et al., 2001).

The formation and maximum size of sinkholes that can occur are dependent on the following factors (Buttrick et al., 2001):

- The thickness of the blanket layer,
- size or width of the throat (gryke or fissure), and
- the estimated 'angle of draw' in the various soil horizons.

Wad and residual dolomite are usually found at the bedrock-soil interface and in grykes in an unsaturated, non- to highly-reworked, state. These are critical areas for ground stability of a dolomite site (Buttrick, 1986). Therefore, the mechanical, geochemical and structural properties of non-reworked material need to be established first, followed by the influence of the reworking process on the behavioural and characteristic properties. Richardson (2013) stated that the majority of sinkholes are trigger by ingress water. Thus, the relationship between water and a unique material such as dolomitic residuum needs to be investigated.

This research aims to better understand the geotechnical properties and hydrological behaviour of unsaturated wad and residual dolomite in relation to the grading, fabric and geochemical composition and the microstructure of the particles of the material, and how the reworking processes alter these characteristic properties. A secondary aim is to investigate the value in the results from, and limits of, rigorous geotechnical testing on the material.

This study will improve the understanding of dolomitic residuum at variable saturations in the vadose zone. To study this unique material, a good bases of the understanding of unsaturated soil behaviour is needed and will be elucidated in the next chapter.

2. Hydromechanical behaviour of unsaturated residuum.

Majority of the research during the development and understanding of classic soil mechanics was done in regions where soil conditions are generally wet, and the ground water table was close to the surface. Consequently, the assumption that soil is saturated during the analysing of field data of a geotechnical investigation is generally accepted. The advances in soil mechanics in the geotechnical practice have proven that this assumption is not always valid, especially in semi-arid regions such as South Africa. The advances in unsaturated soil mechanics has generally focused on dry sands due to ease of modelling and simplicity of the material.

Residual dolomite or wad is generally found in the vadose zone in an unsaturated state and the variation of moisture due to external natural and anthropogenic processes results in a significant change in behaviour of the material. To understand the alterations of the material behaviour with a change in soil moisture, a good knowledge of unsaturated soil mechanics, and how this differs from saturated soil mechanics, is needed.

2.1. Unsaturated soil mechanics

Saturated soil mechanics is a two-phase system that deals with soil that has one fluid phase, generally water, with positive pore-water pressures, and one solid phase, the soil matrix. The fundamental difference between saturated and unsaturated soil mechanics is the presence of a third phase, which is the air present in the pore spaces. Thus, unsaturated soil mechanics is referred to as a three-phase system (Fredlund et al., 2012). The presence of negative pore-water pressure in the soil relative to the internal and external air pressure gives rise to the behaviour of unsaturated soil. Terzaghi (1943) emphasised the significant role of the air-water interface in the understanding of unsaturated soil behaviour. Fredlund and Morgenstern (1977) justified the need to recognize the unique influence of the air-water interface or contractile skin as a fourth phase in unsaturated soil.

The contractile skin at the air-water interface acts as a thin membrane interwoven throughout the voids of the soil (Fredlund et al., 2012). The presence of this thin partition can cause an unsaturated soil to change volume, water content and shear strength when the stress state changes in the contractile skin (Fredlund et al., 2012). The air-water interface is responsible for the increased strength of unsaturated soil through two components, surface tension and matric suction (Kim & Hwang, 2003). Surface tension acts along the air-water interface and matric suction acts across the interface due to the pressure differences (u_a - u_w) (**Figure 2–1**) (Kim & Changsoo, 2003; Gaspar, 2017).

Surface tension

Surface tension manifests from intermolecular forces acting on molecules in the contractile skin (Fredlund et al., 2012). This property gives a fluid the ability to support the weight of an object with a higher density on its surface (Gaspar, 2017) and to understand this phenomenon; an investigation on a molecular level is needed (Hunter, 2001). Sophocleous (2010) provides a comprehensive explanation for the presence of this 'elastic skin' around a fluid.

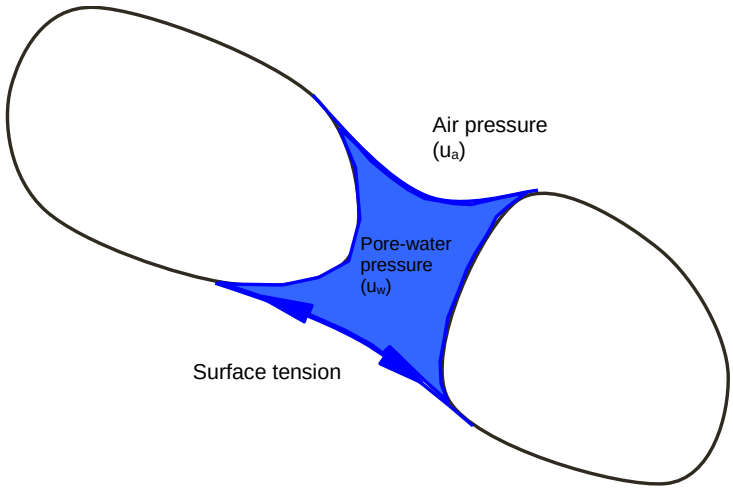

Figure 2–1: Components contributing to increase strength in unsaturated soil.

The molecules in the interior of a fluid experience both attractive and repulsive forces of equal magnitude in all directions. The intermolecular forces act to stabilize the system through interaction between near neighbouring molecules that results in a reduction of their potential energy. These interactions give rise to cohesion among molecules in a fluid and adhesion or adsorption between molecules of that liquid and any bounding solid surface. Referring to **Figure 2–2**, Molecule A will experience equal forces in all directions and will have a lower potential energy than molecules close to the contractile skin of the fluid. Molecule B will have fewer neighbouring molecules in the gaseous region above, leading to a greater energy potential. Furthermore, the molecules near the surface (Molecule B) will experience an unbalanced force distribution of weaker forces from above and a subsequent net downward force pulling the molecule into the bulk fluid will arise. Work needs to be done to counteract this force or to take Molecule A to the Molecule B position. To maintain equilibrium at the surface of a fluid a tensile pull is generated along the contractile skin. Therefore, molecules near or at the surface will possess a positive potential energy, which is termed surface tension (Sophocleous, 2010). Surface tension is tangential to the contractile skin and is measured as a tensile force per unit length of contractile skin (i.e., units of N/m) (Fredlund et al, 2012).

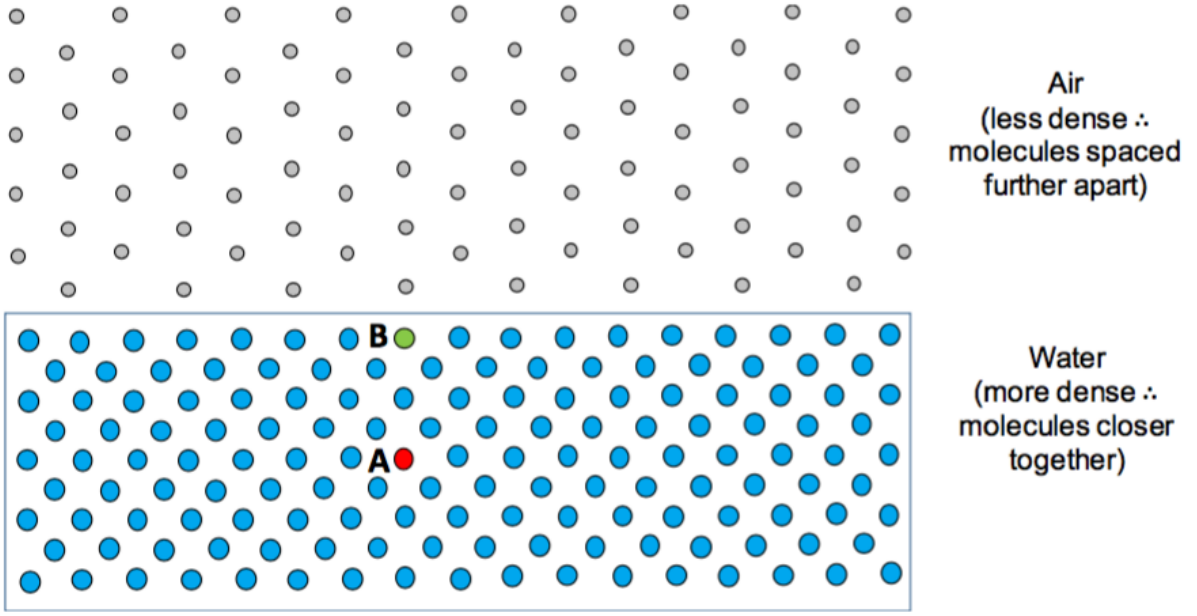

Figure 2–2: Interaction between liquid and gaseous phase (Gaspar, 2017)

The contractile skin reacts in a very similar manner to the membrane of an inflated balloon, which has a higher pressure on the inside than the outside. The pressure difference across the balloon skin causes the membrane to adopt a concave shape towards the larger pressure and exert a tension force along the membrane in order to stay in equilibrium (Fredlund et al., 2012). The meniscus in unsaturated soils will always orientate itself concave towards the gaseous phase as the air-pressure is assumed to be atmospheric ($u_a = 0$) and the pore-water pressure is generally assumed to be negative ($u_w < 0$) (Fredlund et al., 2012). Referring to **Figure 2–3**, the pressures acting on either side of the meniscus are u and ($u + \Delta u$), and since the system is in equilibrium, the pressure difference can be related to the radius of curvature (R_s) of the meniscus and surface tension (T_s) acting along it as shown in **Equation 2-1**.

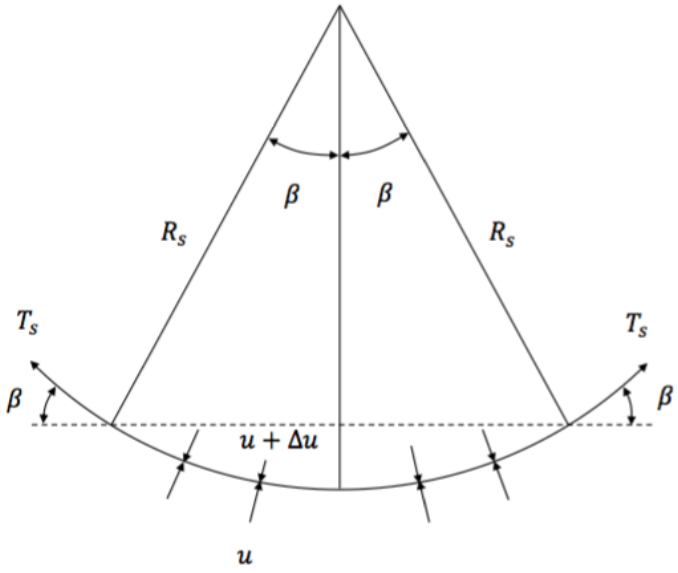

Figure 2–3: Forces acting on the air-water interface (Fredlund et al., 2012)

Assuming force equilibrium in the vertical along the interface: $\Sigma F_Y = 0$

$$2T_s \, sin\beta = 2\Delta u \, R_s \, sin\beta \quad (2\text{-}1)$$

Where:

- $2T_s \, sin\beta$ = length of the membrane projected onto the horizontal plane

Therefore, rearranging **Equation 2-1**:

$$\Delta u = \frac{T_s}{R_s} \quad (2\text{-}2)$$

Equation 2-2 allows one to determine the pressure difference along a two-dimensional surface. For a three-dimensional membrane, **Equation 2-2** can be extended using the Laplace equation (Fredlund et al., 2012):

$$\Delta u = T_S \left(\frac{1}{R_1} + \frac{1}{R_2}\right) \quad (2\text{-}3)$$

Where:

R_1, R_2 = radii of curvature of a warped membrane in two orthogonal principle curves

If it is assumed that radius of curvature is the same in all directions ($R_1 = R_2 = R$) **Equation 2-3** becomes **Equation 2-4**:

$$\Delta u = \frac{2T_S}{R_s} \quad (2\text{-}4)$$

As previously mentioned, the pressure acting on the air-water interface in unsaturated soils are the pore-air pressure (u_a) and the pore-water pressure (u_w). The pressure difference that causes the air-water interface in an unsaturated soil to bend to a curvature shown in **Equation 2-5** (Fredlund et al., 2012):

$$u_a - u_w = \frac{2T_S}{R_s} \quad (2\text{-}5)$$

The pressure difference across the contractile skin in an unsaturated soil is termed matric suction ($u_a - u_w$). It becomes evident when examining **Equation 2-5** that the radius of curvature of the contractile skin decreases as the matric suction of the soil decreases. When the matric suction value is zero (i.e. no pressure difference) the radius of curvature tends to infinity and a flat air-water interface will develop (Fredlund et al., 2012). Under these conditions, the surface tension property will remain at a constant value (Fredlund et al., 2012). The combined effect of matric suction and surface tension, across and along the contractile skin, renders granular unsaturated soils with tensile strength and cohesion (Kim & Hwang, 2003). Matric suction is one component of total soil suction, osmotic suction being the other, and will be explained the next.

Soil suction

Total soil suction (or soil-water potential) can be defined as the thermodynamic potential of soil-water relative to a reference potential of free water (Lu & Likos, 2004). Free water is defined as pure water that is free of solutes, has a flat surface, is in equilibrium with the saturated vapour pressure above the surface and has no external forces acting on it other than gravity (Lu & Likos, 2004). Soil-water has additional forces acting on it caused by the surface tension of the curved surface (meniscus), which reduces the vapour pressure above the surface (Ng & Menzies, 2007). The physical and physiochemical mechanisms responsible for the soil suction act to decrease the potential of the soil-water relative to the reference state (Lu & Likos, 2002). The stress holding the water molecule in the meniscus (i.e. the soil suction) is directly related to relative humidity immediately above the curved surface (Fredlund, 2012; Ng & Menzies, 2007). The primary mechanisms that reduce the potential of soil-water include matric suction, osmotic effects and short-range adsorption. The

adsorptive forces contribution is included in the matric suction component, which will be elucidated next. Thus, matric suction and osmotic suction originate from physical interaction effects and chemical interaction effects, respectively. **Equation 2-6** shows the mathematical relationship of the components of soil suction (Fredlund et al., 2012):

$$\psi = (u_a - u_w) - \pi \qquad (2\text{-}6)$$

Where:

ψ = Total soil suction (kPa)

$(u_a - u_w)$ = Matric suction (kPa)

π = Osmotic suction (kPa)

Matric Suction

The matric suction component of total suction includes the effects of both capillarity and short-range adsorption (Lu & Likos, 2004). **Figure 2–4**, presented by Janssen and Dempsey (1980), best illustrates the concept of capillarity where soil pores are interpreted as capillary tubes partially submerged in a container of water. The combined effect of adhesion, between soil (solid) surface and water, and cohesion, in the water, result in capillarity in the glass tubes and soil pores. The adhesion forces manifest the rise in water and the intermolecular cohesion force provokes all the water molecules to follow the upward pull (Sophocleous, 2010), therefore a negative pressure will be generated in the capillary tube.

The tension-saturated base portion of the vadose zone is called the capillary fringe and is located immediately above the phreatic surface (also referred to as the water table) where the pore-water pressure equals the atmospheric pressure. Referring to **Figure 2–4**, the capillary fringe in fine-grained soils, with narrower pore spaces, will extend higher into the vadose zone, and experience greater pressures, than in coarse-grained soils.

The short-range adsorptive effect arises from electric and van der Waals force fields occurring in the immediate vicinity around fine-grained clay particles that have significant net surface charges and relatively large surface areas (Lu & Likos, 2004). The adsorptive component of the matric suction is important at relatively low water content when only thin films of water exist on fine-grained particle surfaces (Lu & Likos, 2004), but it is difficult to isolate and quantify (Fredlund et al., 2012). It has been suggested that the presence of fine, silt-sized particles with considerably large surface areas and significant net charge play an

important role in sustaining highly negative pore-water pressures (Fredlund et al., 2012). Manganese oxides usually occur as fine-grained material with significantly large surface area per unit mass. This phenomenon will be explained in Section 3.3.

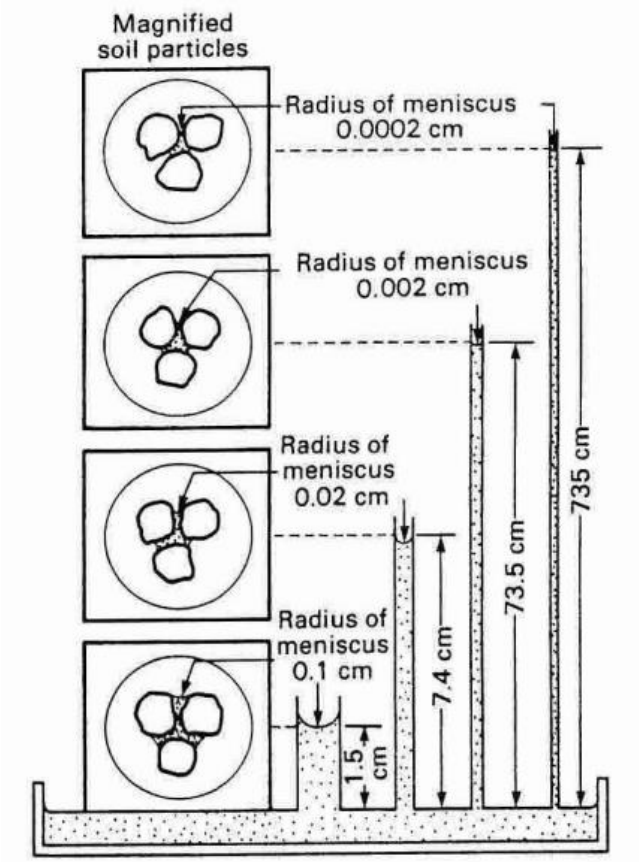

Figure 2–4: The effect capillarity in soil pores illustrated by capillary tubes (Janssen & Dempsey, 1980).

Osmotic suction

Osmotic suction is the component that takes the salt content, or dissolved ions, in the pore-water into account. Osmotic pressure is a term given to the mechanism of water flowing from a position of low dissolved ion concentration to an area of high dissolved ion concentration (Barbour & Fredlund, 1989). If the salt content of the pore-water is changed, changes in the physical properties of the soil can occur, but this component is usually ignored in geotechnical engineering practice (Fredlund et al., 2012). Osmotic suction becomes relevant in a physicochemical process in clays termed osmotic consolidation (Fredlund et al., 2012). Barbour & Fredlund (1989) provide a comprehensive explanation of the volume changes in a clayey profile due to osmotic consolidation.

2.2. The Soil Water Retention Curve

The relation between soil moisture content, either gravimetric or volumetric, or degree of saturation, and soil suction is the most important and fundamental constitutive relationship in unsaturated soil mechanics. The Soil Water Retention Curve (SWRC) illustrates this relationship and it is used to describe behaviour of unsaturated soil and estimate the unsaturated soil property functions (USPFs) (Fredlund, 2017; Lu & Likos, 2004). In the geotechnical engineering practice, SWRC is implemented to better understand the shear strength, volume change and flow of water through unsaturated soil (Fredlund, 2017). Over the entire range of the SWRC the osmotic suction remains constant, if the concentration of dissolved solutes remains the same (Lu & Likos, 2004), and the matric suction changes with change in saturation as will be shown in the following paragraphs.

Referring to the SWRC in **Figure 2–5**, consider a soil medium at 100% (or 1.0) saturation, with the pore-water pressure equal to the atmospheric pressure and matric suction at zero, undergoing a drying cycle, either by drainage or evaporation. As the drying process begins, the soil media is in the capillary regime, where the pore-water pressures are lower than the air-pressure (i.e. negative) and the matric suction becomes positive. In this regime, the degree of saturation remains close to 1 with an increase in suction. The liquid meniscus at the boundary of the soil-water interface pulls inward due to the drying cycle and the matric suction rapidly increases until, at a certain suction value, air enters into the soil media, termed the air-entry value (AEV). The AEV is inversely proportional to the pore size of a soil with sand having a low, well-defined AEV due to the larger pore spaces. By comparison, clay has a higher, poorly defined AEV (Lu & Likos, 2004). The AEV usually occurs between the values of 0.90 to 1 degree of saturation (Cho & Santamarina, 2001). The point of the AEV is a function of the log scale instead of a natural change in the SWRC (McQueen & Miller, 1974).

In the funicular regime, after the AEV has been reached, a state of unsaturation arises as air starts to enter the soil media, but the pore-water is still in a continuous phase with the water-pore being present in both liquid bridges and in pores. In this regime, the matric suction gradually increases as air continuities to replace the pore-water. The suction mechanism is primarily governed by the capillarity and lesser by the short-range adsorption. The gradient of the quasi-linear slope in the funicular regime gives rise to the pore size distribution of the material. A relativity steep slope is represented by a wide pore size distribution (i.e. a well graded soil and a narrow pore size distribution is indicated by a more gradual slope on the SWRC (Lu & Likos, 2004).

Eventually, the pores are mostly filled with air and the pore-water becomes discontinuous, leaving very thin films of water around the soil particles or adsorbed on the surface of the particles resulting in high suction values (Jindal, 2016). This is the point referred to as the residual degree of saturation, Sr, and is defined as the degree of saturation after which a relatively small change in moisture content can result in enormous change in matric suction (Fredlund et al., 2012). This is the start of the pendular regime in which short-range adsorption effect, between the discontinuous water phase and the surfaces of soil solids, is the dominant suction mechanism (Lu et al., 2009).

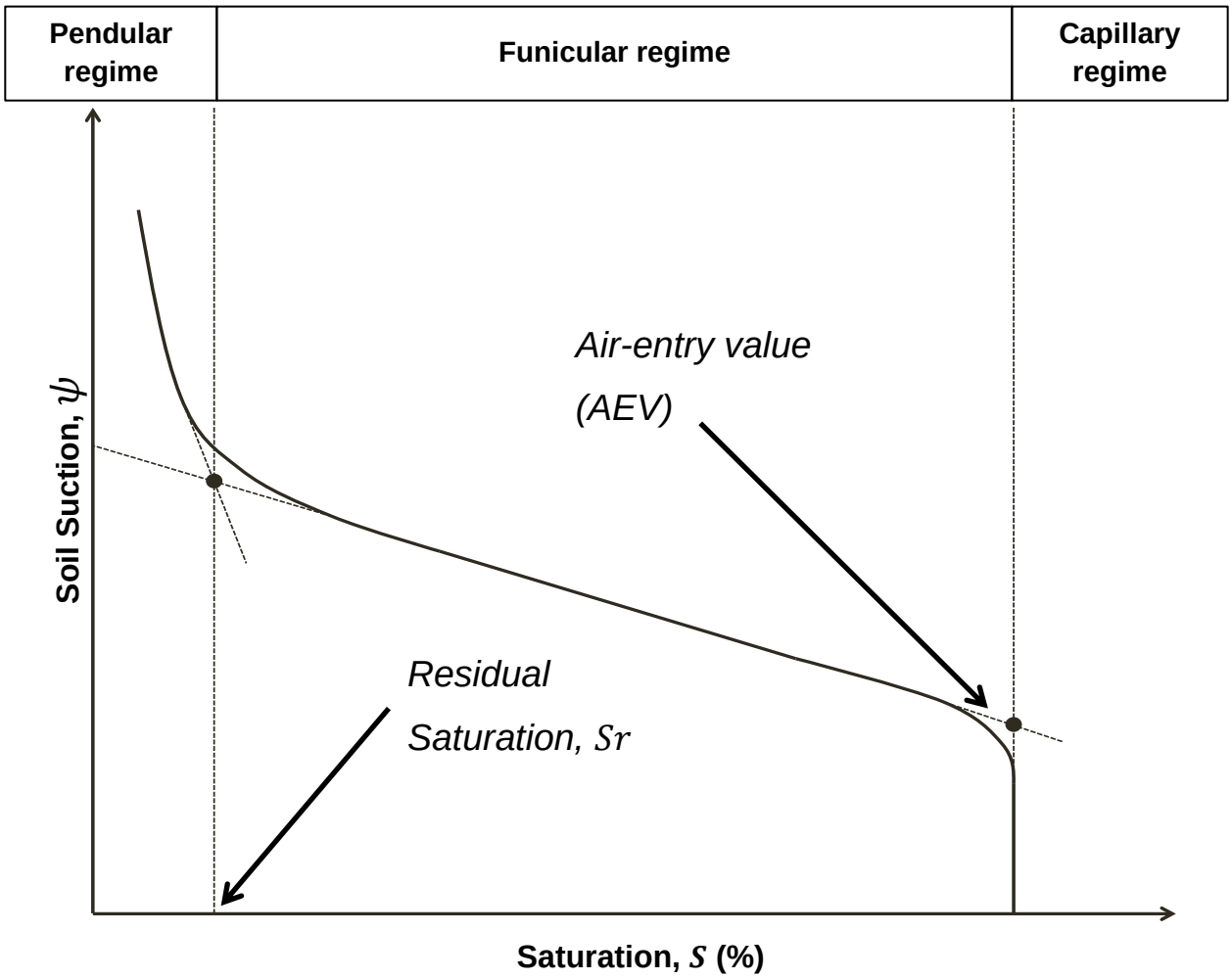

Figure 2–5: Typical Soil Water Retention Curve regimes.

The shape of the SWRC is dependent on the type of soil, grain size distribution, pore size distribution, void ratio, density, organic matter content, clay content and mineralogy (McQueen & Miller, 1974; Imam et al., 2016; Lu & Likos, 2004). The difference in the behaviour of the SWRC can be seen in the typical curves for sand, silt and clay soils shown in **Figure 2–6**.

The SWRC exhibits hysteretic behaviour contingent upon the type of cycle the soil has undergone and a distinct difference exists between the wetting and drying curves as seen in **Figure 2–7**. As previously state, a soil sample starting a drying cycle at saturation will follow the Primary Drying Curve. Before the wetting cycle, the soil is oven dried and will follow the Primary Wetting Curve as the sample is inundated with water. The soil undergoing the wetting cycle will experience a lower value of suction at a certain moisture content value than a soil undergoing a drying process at the same moisture content value. The mechanisms attributing to the hysteretic behaviour are stated in Lu & Likos (2004). The drying and wetting curves or boundary curves form an envelope within which all possible states of the soil can exist (Toll, 2012). Small wetting and drying cycles that can follow an infinite amount of scanning curve exists within the boundary curves (Lu & Likos, 2004). In **Figure 2–7**, Point A is a soil sample at certain initial moisture content that undergoes either wetting or drying. The curve will follow the scanning curve to Point B or Point C, respectively, after which the curve will follow the Primary Wetting or Drying Curve (Lu & Likos, 2004).

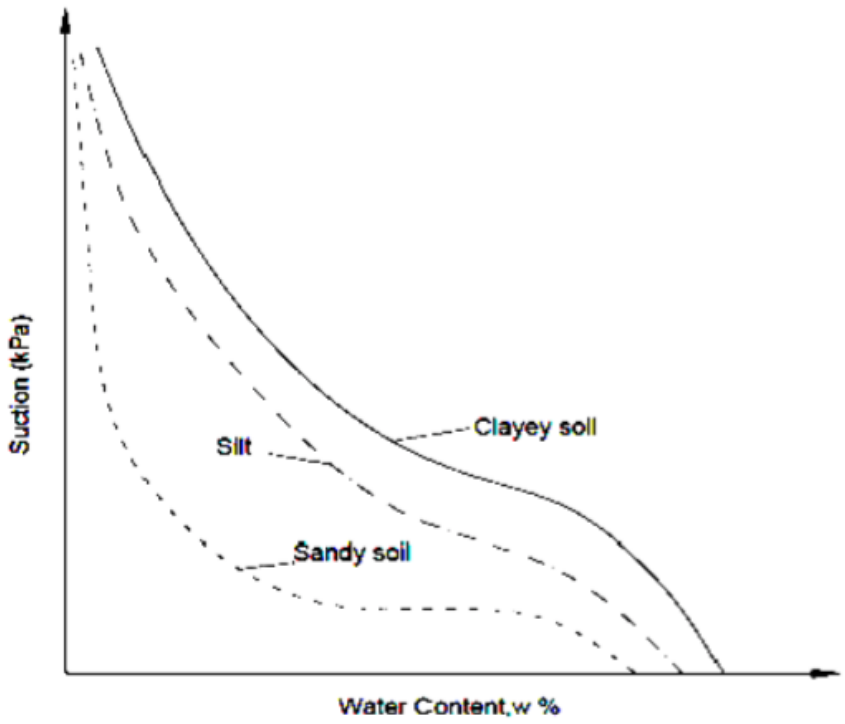

Figure 2–6: Typical SWRCs for sandy to clayey soil (McQueen and Miller, 1974).

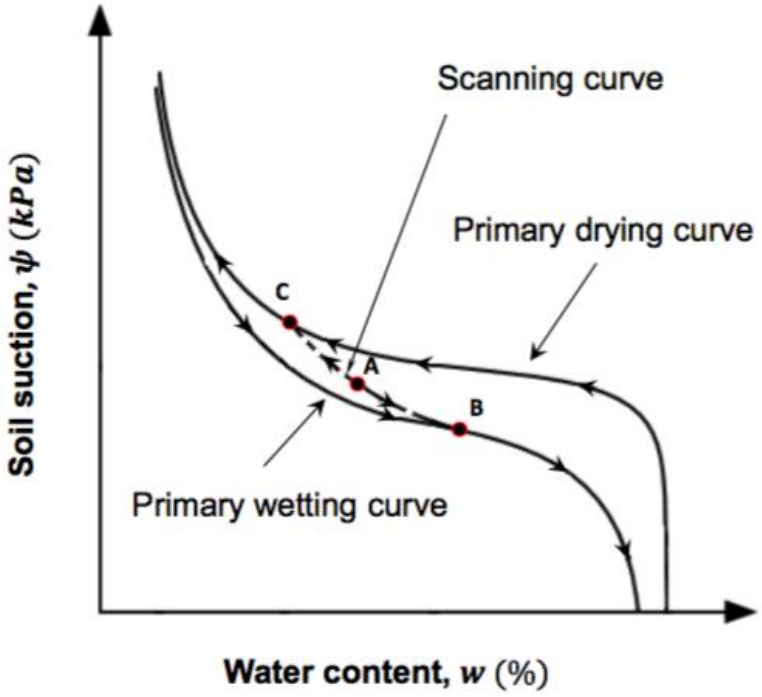

Figure 2–7: SWRC hysteresis (adapted from Lu & Likos, 2004; taken from Gaspar, 2017)

2.3. Influence of soil suction on shear strength of unsaturated soils

The stress state of soils is directly influenced by relative changes within the three-phase system of unsaturated soils. Deviations in a stable system, (i.e. changes in boundary conditions from anthropogenic processes) will affect stress states at particle-particle contacts and ultimately influence the physical behaviour of the soil mass (Lu & Likos, 2004). Terzaghi (1936) first described the principle of effective stress in soil behaviour and suggested that it governed all the changes in the stress state of soil. It has become basic understanding that pore water in relatively dry soils creates a high tensile force that increases the soil strength by pulling the soil grains together (Lu & Likos, 2004).

Equation 2-7 was proposed by Bishop (1959) to determine the effective stress of soils at variable saturations:

$$\sigma' = (\sigma - u_a) + \chi(u_a - u_w) \quad (2\text{-}7)$$

Where:

σ' = Effective stress (kPa)

σ = Total stress (kPa)

u_a = Air pressure (kPa)

u_w = Pore water pressure (kPa)

χ = Empirical factor to degree of saturation

The variable χ created a simple constitutive relationship for the stress state of a soil at a range of degree of saturation. When a soil is completely saturated, χ = 1 and the equation reduces to the classic saturated soil mechanics for effective stress (Fredlund & Rahardjo, 1993). The equation explains the behaviour of the effective stress but fails to describe the stress state of the soil (Fredlund & Morgenstern, 1977) and to incorporate the potential volume change upon wetting (i.e. collapse) (Jennings & Burland, 1962). Burland (1965) explained that the suction increases a soil's shear resistance by increasing the contact stresses between particles as well as stabilises the soil mass due to the presence of the surface tension at the menisci. This ultimately proved that the principle of effective stress does not solely govern the behaviour of unsaturated soils (Toll, 2012).

The importance of separating the two stress state variables was highlighted by Burland (1965). Fredlund & Morgenstern (1977) proposed the need to determine the stress variables, net stress $(\sigma - u_a)$ and the matric suction $(u_a - u_w)$, independently. The use of two independent stress variables has proven adequate to describe the shear strength and volume change in unsaturated soils (Fredlund & Rahardjo, 1993).

2.4. The Extended Mohr-Coulomb failure criteria

Fredlund et al. (1978) devised an extended Mohr-Coulomb failure envelope that best describes the shear strength behaviour of an unsaturated soil. **Equation 2-8** allows for independent determination of the internal friction angles associated with the different stress variables:

$$\tau = c' + (\sigma - u_a)\, tan\, \phi^a + (u_a + u_w) tan \phi^b \quad (2\text{-}8)$$

Where:

τ = Shear strength (kPa)

c' = Effective cohesion [when $(\sigma - u_a); (u_a - u_w) = 0$] (kPa)

ϕ^a = Internal friction angle associated with net normal stress (°)

ϕ^b = Internal friction angle associated with matric suction (°)

Equation 2-8 accounts for the change in the rate of increase of the effective stress angle of internal friction (ϕ'), below and above the air-entry value, during a desaturation cycle of a soil. When a soil is saturated, the increase in strength is governed by the net normal stress, as classic saturated soil mechanics suggest, and the value of ϕ^a would be equal to the ϕ' and constant through desaturation cycle (Fredlund et al., 1978). Once desaturation occurs, at the air-entry value, the increase in strength is dependent on the increase in matric suction (Fredlund et al., 1978). Fredlund et al. (1978) noted that the increase in strength above the air-entry value is less significant than below this value as shown in **Figure 2–8**.

It was shown that ϕ^a has greater values than ϕ'at lower degrees of saturation due to the presence of aggregations causing the soil to perform as a coarser material than the grading suggests (Toll, 2012). The aggregated fabric in an unsaturated soil is unaffected during shearing as the suction gives the material strength, whereas in a saturated soil the aggregations would break down and not affect the shear strength (Toll, 2012).

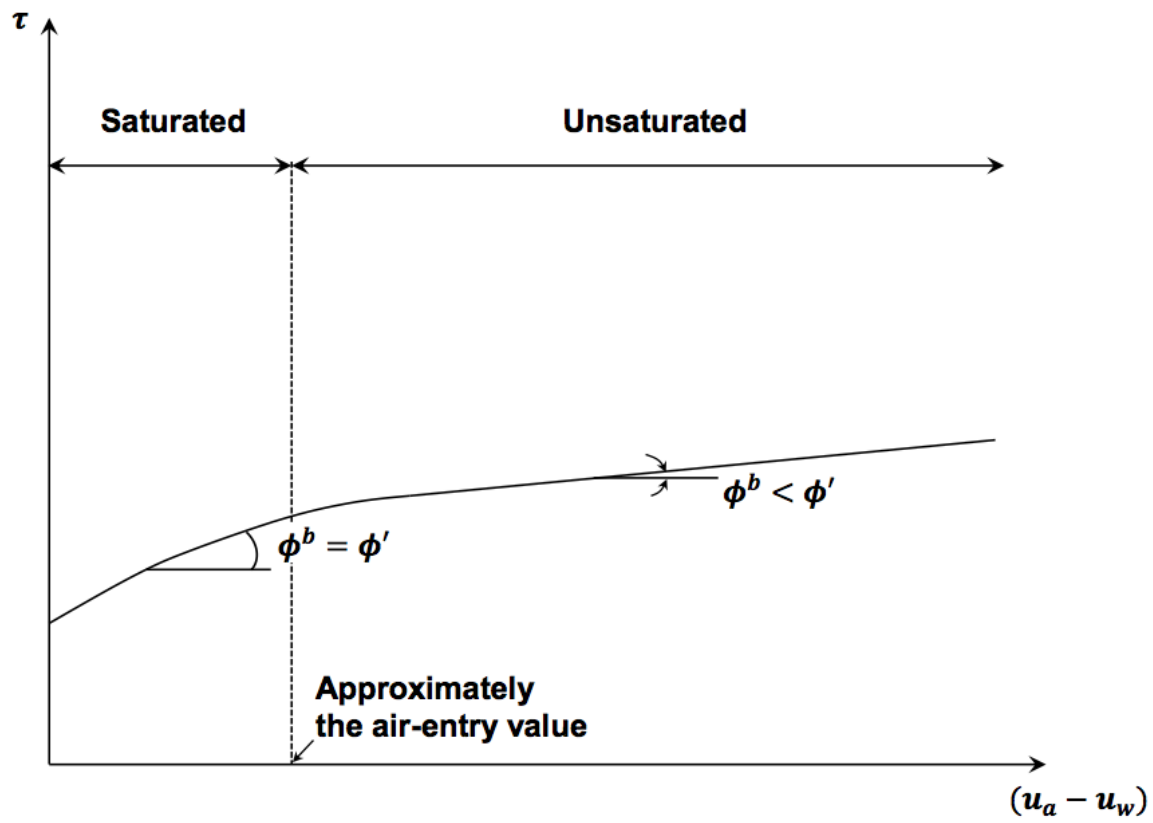

Figure 2–8: Deviation of ϕ' with an increase in matric suction (adapted from Fredlund et al., 1978; taken from Gaspar, 2017)

2.5. Laboratory testing of unsaturated soils

Testing unsaturated soils in the laboratory allows for the control of boundary conditions of the degree of saturation of the sample and pore water pressures experienced (Jacobsz, 2018). Suctions up to 100 kPa are readily tested in the laboratory, however high cost equipment is needed to record suction readings at greater than 100 kPa during a drying cycle. Jacobsz (2018) describes low-cost pore pressure tensiometers, developed at the University of Pretoria, which can routinely measure suctions up to 500 kPa and has proven to take readings up to 600 kPa until the cavitation or air entry value of tensiometers is reached. OcThe tensiometers are primarily used to developed SWRC during a drying cycle, and additionally, this equipment has the ability to record positive pore-pressure readings up to a pressure range of 7 bar (Jacobsz, 2018).

These tensiometers were used in this dissertation to develop SWRC for residual dolomite and wad because of the ease in preparing the sample, saturating the tensiometers and recording highly sensitive real time data during the running of the tests. The tensiometer set up comprises of a commercially available pressure sensor, MS54XX pressure sensor, fitted

to a porous ceramic filter sealed in epoxy. The design and construction of these low-cost tensiometers are specified by Jacobsz (2018)

2.6. Importance of unsaturated residual dolomite behaviour above an open cavity

The contractile skin present as a weaved netting through the soil matrix, due to the existence of the third phase, has immense impacts on the behaviour of unsaturated soil, as shown in Section 2.1. The surface tension and matric suction increases the strength at lower degrees of saturation and produces an inter-particle bonding effect in unsaturated soils, more notably in coarse grained material. The increase in strength is greater in finer material that possesses narrower pore spaces, allowing for sustained matric suctions through a greater range of partial saturation. The increase of saturation causes a loss of matric suction and therefore, a loss of strength. This is evident, and partly responsible, for the collapse in some soils exhibiting fabric with an open structure.

Jennings et al. (1965) proposed the conditions needed for sinkhole to form. An open cavity in the soil material, usually found in the vadose zone, must exist above a receptacle, as this will receive and remove the material as the cavity grows above. A disturbance is required to disrupt the equilibrium in the arch, such as water that results in loss of strength and washing out of key binding material and causes the material to collapse. Wagener (1985) described two such scenarios, dewatering (lowering of water table) and water ingress (static water table). Water ingress scenarios accounts for majority of the sinkholes that form in dolomite areas within South Africa (Richardson, 2013; Constantinou & van Rooy, 2017). Water ingress results in transient pore pressure gradients in the arch material and is the most common cause of failure of cover-collapse sinkholes (Tharp, 1999).

The arch material generally comprises of an unsaturated fine matrix with chert gravel and cobble-sized slabs. The overall support of the material is generally provided by competent components, such as dolomite pinnacles or dykes, located adjacent the arch (Brink, 1996). The stability within the arch is generated due to the suction pressures in the soil, whereby creating a bonding agent between the coarser chert material (Jacobsz, 2016). The material at the free face of the arch experiences zero vertical stress and the major principle stress acts in a horizontal direction (Jennings et al., 1965). If the minor principle stress exists at zero, and a failure envelope is drawn with a typical friction angle and a cohesive value greater than zero, the Mohr circle will show the material must possess some degree of tensile strength (Gaspar, 2017; Tharp 2003). The majority of the tensile strength will exist as

cohesive strength due to the suctions in the soil matrix. Therefore, an understanding of the flow regimes of water and the influence it has on the change of saturation in the vadose will assist in the understand of the mechanism of mobilisation in the arch during the ingress scenario.

2.7. Vadose hydrology of residual dolomite

The hydrology of the vadose zone has been intensely investigated, with authors describing various flow mechanisms in a soil region where pore pressures are lower than atmospheric and the system is governed by forces of capillarity and gravity (Dippenaar 2012; 2014a; 2014b; Dippenaar & van Rooy 2018; 2014; Brouwers & Dippenaar, 2018; Toll, 2012; Lu & Likos, 2004). Though, very little work contributing to the vadose zone properties of residual dolomite exists (Dippenaar et al., 2018). Redefining residual dolomite will be beneficial in understanding the link between the bedrock mineralogy and the overburden properties (Dippenaar et al., 2018). This new understanding may give insight to the contribution that residual dolomite has in sinkhole formation, especially during the ingress scenario.

The flow and permeability in unsaturated soils has been thoroughly investigated and described by numerous authors (Lu & Likos, 2004; Toll, 2012; Fredlund et al., 2012; Dippenaar et al., 2014c). The type of flow, be it pore water or pore vapor flow, through an unsaturated medium is dependent on the water content and pore size or soil texture (Lu & Likos, 2004). **Figure 2–9** illustrates the conceptual regimes of pore airflow and water flow relative to the water content and pore size in an unsaturated soil. The boundary flow limits are represented by the residual water content or residual saturation, explained in Section 2.2, and the occluded-air-bubble water content. The occluded-air-bubble point is achieved when the water content in the system results in isolated air bubbles in the pore water (Lu & Likos, 2004). The increasing water content and pore size and connectivity, results in water flow to be dominant in an unsaturated soil, the rate which is dependent on the factors controlling the hydraulic conductivity.

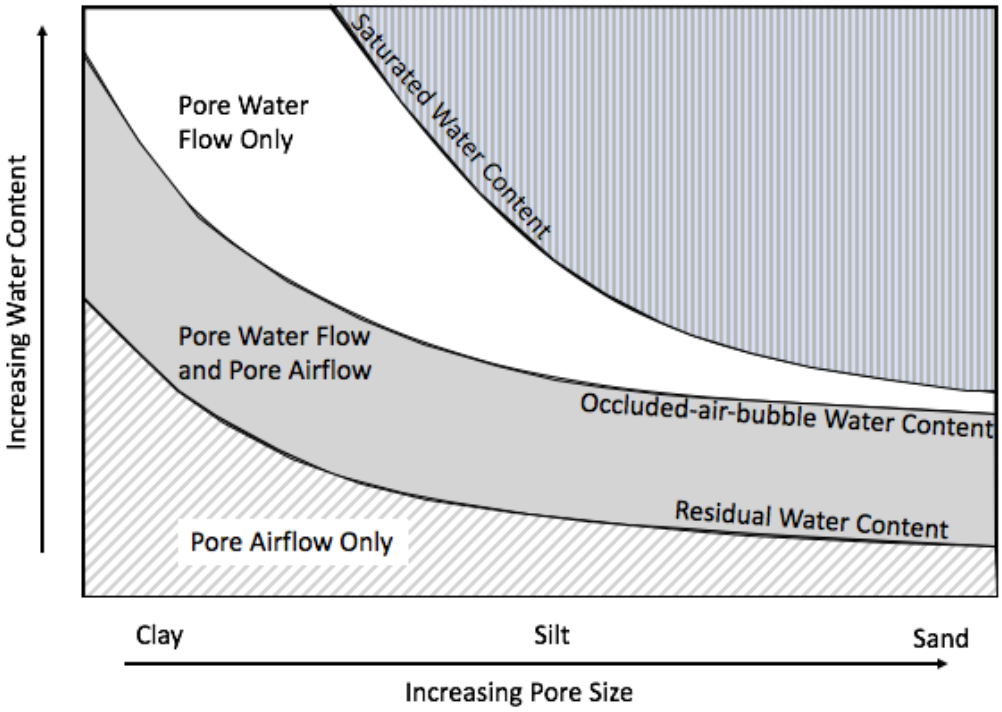

Figure 2–9: Conceptual regimes of pore airflow and pore water flow in unsaturated soil (adapted from Lu & Likos, 2004)

Hydraulic conductivity in unsaturated soils is dependent on the fluid properties, the material attributes (pore structure, void ratio and grading) and the relative degree of saturated present in the pore openings. The variability of flow in unsaturated soils is also a function of the initial water content prior to an alteration of moisture conditions in the system. The SWRC exhibits hysteresis, and since the hydraulic conductivity is a function of matric suction, it will follow the same trend (Lu & Likos, 2004). The hydraulic conductivity is greater along the primary drying curve compared to along the primary wetting curve at the same degree of saturation.

Figure 2–10 shows the relationship of the unsaturated hydraulic conductivity to increasing water content. This relationship shows that higher degrees of saturation achieves a higher hydraulic conductivity and that saturated hydraulic conductivity is always greater than unsaturated hydraulic conductivity for the same soil. The extent of influence of the water content to the relative conductivity is dependent on the soil texture and pore size (Lu & Likos, 2004). The hydraulic conductivity of sand will have a significant reduction in value at a point that coincides with the AEV on the SWRC compared to a finer-grained soil material at the same water content (Lu & Likos, 2004). Sand grains house larger pores between the particles than silt-sized aggregate. As water drains out of the soil, the hydraulic conductivity reduces as the water content reduces relative to the pore size. The relative water content

rapidly reduces in the larger pores between the sand grains at much lower suctions than the silt grains. Therefore, finer grained soils are able to conduct water at significantly larger suctions than coarse-grained soil (Lu & Likos, 2004). This is an important concept in lateral flows and capillary barriers in soils and at the soil-rock interface found in the vadose zone as shown by Dippenaar & van Rooy (2018).

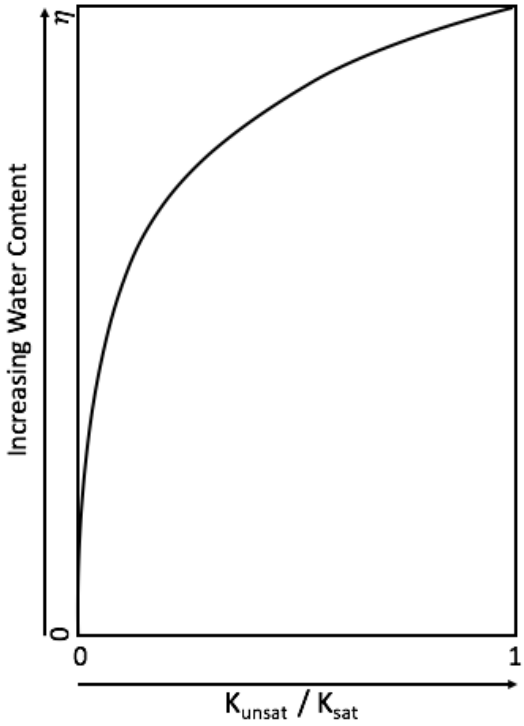

Figure 2–10: Influence of water content on relative hydraulic conductivity (adapted from Fitts, 2002).

As mentioned, the arch material is commonly comprised of chert coarse gravel. A rapid increase in soil saturation may be achieved as water flows along the impermeable material surface and congregates to the soil between the chert slabs and coarse gravel. The resulting stability will depend on numerous factors, one being the possibility of a capillary barrier forming as elucidated by Brouwers & Dippenaar (2018). Kleinhans & van Rooy (2016) explained that a competent surface is needed for the soil to mobilizes against. Ingress water accumulates together as its diverged from a vertical direction by the competent component. The increased saturation, against the virtually impermeable material, may cause a loss in surface tension, resulting in loss of cohesion, and causing an increase in hydraulic conductivity sufficient enough to trigger mobilisation of the material. The scale of this scenario has the potential to occur from a few millimetres between chert gravel causing collapse of the arch, to meters wide slip face along a dolomite pinnacle.

The need to broaden the knowledge of the unsaturated hydromechanical behaviour of a material so unique as residual dolomite, which occurs in such a vital zone of importance for sinkhole formation, cannot be overlooked. This dissertation will aim to gather and compare new and old data to fill the gaps in the basic understanding of the material and to look at the basic fundamental unsaturated behaviour of residual dolomite. The properties of residual dolomite are highly dependent on the material's history, formation and chemical components. The parent rock, formation process, material components and influences of the these will be looked at in the following sections.

3. Geology

3.1. Geology of dolomite in Southern Africa

Residual dolomite is formed from leaching of a calcium-magnesium-rich carbonate rock called dolomite (Buttrick, 1986). The dolomitic areas investigated in this research are housed in the Malmani Subgroup found in the Chuniespoort Group, of the Transvaal Supergroup and has been intensely researched by numerous authors (Brink, 1979; Obbes, 1995; Eriksson et al., 2006). **Figure 3–1** displays the five formations of dolomitic rocks found in southern Africa, namely the Oaktree (oldest), Monte Christo, Lyttleton, Eccles and Frisco Formations (youngest) (Obbes, 1995). The formations have been subdivided based on chert content, and the presence and morphology of stromatolites (Obbes, 1995). The Malmani Subgroup is confined by the lower Black Reef Formation and, depending on the location, by the upper iron-rich Penge Formation, as shown in **Figure 3–2** (Eriksson et al., 2006), or the Pretoria Group (Hammerbeck, 1976). The subgroup dips at 15 to 20 degrees and varies in orientation from northeast to northwest (Obbes, 1995). The tilting occurred during the emplacement of the Johannesburg basement granite-gneiss dome and the intrusion of the Bushveld Igneous Complex (Trollip, 2006). Thus, the dolomite formations outcrop in the area south of Pretoria and along the western and eastern limbs of the Transvaal Basin (Eriksson et al., 2006; Hammerbeck, 1976).

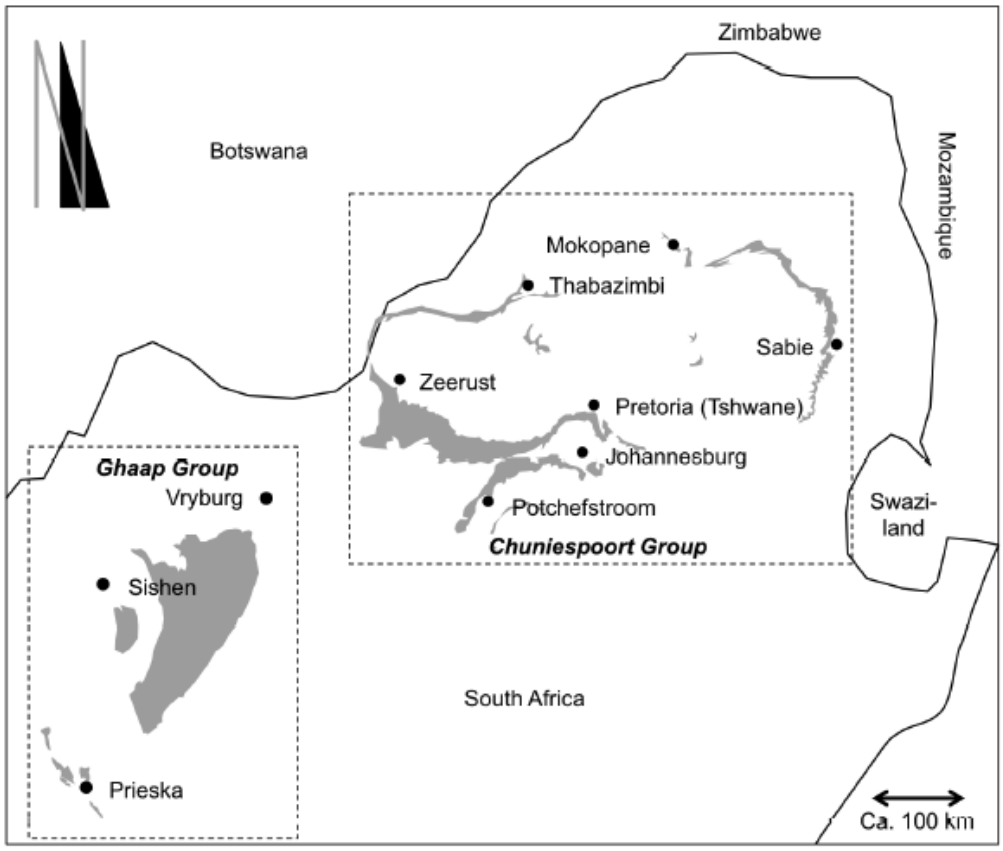

Figure 3–1: Distribution of the major dolomites of South Africa shown in grey shading Taken from Dippenaar et al., (2018); adapted from Eriksson et al., (2006).

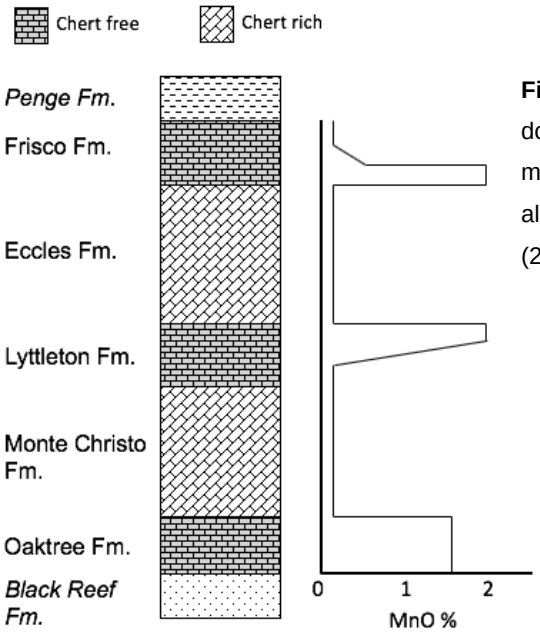

Figure 3–2: Stratigraphic section of Malmani dolomites with basic representation of manganese content. Adapted from Beukes et al., (1999), Brink (1979) and Eriksson et al., (2006).

The Malmani dolomites are replacement products of limestone alternation through the process of dolomitization and chertification during the late Archean and early Proterozoic (Obbes, 1995). The precursor carbonates that formed in the Transvaal Supergroup Epeiric Sea some 2550 Ma ago are stromatolitic deposits or the direct result of erosion and weathering of stromatolites (Eriksson and Altermann, 1998). Dolomite rock contains more than 90% dolomite (mineral) and less than 10% calcite, secondary silica (chert) and detrital minerals. The best representation of the range of the dolomite compositions that forms, namely calcian to magnesian dolomites, is $Ca_{(1+x)}Mg_{(1-x)}(CO_3)_2$ as dolomites are rarely stoichiometric ($CaMg(CO_3)_2$) (Warren, 2000). Dolomite can be “enriched” iron (Fe) or manganese (Mn), but these are usually minor amounts in the overall rock (Buttrick, 1986).

Buttrick (1986) states “the fabric developed in the wad is determined by the nature of the fabric inherent in the parent dolomite”, therefore the diagenesis and especially the stress history of dolomite influences the properties of wad. The dolomites in the Chuniespoort Group have areas of stress build up from tectonic activity such as faulting and folding under low temperatures after intrusions of sills and dykes (Buttrick, 1986). The variation of stress concentrations results in a change in structure over a relatively small distance without changing the chemical composition of the rock (Buttrick, 1986). The stress acting on the dolomite forms a layered fabric or laminations in the previously massive rock, which has no visible features (Buttrick, 1986). The structure of the dolomite is believed to survive the leaching process of dolomite to residual dolomite that is summarised in the ‘Guideline for engineering geological characterisation and development of dolomite land’ (2003). The

leaching processes has resulted in a variety of karst formations, and the different accepted models are explained by Kleinhans & van Rooy (2016).

3.2. Formation of residual dolomite

Beukes et al. (1999) concluded that the dolomite residuum present today formed after the break-up of Gondwanaland (~180 ma.), where conditions were humid and warm resulting in moderately acidic to weakly alkaline and oxidizing conditions. These conditions allow for deep, chemical weathering to form typical wad material from dolomite. Rainwater that precipitates, infiltrates and eventually percolates to dolomite bedrock becomes slightly acidic due to the particle pressure of carbon dioxide in the atmosphere and the soil, to form a weak carbonic acid (H_2CO_3) (Council of Geoscience, 2003). The meteoric water flowing through the discontinuities in the dolomite rock mass causes leaching of the soluble carbonate minerals, resulting in a bicarbonate-rich water that leaves behind the insoluble material (Council of Geoscience, 2003). **Equation 3-1** simply represents this process (Council of Geoscience, 2003):

$$CaMg(CO_3)_2 + 2\ H_2CO_3 \rightarrow Ca(HCO_3)_2 + Mg(HCO_3)_2 \qquad (3\text{-}1)$$

The leaching process is most intense in the joints and fractures that open up over time forming various shaped grykes between pinnacles of fresh sub-rounded dolomite rock (Buttrick, 1986). Further weathering results in Fe and Mn elements oxidise to Fe^{3+} and Mn^{4+}, unlike the alkali earth metals that weather to Ca^{2+} and Mg^{2+}, and can be represented by **Equation 3-2** and **Equation 3-3** (Buttrick, 1986):

$$2MnCO_3 + H_2O \rightarrow 2Mn(HCO_3) \qquad (A)$$
$$2Mn\ (HCO_3)_2 + H_2O + O_2 \rightarrow 2MnO_2 + 4H_2CO_3 \qquad (B)$$

$$(A) + (B): 2MnCO_3 + 2H_2O + O_2 \rightarrow 2MnO_2 + 2H_2CO_3 \qquad (3\text{-}2)$$

$$4FeCO_3 + 4H_2CO_3 \rightarrow 4\ Fe(HCO_3)_2 \qquad I$$
$$4Fe(HCO_3)_2 + 4H_2O + O_2 \rightarrow 2Fe_2O_3 + 8H_2CO_3 \qquad (D)$$

$$I + (D): 4FeCO_3 + 4H_2O + O_2 \rightarrow 2Fe_2O_3 + 4H_2CO_3 \qquad (3\text{-}3)$$

The continued leaching of the dolomite results in a material known as residual dolomite or wad. Iron (Fe) and manganese (Mn) solubilities are greatly reduced in highly oxidising

environments to the point where the Fe and Mn oxides are deposited, with other soluble materials from the parent rock, to form the residuum (Snyman, 1981; Buttrick, 1986). Buttrick (1986) analysed wad at increasing distance from a fresh dolomite floater in a profile in the Oaktree Formation. The wad in close proximity had a decrease in SiO_2, MgO and CaO content; the initial depletion of Mg and Ca is expected during weathering (Buttrick, 1986). This depletion in ions causes a relative enrichment of Al_2O_3, Fe_2O_3 and MnO, ferric iron having the greatest increase (Buttrick, 1986). The relative increase of Fe to Mn is inferable to the lower oxidation potential required to convert ferrous iron (Fe^{2+}) to ferric iron (Fe^{3+}), therefore precipitates more readily (Buttrick, 1986), as opposed to the oxidation potential of Mn^{2+} to Mn^{4+}. Wad samples further away typically had an increase in Si^{4+}, as silica, and manganese oxide, and a relative decrease in Al_2O_3 and Fe_2O_3 and a continued depletion of Mg^{2+} and Ca^{2+} (Buttrick, 1986).

Wad is recognized for being enriched in Mn and Fe, some of the most enriched Mn soil in the world, with Mn contents as high as 17% (Dowding, 2007). De Villiers (1960) found wad to contain 21 - 28 weight percent (w%) Mn_2O_3 and 22 - 44 w% Fe_2O_3. Wad located on the East Rand was rich in Mn and Fe, at values of 19,2w% and 36,1w% respectively, and contained almost pure Mn oxide (Hawkins et al., 1986) The two elements are diadochic (Buttrick, 1986), and will often substitute with one another in a morphed crystal lattice and exist as a mass of fine-grained oxides in wad. Buttrick (1986) found the iron content is generally double the manganese content in a typical non- to slightly reworked wad. Wad inherits the fabric present in the parent rock when formed through weathering and leaching of the dolomite (Buttrick, 1986). The preserved relict structure results in the same volume with a significantly lesser amount of material resulting in a highly voided and low-density material (Buttrick, 1986). The description of wad is generally given as a dark, fine-grained, insoluble material that formed from weathering of manganese-rich dolomite resulting in a Mn enriched material.

Chert is nearly insoluble and weathers to a white chalky material (Buttrick, 1986) and usually exists as layers in the dolomite. After the soluble dolomite has leached out, chert remains intact in the residuum. Over an extended period of time, the chert will break up due to mechanical processes leading to chert coarse gravel and cobbles to be present or exist as sand grains in residual dolomite. The addition of this chemically inert material into the finer wad matrix results in a relative decrease in metal oxides, an increase in silica, and an increase in density and coarser grading in the overall residual material. The description of the residual dolomite is usually described as reddish brown, sandy silt with variable chert gravel and clay.

When working with wad or residual dolomite, dark staining of the fingers is an attribute associated with presence of Mn oxides in the soil. The effect on soil behaviour that metal oxides have in wad might not stop there. To understand the possible behavioural influences, a brief summary of the metal oxides previously found in wad may be beneficial.

3.3. Role of manganese and iron oxides in residual dolomite

The influence that Mn oxides have on the behaviour of soil has been thoroughly studied terms of soil science and its reducing and oxidizing ability (Greathouse et al., 2014) and has been the subject of immense success in the application of water treatment due to its uniquely large surface area (Chen et al., 2011). Very little has been researched on the effect that Mn has on the geotechnical behavioural characteristics of soil. A small soil mass can have a relatively large reactive surface area due to the presence of layered silicate clays and silt-size metal (oxyhydroxides), namely gibbsite, goethite, ferrihydrite, birnessite and other Mn-oxides (Perdial et al.,2015). The variable surface charge of the metals area is dependent on the pH of the soil (Perdial et al., 2015).

Mn oxides commonly form coatings on other minerals (Post, 1999), and can form reactive surfaces on inert chert or quartz grains. Metal (Fe and Mn) oxides in wad have recently been thought to influence the variable and high liquid limits to a much greater extent than previously thought (Bear Geoconsulting, 2016), especially the presence of certain Mn-oxides. Jenne (1968) stated that the chemical influences that Mn-oxides have on the surrounding environment and aqueous solutions far outweighs their concentrations. The chemistry of Mn-oxides is complex due to the variety of oxidation states, though Mn oxides in soils are limited to Mn^{3+} and Mn^{4+} (McKenzie, 1972). A continuous series of different Mn compositions exists as Mn can oxidize without changing positions in the crystal lattice, with the addition of conversions of ligands to maintain electrical neutrality (McKenzie, 1972). Mn-oxides are typically poorly crystalline (i.e. amorphous) and generally no attempt is made to distinguish the exact Mn mineral (Post, 1999). Dowding (2007) studied the Mn-rich soils in the Graskop, Mpumalanga, area and identified Mn and Fe minerals commonly found in wad to be lithiophorite, birnessite and todorokite, and goethite, haematite and maghemite, respectively. Beukes et al. (1999) determined that ferromanganese wad composed of amorphous Mn- and Fe-oxyhydroxides containing birnessite, lithiophorite and haematite with subordinate quartz, muscovite and kaolinite.

The definition of wad implies that the material is enriched Mn, though pervious authors have shown that the material is often enriched Fe, occasionally is amounts greater than Mn

(Buttrick, 1986). To better understand the influence of Mn-oxides, a concise summary of the material found in wad has been put together below.

Birnessite [(Na, Mg,Ca,Mn^{2+})Mn_7O_{14}] (simplified to δ-MnO_2 in geochemical literature) is the most common Mn oxide in soil and marine deposits (Burn & Burn, 1977; McKenzie 1972). It comprises of layers of edge sharing MnO_6 octahedra alternating with planes of cations, mainly Ca, Mg, Na and Mn^{2+} and H_2O (Figure 3a) (Dowding, 2007). Birnessite is mostly found in neutral to alkaline conditions (Ross et al., 1976; Taylor et al., 1964) and it is believed the structure and chemistry of the mineral is influenced by the pH of the soil (Dowding, 2007). It is also believed to have a strong influence on soil and groundwater chemistry as it readily participates in oxidation-reduction and cation exchange reactions (Post, 1999). Vernadite is a variety of birnessite that is analogous to the synthetic phase of δ-MnO_2 and has been found to have 15-25% of its weight to be H_2O (Post, 1999). Found the surface area of a fine-grained birnessite to be approximately 300 m^2/g (Buser & Graf, 1955). An abundance of this oxide could allow for a much greater water holding capacity compared to the Mn being present in a different mineral and crystal form. Birnessite occurs as black or reddish brown, fine-grained, generally silt-size, poorly crystalline aggregate, or as an amorphous surface coating on rocks or soil grains, in nature (Post, 1999; Herman, 2012). The mineral structure, when not amorphous, is typically described as being similar to highly voided coral or sponge material (Cheney, et al., 2008; Jiang, et al., 2010; Bruins, 2016). It is identified by its red-brown streak and is commonly admixed with hydrated Fe and Mn oxides in soil (Herman, 2012). It has been suggested that disordered birnessite, lithiophorite, hollandite and todorokite oxidises form a well-crystalline birnessite, depending on the soil conditions (McKenzie, 1972)

Lithiophorite [(Al,Li)$MnO_2(OH)_2$] has a similar structure to that of birnessite expect the alternating layers, between the MnO_6 octahedra, are Al-hydroxy sheets, where lithium is contained in the in the Al octahedral vacancies (Figure 3b) (Dowding, 2007). The Al-hydroxy sheet suggests that lithiophorite forms under acid conditions (Golden et al., 1993), this agrees with Dowding (2007) findings that lithiophorite exhibitions weaker oxidizing capacity than the other Mn minerals and is the end member of the Mn weathering sequence, after K, Na and Mg cations have been leached out, leaving the aluminous Mn oxide; thus is persevered in old, highly weathered, acid soils. It typically occurs as a finely crystalline mass (Post, 1999) and Dowding (2007) concluded that lithiophorite dominates the mineralogy of the clay fraction in the highly acidic, wad rich, soils of the humid Graskop area, Mpumalanga.

Todorokite [(Na,Ca,K,Ba,Mn^{2+})$_2Mn_5O_{12}.3H_2O$] is made up of triple chains of edge-sharing MnO_6 octahedra that link up to form 3x3 tunnels (Figure 3c) (Post and Bish, 1988). The tunnels in the middle of the triple chain can accept Na, Ca, K, Ba, Sr and H_2O molecules, whereas the octahedral at the edge of the triple chains are slightly larger, therefore can accommodate for larger cations (Post and Bish, 1988), Mg^{2+} being the most common (Turner, 1982). Dixon (1988) suggests that todorokite will not be expected in highly weathered, acid environments due to the fibrous morphology and influence of magnesium in the formation of the mineral. Post (1999) suggests todorokite is an important phase in Mn coatings and varnishes.

Manganite [γ-MnOOH] has a crystal structure very similar crystal structure to pyrolusite (Figure 3d) (Post, 1999) and is the most common MnOOH polymorph. Pure manganite has never been recorded in wad, but it is common in manganese rich soils. *Groutite* [α-MnOOH] is isostructural to the Fe-oxide goethite (α-FeOOH) and is classified in the same group of Mn polymorphs with manganite but exhibits slightly larger tunnels in the crystal structure than pyrolusite (Figure 3d). Both Fe and Mn are abundant in wad with most of the Fe being present in goethite (Dowding, 2007). It has been suggested by Hawkins & Thompson (1988) that Mn and Fe substitution, particularly in the goethite structure, results in goethite and manganite, or groutite, occurring as an admixture. **Figure 3–3** shows the typical atomic structure of the aforementioned oxides.

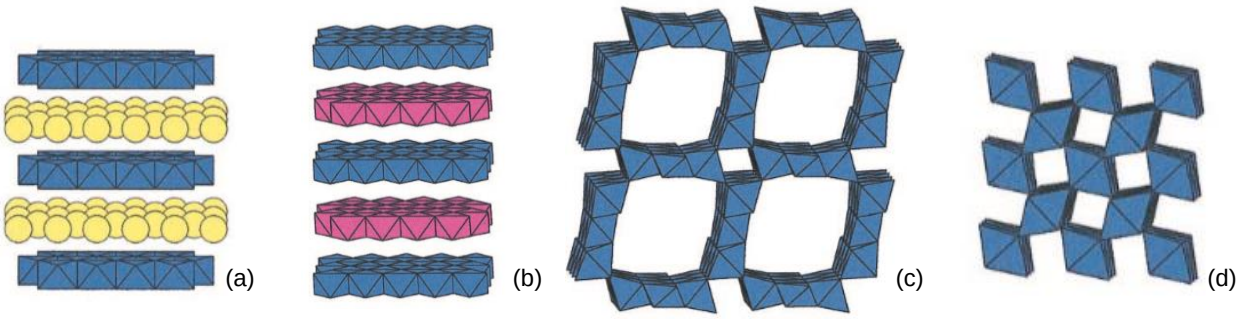

Figure 3–3: Polyhedral representation of the crystal structures of (a) birnessite-like phase showing disordered Na/H_2O sites (yellow) in between the Mn octahedral sheets; (b) lithiophorite exhibiting alternately stacked layers of MnO_6 (blue) and (Al, Li)$(OH)_6$ (red) octahedral, (c) todorokite having large tunnel structure made up by the triple chain structure, (d) pyrolusite made up of single chain structure of edge sharing Mn(IV)O_6 (Adapted from Post, 1999).

The aforementioned oxides usually exist as nanoparticles that exhibit a rod and fibrous structure to an amorphous, irregular sized, mass of particles depending on the element constitutes that make up the oxide (Gotić, et al., 2012). As previously mentioned, Fe and Mn are diadochic and readily substitutes with one another. This substitution causes oxides to alter and morph the crystal lattice. Gotić, et al. (2012) found that mixing Fe^{2+}, whereby

allowing it to substitute in, and modify, a crystal lattice, with a mass of synthesized MnO_2 hollow nanotubes and nanorod particles, the material would form relativity large 3D irregular sized particles with smaller amorphous nanoparticles and nanorod particles absorbed on the larger aggregates' surface. This change in morphology of the larger sized particles may result in the reduction of the large surface area and may affect the water holding capacity of the oxides. However, Borggaard (1983) determined that amorphous Fe-oxide nanoparticles can possess a specific surface area slightly greater than 300 m^2/g, and the nanoparticles material is known for its large surface area (Nguyen et al., 2012).

The influence of amorphous iron hydroxide coatings around clay particles on interparticle relations and water-holding capacity of the soil was intensely investigated by Yong et al. (1992). Yong et al. (1992) found the quantity of amorphous complexes, relative to clay, and composition of it has a direct link to the specific surface area and surface charge that contributes to the water-holding capacity and bonding action of the overall material. The effect of this will further influence the water holding-capacity of the soil. It is clear that the presence of both Mn and Fe have the ability to influence the liquid limits as both can take up relatively large volumes of water.

Difficulty arises in identifying material of this nature, especially when attempting to make use of X-ray powder diffraction (XRD). XRD is used to identify crystalline material by measuring unit cell dimensions and recording intensity of reflected X-rays that are diffracted off the investigated sample. When a large quantity of Fe-ions are present in the soil, an extensive amount of substitution with the Mn-oxides will occur, and change in the environment will cause continuous change in oxidation state of the Mn-oxide, resulting in the crystal structure to morph and the infrared (IR) spectra, or XRD 'peaks' used to identify the minerals, to broaden and shift (Hawkins & Thompson, 1988). Birnessite IR spectra may shift and broaden in X-ray powder patterns due to alterations in the particle size as it possesses a high sorption capacity and can easily accepts foreign elements (>0.5 mole per mole in slightly alkaline conditions). It has CEC of 1.5 of equiv. per 100g at pH 8.3, compared to 0.1 for montmorillonite even though it has a much larger surface area (McKenzie, 1972). Further difficulty is experienced as many of the common Mn-oxides found in wad share similar IR spectra to other common minerals found in soil. Mn-oxides that are commonly mistaken for more common soil minerals are: birnessite for kaolinite, manganite for goethite, and todorokite for common micas and gibbsite (Dowding, 2007).

The combination of XRD, x-ray fluorescence (XRD) and a scanning electron microscope (SEM) is needed to more accurately determine the Mn-oxides present in the soil. Photos

taken under SEM will give in sight to the morphological state of Fe- and Mn-oxides. The presence of the different metal oxides may provide reasons for some of residual dolomite and wad's variable behaviour properties, especially the water holding capacity. Investigating pervious work done on residual dolomite with new information of the chemical components might divulge more understanding of the material. Therefore, the existing data of residual dolomite will be summarised in the next section.

4. Geotechnical testing on residual dolomite

The majority of the research conducted on wad was performed in the 1980s. The material used was generally found in close proximity to chert-poor dolomite formations and has resulted in a good understanding of the behaviour and properties of wad. Since then, very little work has been done on residual dolomite and wad. A comprehensive summary on the known characteristics of wad is given in this chapter.

Day (1981), Wagner (1982) and Buttrick (1986) agree upon the definition that wad is a dark, fine-grained, insoluble material formed from weathering of manganese-rich dolomite and is divided into two groups assessed on the fabric, being structured or laminated and non-structured or massive wad. Day (1981) and Wagner (1982) use the term 'non-structured' to describe wad with no inherent parent structure present that might have been reworked by mechanical processes or compression from overburden that destroys the structure resulting in a powdery wad appearance. Buttrick (1986) uses the terms 'non-structure' or 'massive' to describe wad material with no distinguishing features and defines 'reworked' wad to have been mechanically reworked, destroying the relict structure of the residual massive or laminated wad material, and undergone addition of external impurities. Buttrick (1986) further divides laminated and massive wad, due to secondary features, into fissure or intact wad. Laminations in the wad are primary features and exhibits two-dimensional anisotropic behaviour that influences upper limits of drained and undrained shear strength (Buttrick, 1986). Secondary features further influence the shear strength parameters by producing three-dimensional anisotropic behaviour (Buttrick, 1986). In this document, the terms structured, non-structured, and reworked wad will be used to describe the wad fabric.

When wad is non-reworked, be it structured or non-structured, it typically grades as a clayey silt or silty clay with a low density and high void ratio (Wagener, 1982; De Beer, 1985; Buttrick, 1986; Bester et al., 2017). Roux (1981) recorded wad dry density to be as low as 80 kg/m^3. Although, wad can contain a high amount of sand especially when reworked, which may grade as a sandy clayey silt (Day, 1981; Buttrick, 1986). Jones and Wagener (1981, 1982) reports presented interpreted SEM data of wad material from sites located on the Oaktree Formation and Black Reef Quartzite Formation that indicated the material resembles "rice crispies", having large voids between interlocking grains with not cementing material present. The wad from these investigations have been found to have a void ratio of 0,9 to 11,2 and possess a high permeability (Wagener, 1982). Hawkins et al. (1986) retrieved and analysed wad samples from the Thokozo area on the East Rand. The laminated wad material had a low dry density of 500-600 kg/m^3 (Hawkins et al., 1986). Brink (1979) sample

wad from various sites that included the Black Reef Formation and the Oaktree Formation, and found the average void ratio of 3,9 and a maximum of 9,6 in fissured wad and an average specific gravity of 3,2. Bester et al., (2017) wrote a comprehensive summary of the research done on the properties of wad on the chert free Oaktree formation.

The author interpreted the published Jones and Wagener (1981, 1982) reports from site investigations conducted on the Farm Rooihuiskraal in Centurion and a review report from Bear Geoconsultants' (2016) of an investigation on Monavoni Extension 11. These investigations were done on the Oaktree formation; this allows for the wad to be evaluated using conventional soil mechanics tests (Bester et al., 2017). Chert poor wad of the Oaktree formation exhibits similar properties of a firm clayey silt or silty clay while having a low density and average clay content of 41% (Bester et al., 2017). Bester et al. (2017) state that wad is not a highly dispersive soil, this agrees with Buttrick's (1986) statement of wad being non-dispersive but erodible. The accuracy of dispersive tests is questioned when dealing with a unique soil such as wad as different tests, be it crumb test or pinhole test, yield different results (Maharaj, 2013).

Buttrick (1986) presents the most recent detailed research on the geotechnical properties of wad. This work emphasises the importance of macroscale structural division as well as that of the fabric description of wad material, highlighting that wad possess both poor and positive behavioural characteristics, which is influenced by the environment and compositional features. Day (1981) states structure is essential when assessing wad compressibility as it influences the compressibility more than any other factor. Brink (1979) and De Beer (1985) indicate that wad is regarded as an extremely compressible material and exhibits low strength. Beukes et al. (1999) found that the bedding of the dolomite is preserved in the residuum, however the material experienced 60% to 70% compaction during the transformation from dolomite to wad. The shear strength of wad has no correlation to the dry density of the material (Wagener, 1982).

Buttrick (1986) concluded that structured wad possesses more than double the average void ratio value than non-structured wad. The high void ratio values, usually greater than one, highest value being 16,6, are due to the leaching process that forms the residual soil, the inherent structure of the parent rock and the volume that the residual soil occupies (Buttrick, 1986). The volume occupied by the parent rock and soil is the same after leaching resulting in a high porosity and low permeability soil (Buttrick, 1986). The natural moisture content usually exceeds the liquid limit (Buttrick, 1986; Wagener, 1982; De Beer, 1985; Brink, 1979). The intact structured wad typically has low to very low permeability and the massive wad a

low permeability, values for both types are generally in the order of 10^{-7}m/s. Thus, the water percolating through the wad material cannot reach the required seepage for piping or erosion to occur, therefore making it hydrodynamically stable (Buttrick, 1986). Wagener (1982) and Day (1981) found that the wad structure breaks down because of high pore pressures or shock loading that liquefies the material. The reworking process will generally increase the permeability as well as allow the material to be more readily and easily eroded away (Buttrick, 1986).

Buttrick (1986) theorised the high liquid and plastic limits as well as the high-water holding capacity exhibited by certain wad materials is related to the porous nature and the high specific surface area of the fine-grained material allowing for large quantities of hydroscopic water in the material. However, some grading analyses show low clay content for the high plastic limit material. The dispersant agent used in the grading analysis may not function accordingly, thus leaving the clay particles as flocculated clusters greater than 2 microns, resulting in a misleading low clay content value (Buttrick, 1986). The high liquid limits and water holding capacity may also result from adsorption of water onto metal (Fe and Mn) oxide surfaces rather than the fine material (Bear Geoconsultants, 2016). Buttrick (1986) recommended further research on geomechanical properties of remoulded and reworked wad samples, bearing in mind the extent of reworking, and that liquefaction of wad needs to be better understood as well as the geochemical makeup of material that is intact or non-reworked. **Table 4–1** and **Table 4–2** provides a summary of the properties of wad from tests conducted by various authors.

Table 4-1: Summarized results from testing previously performed on wad

Author / Report	Fabric	Grading (%)				Dry density (kg/m^3)	Dispersiveness	PI (%)	LL (%)	e	SG (g/cm^3)	Permeability (m/s)
		Clay	Silt	Sand	Gravel							
Brink (1979)	-	<29	-	-	-	285 - 722	-	5-28	47-96	2,7-9,6	1,63-3,47	-
Day (1981)	Structured or Intact and; non-structured or Reworked	30	50	22	-	225 - 1327	-	14-27	61-125	-	-	-
		Clayey silt to silty clay										
Jones and Wagener (1981)	-	29	49	21	1	225 - 1327	-	10-29	61-125	1,1-11,2	2,9	-
		Clayey silt										
Jones and Wagener (1982)	-	Clayey silt to sandy silt				253 - 1481	-	15-23	40-135	-	-	-
Wagener (1982)	Intact (structured)	Clayey silt				225 - 1481	Not dispersive	-	-	0,9-11,2	-	High
	Powdery (non-structured)											
De Beer (1985)	-	11-60	-	-	-	273 - 1558	-	5-27	49-126	0,3-8,9	-	-
		Clayey silt										
Hawkins et al. (1986)	Laminated	-				500 - 600	-	18	71	-	-	-
Buttrick (1986)	Laminated or Structured	48	-	-	-	220 - 1221	Not to slightly dispersive	3-26	28-113	1,3-16,6	2,2-3,1	Very low to intermediate
		Clayey silt to sandy silty clay										
	Massive or Non-Structured	Sandy clayey silt				406 - 1516		11-27	27-136	0,9- 6,2	1,94-3,0	Very low to low
Bear Geoconsultants (2016)	"pure" wad (Non-structured or Structured)	-				576 - 1075	Not dispersive	10-40	57-93	2-12	-	$1,5x10^{-6}$ - $1,2x10^{-8}$
PI - Plasticity Index; LL - Liquid Limit; e - void ratio; SG - specific gravity												

Table 4-2: Summarized results from testing previously performed on wad

Author / Report	Fabric	Grading (%)				Dry density (kg/m^3)	Triaxial			
		Clay	Silt	Sand	Gravel		Structured	Non-Structured	Reworked	Not Specified
Brink (1979)	-	<29	-	-	-	285 - 722	-	-	-	-
Day (1981)	Structured or Intact and; non-structured or Reworked	30 Clayey silt to silty clay	50	22	-	225 - 1327	ϕ' = 22° c' = 55 kPa ϕ = 18° c = 59 kPa	-	-	-
Jones and Wagener (1981)	-	29 Clayey silt	49	21	1	225 - 1327	ϕ' = 24,1° - 25,4° c' = 23 - 51 kPa ϕ = 17,1 - 18,6° c = 30 - 48 kPa	-	ϕ' = 20,9° c' = 63 kPa ϕ = 14,7° c = 74 kPa	ϕ' = 17,1° c' = 40 kPa ϕ = 17,1° c = 48 kPa
Jones and Wagener (1982)	-	Clayey silt to sandy silt				253 - 1481	-	-	-	-
Wagener (1982)	Intact (structured) Powdery (non-structured)	Clayey silt				225 - 1481	-	-	-	-
De Beer (1985)	-	11 - 60 Clayey silt	-	-	-	273 - 1558	-	-	-	ϕ = 26° c = 40 kPa
Hawkins et al. (1986)	Laminated	-				500 - 600	-	-	-	-
Buttrick (1986)	Laminated or Structured	48 Clayey silt to sandy silty clay	-	-	-	220 - 1221	ϕ' = 21° - 25° c' = 23 - 63 kPa ϕ = 15° - 19,3° c = 26 - 74 kPa	ϕ' = 23° - 29° c' = 4,0 - 53 kPa ϕ = 21,5° - 33,3° c = 1,0 - 65 kPa	-	-
	Massive or Non-Structured	Sandy clayey silt				406 - 1516				
Bear Geoconsultants (2016)	"pure" wad (Non-structured or Structured)	-				576 - 1075	-	-	-	ϕ = 16,9° - 28° c = 20 - 61 kPa

5. Materials and Methods

This section will elaborate on the successfully retrieved samples, the locality of the samples and described the tests conducted on the samples. The samples condition ranges from highly reworked wad to slightly to non-reworked, non-structured wad and non-reworked, structured wad, all located within the Malmani Subgroup, of the Chuniespoort Group, found in the Transvaal Basin of the Transvaal Supergroup. The samples were retrieved in accessible areas such as roadcuts and open excavations with the coordination of farmers, consultants and active mining corporations. Determination was placed in spreading the sample localities across the eastern and western Transvaal limbs and the area south of Pretoria. **Table 5–1** provides a summary of the samples successfully retrieved and tested for this dissertation. The sample localities will be split into three regions and individually described. The methodology of tests conducted on the samples will be elucidated thereafter.

Table 5–1: Summary of sample type and location.

Sample Name	Fabric	Sample type	General locality	Province
Highveld	Structured	Block	Excavation south of Pretoria	Gauteng
R533	Non-structured	Disturbed	Road cut near Pilgrim's Rest	Mpumalanga
Doornhoek	Non-structured	Shelby	Old mine south of Zeerust	North West
Sudwala Caves	Slightly reworked	Disturbed	Excavation at Sudwala caves	Mpumalanga
Mooiplaas	Reworked	Shelby	Active mine near Laudium	Gauteng
Bokkraal	Reworked	Shelby	Old mine south of Zeerust	North West
Carletonville	Reworked	Block	Sinkhole at Khutsong	Gauteng
South Downs	Reworked	Disturbed	Sinkhole at South Downs	Gauteng

5.1. Sample localities

Figure 5–2 shows location of samples retrieved, denoted by yellow and orange dots. The yellow dots represent a single sample taken with the name given to sample. The orange dot symbolises multiple samples taken in the area south of Pretoria. An extract of the 1:50 000 2328 CC Lyttleton geological sheet expands on the exact location of the sample points in **Figure 5–1.** The regions will be split into western and eastern limbs and the area south of Pretoria.

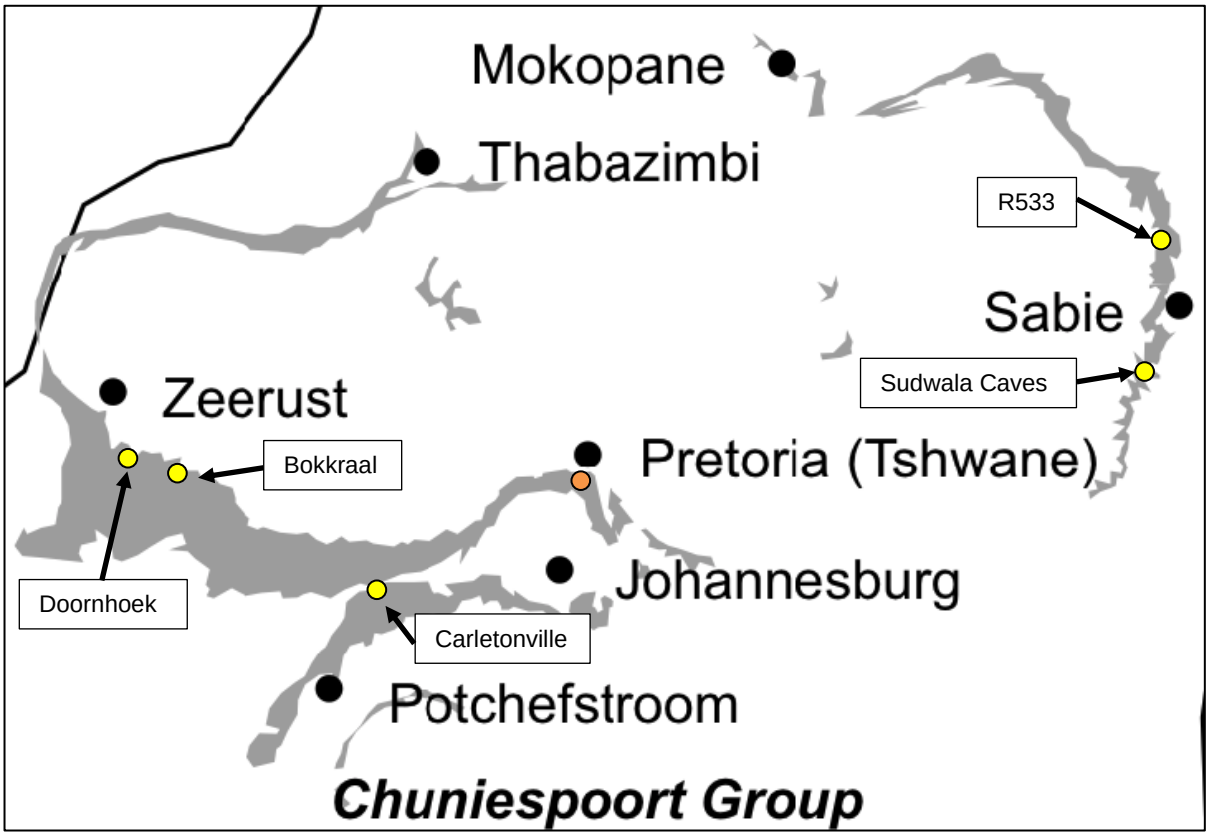

Figure 5–2: Sample locality positions placed on extract of Chuniespoort Group dolomites found in the Transvaal Basin (Adapted and taken from Dippenaar et al., 2018; adapted from Eriksson et al., 2006).

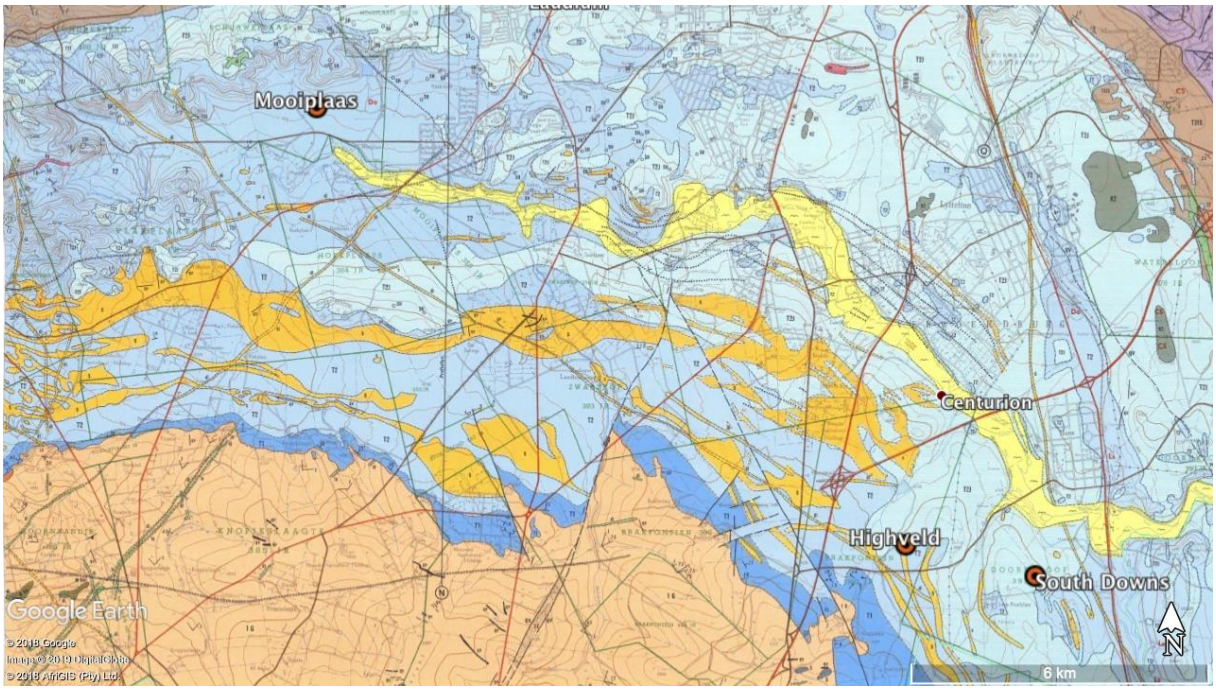

Figure 5–1: Cropped section of the 1:50 000 Lyttleton 2528 CC geological sheet showing sample localities in the area south of Pretoria.

Western Limb

The area to the south and southeast of Zeerust has a Weinert N-value of between 5 and 4 and the Khutsong area falls into a N-Value of between 4 and 3 (Weinert, 1980). This sample area is the driest area with the lowest rainfall of all sample areas, though chemical weathering is still expected to be prominent in the areas of Doornhoek, Bokkraal and Khutsong (Weinert, 1980). The Doornhoek and Bokkraal dolomites have both been exposed due to presence of drainage channels that eroded above Pretoria Group sediments. The sample locations exist in previously excavated material in the valley face of the drainage channels.

The Khutsong area, north west of Carletonville, dolomites were exposed due to a sinkhole that formed from ingress water. The dolomites exhibited numerous chert bands and lineation's. The dolomites are believed to be part of the Eccles Formation. The saprolite was mainly comprised of reddish brown, loose to medium dense, gravelly sandy silt, with pockets of dark brown to black loose, gravelly sandy silt. The material can be characterised as reworked wad to silty chert gravel residuum. Disturbed samples were taken, and block samples were cut out from the sinkhole's slip face at approximately 3 to 4 mbgl (**Figure 5–3**).

Hammerbeck (1976) states that the upper series of the Malmani Subgroup SSW of Zeerust outcrop on the farms Bokkraal 344 JP and Doornhoek 305 JP. The shales and quartzites of the Pretoria Group overlie the dolomite on these farms. Thus, it can be deduced the dolomite rocks on these farms are part of the Frisco Formation, this corresponds with the 1:250 000 2526 Rustenburg Geological sheet. The Frisco Formation consists of chert free dark grey dolomite (Obbes, 1995). The samples at these localities were retrieved from open and underground excavations associated with previous mining activities as the material possessed ore stringers in the form of a lead sulphide named Galena (PbS) (**Figure 5–5** and **Figure 5–5**). Shelby samples and a block sample were obtained from two different localities on the Bokkraal Lead Mine. The block sample and two Shelby samples were retrieved from a wall face in an underground mine shaft approximately 15 metres below ground level (mbgl), and three Shelby samples from a road-cut on the Bokkraal farm. The road-cut face consisted of dark reddish brown, sandy clay, highly reworked wad, all tests were performed on this material. One Shelby tube sample was retrieved at Doornhoek from a fresh excavated face at a depth of 4 to 5 mbgl. The material was described as dark purple-blue, streaked orange and green, stiff, open structured, fine sandy silt and appeared to be slightly reworked non-structured wad.

Figure 5–3: Khutsong block sample taken off dolomite pinnacle in sinkhole.

Figure 5–4: Entrance to old underground mine at Bokkraal.

Figure 5–5: Old mine excavation at Doornhoek.

Eastern Limb

The eastern escarpment receives the most rainfall and it exhibits the wettest conditions of all the sample areas. The Weiner N-Value of Sudwala caves and Pilgrim's Rest area is N<2, implying intense chemical weathering (Weinert, 1980). Sudwala Caves is located at the lower bound, and Pilgrim's Rest near the upper bound, of the Malmani Subgroup as per the 1:250 000 2430 Pilgrim's Rest and 2530 Barberton Geological sheets. The area is mountainous with numerous steep valley sides and deep valley bottoms.

Sudwala caves exhibit chert-rich dolomites and is believed to be part of the Monte Christo Formation. The disturbed sample material was successfully retrieved from an existing excavation face, located near the crest of a hill, that comprised of black brown mottled, speckled and streaked white and orange, stiff to very stiff, blocky and fissured, clayey silt with minor chert gravel (**Figure 5–6**). The material would characterise as reworked to non-structured wad in places. The material was too stiff and contained variable amounts of coarse gravel, which made it difficult to retrieve a Shelby sample.

Figure 5–6: Excavation face at Sudwala caves.

R533 sample was retrieved in a road cut roughly 1.30 km northwest of Pilgrim's Rest on the R533 road. A disturbed sample was retrieved from a hand dug excavation with a profile that can be described as dark brown to black, stiff, blocky, clayey silt (**Figure 5–7**). The sample was recovered very close to a dolomite outcrop that exhibited very little chert. The material is believed to have leached from chert-poor dolomites of the Frisco Formation.

Figure 5–7: R533 sample position in roadcut.

South of Pretoria

The area south of Pretoria has a Weinert N-value of between 3 and 2, indicating that decomposition will be the dominate weathering process (Weinert, 1980). The area is generally flat lying with undulating shallow gradient topography. Three samples were retrieved with the coordination of consultants and an active mining cooperation.

Roux (1981) suggests the chert rich Eccles Formation underlies the township of Laudium and the surrounding area. The PPC Aggregates Mooiplaas Dolomite Mine immediately west of Laudium is in close proximity to the contact between the Lyttleton and Eccles Formation. The material retrieved is believed to be taken from a gryke between dolomite pinnacles of the Lyttleton Formation at a depth of 2 mbgl (**Figure 5–8**). The surrounding area was generally flat with a gentle slope downhill from a chert ridge to the north.

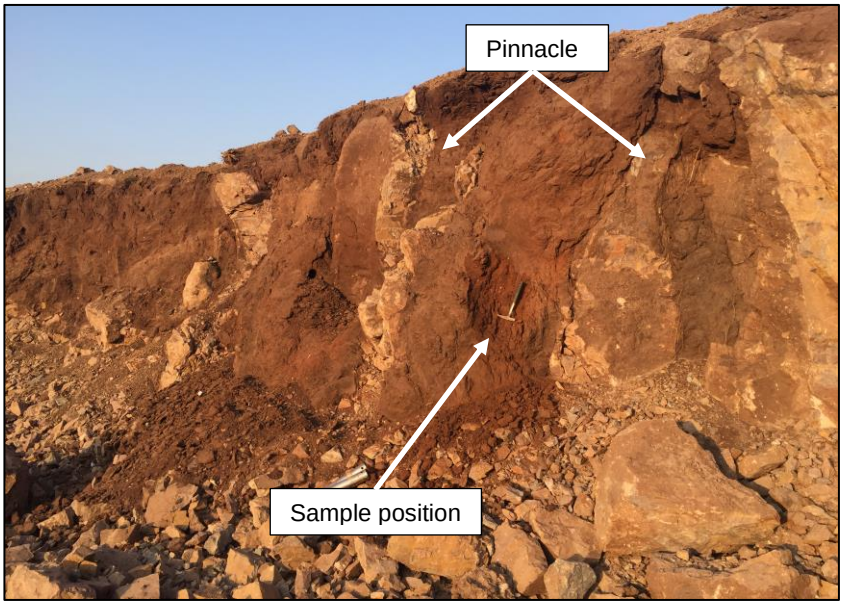

Figure 5–8: Mooiplaas sample position between two pinnacles.

Bester et al. (2017) conducted a review of a dolomite site investigation near Eco-Park Estate, Centurion, which concentrated on the properties possessed by the very dark chert free wad of the Oaktree Formation found in the area. The Highveld sample was provided by Bear Geoconsultants and formed from leaching of Oaktree dolomite into a typical purple black, stiff, indurated, highly voided with relict structure, clayey silt, structured wad (**Figure 5–9**).

Figure 5–9: Example of Highveld sample.

A sinkhole formed in the South Downs area and, according to Trollip (2006), this area is underlain by the chert-rich Monte Cristo Formation. The dolomites present on site were chert

rich and the subsurface soil profile varied with pockets of stiff to very stiff clayey silts with chert sand and gravel at distance from the sinkhole, and in close proximity to the throat of the sinkhole, the material was black to dark brown, loose, open structured, silty sand with minor gravel. Disturbed sample material was retrieved from the area in the vicinity of the throat of the sinkhole at approximately 3 to 4 mbgl (**Figure 5–10**). The material was too powdery and loose to successfully retrieve an undisturbed block sample.

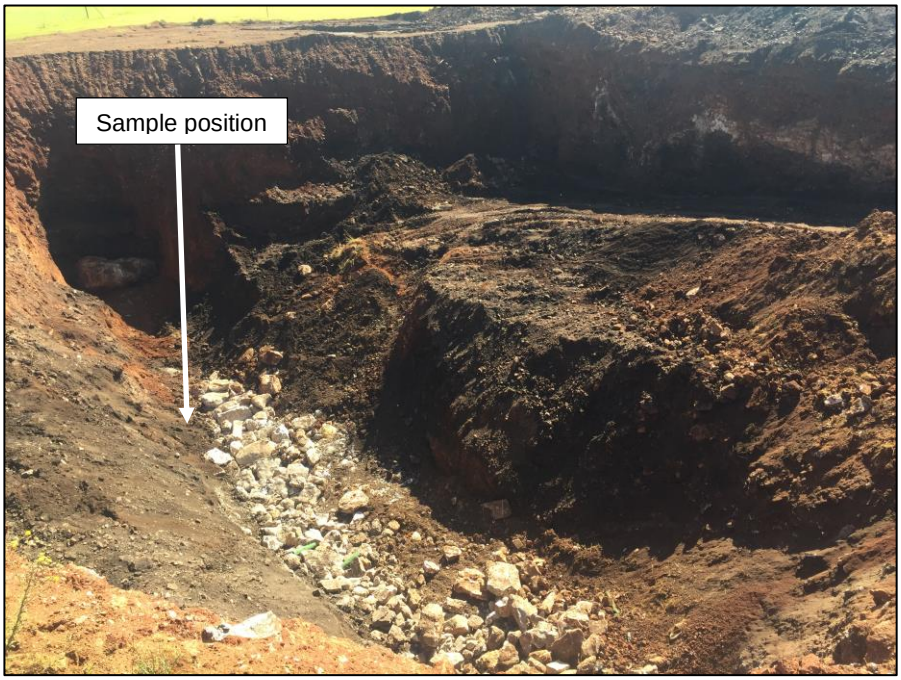

Figure 5–10: South Downs sample locality in sinkhole during rehabilitation.

5.2. Testing Methodology

Five undisturbed, Shelby or block samples, and eight disturbed samples at each locality, were taken from accessible areas at various excavations, sinkholes, road cuts, and abandoned and active mines. The vast sampling area allows for comparing structured, non-structured and reworked wad as well as material from slightly different climates and environments.

The major objective of this project was to evaluate the hydromechanical properties of wad in relation to the geochemical makeup, grading and microstructure of the wad formed from the different dolomite formations found in the Malmani Subgroup. **Table 5–2** provides a summary of tests conducted on the samples. The methodology of each test is explained in this chapter.

Table 5–2: Summary of tests conducted on the various samples.

Sample Name	Test							
	Triaxial	Dispersion	XRD / XRF	FI	Microscopy	SEM	Columns	SWRC
Highveld		•	•	•	•	•	•	•
Sudwala Caves		•	•	•	•	•	•	•
R533		•	•	•	•	•	•	•
Doornhoek	•	•	•	•	•	•	•	•
Mooiplaas	•	•	•	•	•	•	•	
Bokkraal	•	•	•	•	•	•	•	
Carletonville		•	•	•	•		•	
South Downs		•	•	•	•	•	•	

FI - Foundation Indicator

5.2.1. Triaxial test

60mm diameter thin wall Shelby tubes were pushed into various soil faces and excavations by hand to retrieve the undisturbed Bokkraal, Mooiplaas and Doornhoek wad samples. The Shelby tube samples were carefully extruded and cut into 50mm diameter and roughly 100mm to 150mm high cylindrical samples at the University of Pretoria Civil Engineering Laboratory. The ASTM D4767 report is the standard used for the triaxial tests. The samples were encased in a thin rubber sheath with porous disks on either end and placed into the triaxial cell and secured by two rigid plates. The cell was then filled with water, and the fluid exerted a hydrostatic static compressive stress around the sample. Mooiplaas-A, Mooiplaas-B and Mooiplaas-C samples underwent consolidated-undrained (CU) triaxial tests at 50kPa, 100kPa and 200kPa confining pressure respectively, and each was sheared at a rate of 0,01 mm/min after being consolidated at 100kPa isotropic confinement. Side drains were placed on the Mooiplaas-A sample whereas the rest of the samples had no side drains. CU tests were done to better understand the stress path and behaviour of the material by recording the pore water pressure readings during the application of the deviator stress. Three triaxial consolidation and permeability tests were conducted on the Mooiplaas-D, Bokkraal and Doornhoek samples at 100kPa confining pressure.

5.2.2. Crumb test

The crumb test is used to assess disperstivity of a soil. The procedure is described in Maharaj (2013) and was used due to its simplicity and reliability for unique soils. Undisturbed

'crumbs', 40mm in diameter, were taken from each sampling locality and each one was dropped gently into a jar of distilled water as not to disturb the water. Readings were taken at 10 minutes, 1 hour and 2 hours to confirm if the material was either dispersive or non-dispersive.

5.2.3. XRF and XRD

The geochemical make-up of the Bokkraal, Mooiplaas and Doornhoek samples were determined at the University of Pretoria and the Carletonville, Highveld, R533, Sudwala Caves and South Downs samples at UIS Analytical Services in Centurion. The samples from each locality were milled and prepared in the lab. The former XRF samples were analysed using the ARL Perform'X Sequential, and the latter using the ARL ADVANT'X Series, XRF instruments and Quantas software. The XRD samples were prepared according to the standardized Panalytical back loading system, which provides nearly random distribution of the particles. The samples were analysed using a PANalytical X'Pert Pro powder diffractometer in θ–θ configuration with an X'Celerator detector and variable divergence- and fixed receiving slits with Fe filtered Co-Kα radiation (λ=1.789Å). The phases were identified using X'Pert Highscore plus software. The relative phase amounts (weight%) were estimated using the Rietveld method.

5.2.4. Foundation indicators

Eight disturbed samples were sent to BM du Plessis Civil Engineering Labs for Foundation Indicator tests that include grading and Atterberg limits analyses following SANS3001 series as the standard proceed. Cone penetrometer test method, following the procedure stated in the BS: Part2: 1990, was used to determine the liquid limit of the wad.

5.2.5. Stereomicroscope

A stereomicroscope is an optical microscope (model: Zeiss Stereo Discovery V20) designed for low magnification for observation of a sample's microstructure, typically using reflected light from the surface. Undisturbed wad samples and samples post shearing and consolidation were analysed at x20, x34, x45, x70, x94 magnification and photographs of the most representative sections of the samples were taken at these magnifications.

5.2.6. Scanning Electron Microscope

The morphology of undisturbed samples was observed using a Zeiss Gemini SEM under different magnifications best suited for the material. The SEM scans the material surface with the use of a focused beam of electrons, producing an image revealing the surface topography. Investigating the microscopic structure of the soil grain may build an

understanding as to where certain minerals are present and to better establish the governing factors of the high and variable liquid limits.

5.2.7. Columns

The Perspex columns were used for two different tests, namely relative hydraulic conductivity (K) and erosion test. The relative K tests were done to determine the typical flow rate of the material in a partial saturated state and compare results of each material. The erosion tests were performed to establish what parameters are needed for the material to mobilise, what usually erodes out and to compare the material's mobilisation potential to one another.

The test set up comprises of a 450 mm high Perspex pipe with a diameter of 60 mm. The pipe is fixed on a Perspex plate and sealed, using Sikaflex Crystal Clear, to make the connection water tight at the bottom and the top of the pipe is left open. The plate has a 2 mm in diameter hole in the centre of it that allows liquid and fine material to flow through without disruption. The material that flows out is caught in a beaker placed under the column. The basic set up is shown in **Figure 5–11**.

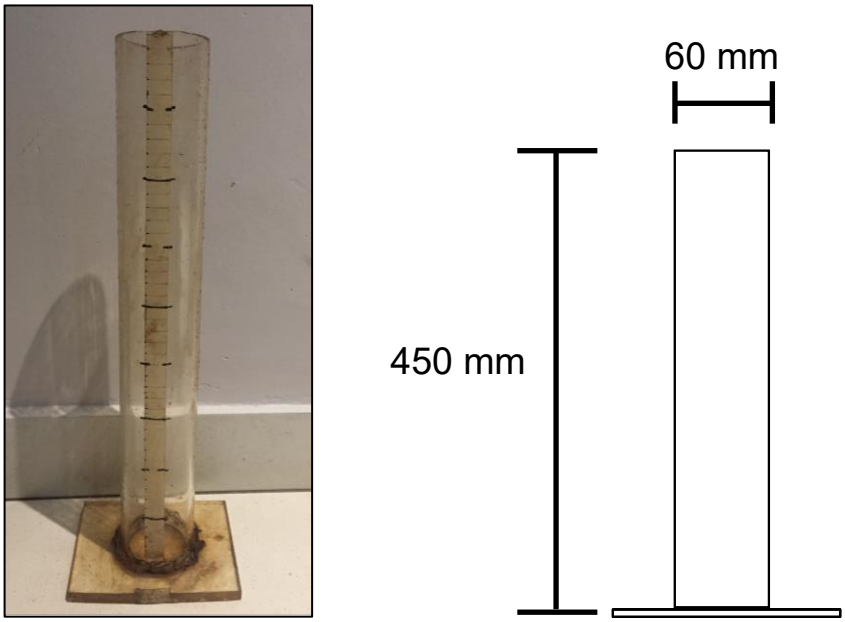

Figure 5–11: Photograph and diagram showing basic column set up.

Falling head tests were conducted on several samples in order to establish the relative K, or permeability, of the soil. Disturbed fine-grained samples were packed in the Perspex column, sandwiched between two coarse-grained, 30 mm in length, quartz filters. The coarse quartz filters are used to ensure material is not entrained when water is introduced from above and will not inhibit flow. After placing the sample between the filters, the column is gently tapped to achieve denser packing. The samples averaged in length between 130 mm and 165 mm,

with a diameter of 60 mm. The initial stage entails introducing an influx of water large enough to create a significant head, which is allowed to flow through the sample with the intent of creating uniform conditions, partial consolidation and partial saturation throughout the length of the sample. The height of the soil column is recorded before and after initial water influx to establish if consolidation took place. Once all the initial gravitational water has drained, the test is started by adding water, increasing the head to that of the initial water influx, and allowing the water to drain through the material. The drop-in head is measured every 15 minutes until all the gravitational water has flowed through. The drop-in head is placed against time to ensure steady state has been reached and to determine the hydraulic conductivity of the remoulded material. The material height in the column is once again measured and the weight of the material after test, and before and after drying, is taken to get an indication of the moisture content of the material during the test. The basic set up is shown in **Figure 5–12.**

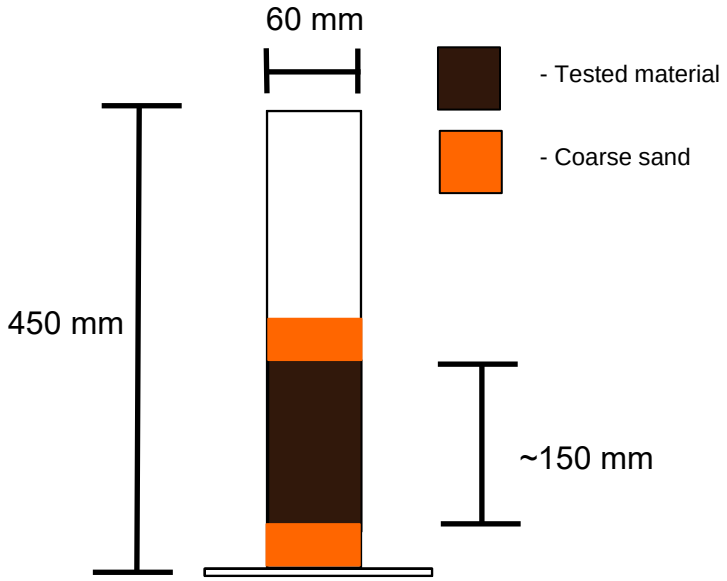

Figure 5–12: Basic schematic showing the K test set up.

The erosion tests were conducted to determine the mobilization behaviour of the material. Disturbed samples were placed in the column without any filter at the bottom of the column. The column used had a 4mm x 2mm slot opening at the bottom. This will allow material to freely move out of the column when the mobilization criteria are met. The sample material was placed to a height of 10 mm in the column followed by a quartz filter placed above the material, to ensure material was not entertain when water was poured into the column. The test comprised of five (5) different scenarios of hydraulic head increases, namely (1) Initial, followed by an immediate (2) rapid head increase and (3) slow head increase, succeeded by a dry out period, a (4) raid head increase, seconded dry out period and final (5) slow head increase.

A relatively large head was introduced into the column and the initial behaviour of the wetting front was recorded and the mobilization of the material out of the column was noted. Immediately after all the free water has flowed out, a new pressure head was rapidly placed in the column and the material behaviour was recorded again until all the free water has once again flowed out. Immediately after the second influx of free water had flowed out, a new pressure head, of the same magnitude as the pervious stage, was introduced into the column at a gradual rate of increasing head. This allows for the comparison of behaviour under different rates of head increase for the material. The material was then left to 'dry out' without any influx of water for 12 hours. Once the column material 'dried out', the rapidly increased pressure head procedure was repeated, and the material was once again left for 12 hours. The final influx of water was introduced at a very slow rate to a pressure head equal to the same height as pervious and the behaviour was once again recorded. The basic set up of the erosion test is shown in **Figure 5–13.**

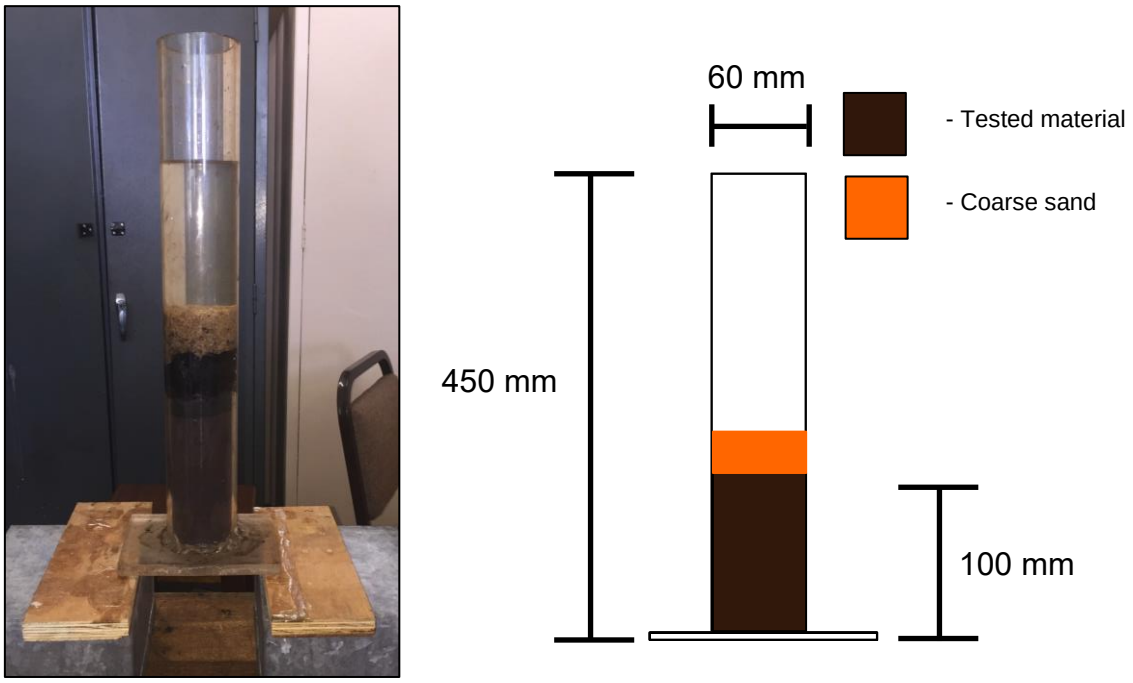

Figure 5–13: Photograph of test underway and basic diagram showing erosion test set up.

The gravitational water and material mobilised was caught by a beaker placed under the column. The beaker was precessed in order to entrain the insoluble particles that mobilised out of the column during testing and a photograph was taken to visually compare samples from the different scenarios of the same material. The water, along with the insoluble mobilised material, was sieved through filter paper. The mobilised material was gathered by the filter paper as the water passed through. The filter paper was placed in an oven set at 105°C to ensure all moisture is removed from the filter paper and mobilised material. The

mass of the mobilised material was determined by recording the weight of the filter paper before the sieve process and after the drying out oven process.

5.2.8. Specific gravity

The specific gravity of each sample was obtained by relating the weight of oven dry soil to the weight of water as stipulated by the ASTM D5550-14 using Micromeritics AccuPyc II 1340 Pycnometer. This method uses Helium gas to create a vacuum to measure the particle density.

5.2.9. Soil water retention curves

The pore pressure tensiometers (PPT), as described by Jacobsz (2018), were used to record the suction pressures in the sample material during a drying cycle from saturation up to, and including, the point of cavitation in the PPT. The full description of the tensiometers design, preparation and set up before and during the test is explained in Jacobsz (2018) and Toker et al. (2004).

The PPTs were dried for 4 hours at 60° C to ensure zero moisture in the ceramic disk. The PPTs were then saturated in deaired water under pressure in a modified triaxial. The calibration process, as stated in Jacobsz (2018), was done in the triaxial whilst the PPTs were connected to a data logger (**Figure 5–14**). Once the PPTs were saturated and the calibration data had been recorded, the PPTs were removed from the triaxial and placed into the prepared saturated sample.

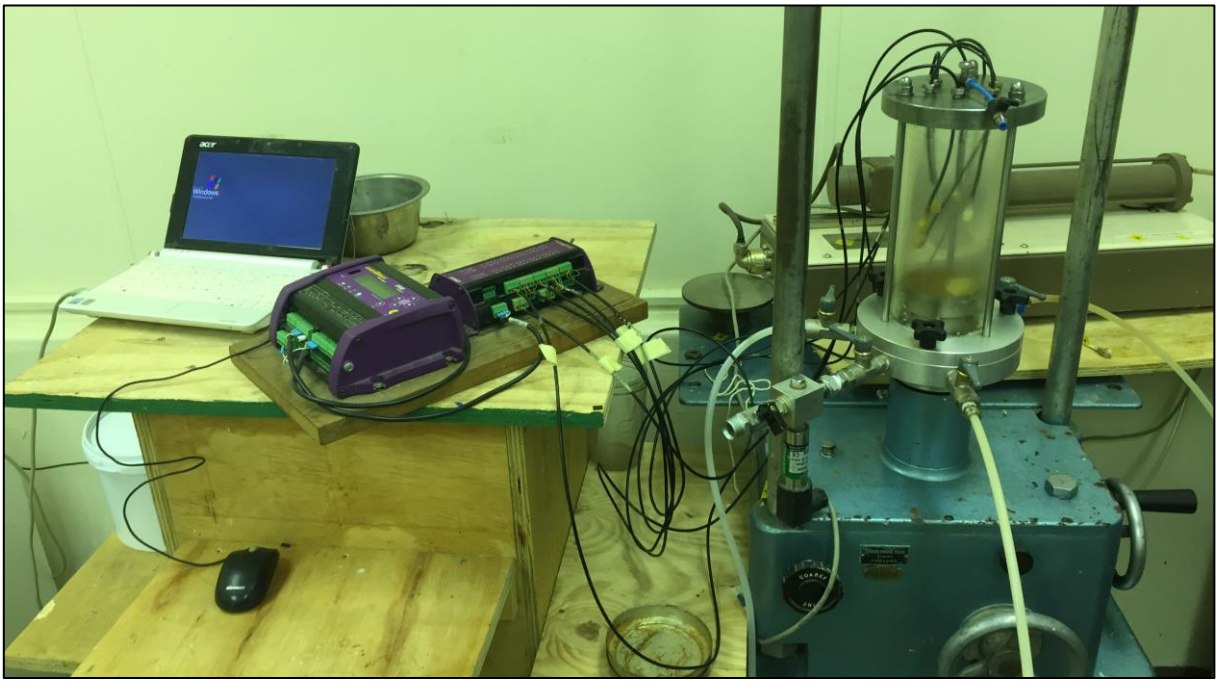

Figure 5–14: Triaxial and datalogger set up during saturation and calibration of tensiometers.

The samples were prepared to a workable dimension and saturated. The sample was placed in a 75 mm diameter and 25 mm high cylinder, packed to desired density if remoulded, or cut out from block sample or Shelby tube to said dimensions. The sample was weighed, and the bottom of the sample was placed into a container with deaired water. The sample was allowed to saturate from the bottom up to ensure all air bubbles vacated the sample pore spaces. Once the sample was saturated, it was weighed and the residue water in the container was removed and container was dried. The prepared sample was placed on a digital scale inside a control box (**Figure 5–16**). The control box was used to ensure similar test conditions for all samples.

A small opening was gently cut into the sample that housed the two tensiometers during the test. The tensiometers were suspended above the sample and fed through a small opening to the data logger. The control box was closed with one fluorescent lamp that stayed on for the duration of the test. The data acquisition was set to record every second for the first 30 and then adjusted to record every 180 seconds thereafter. The same recording schedule was set for the digital scale that takes weight readings during the test.

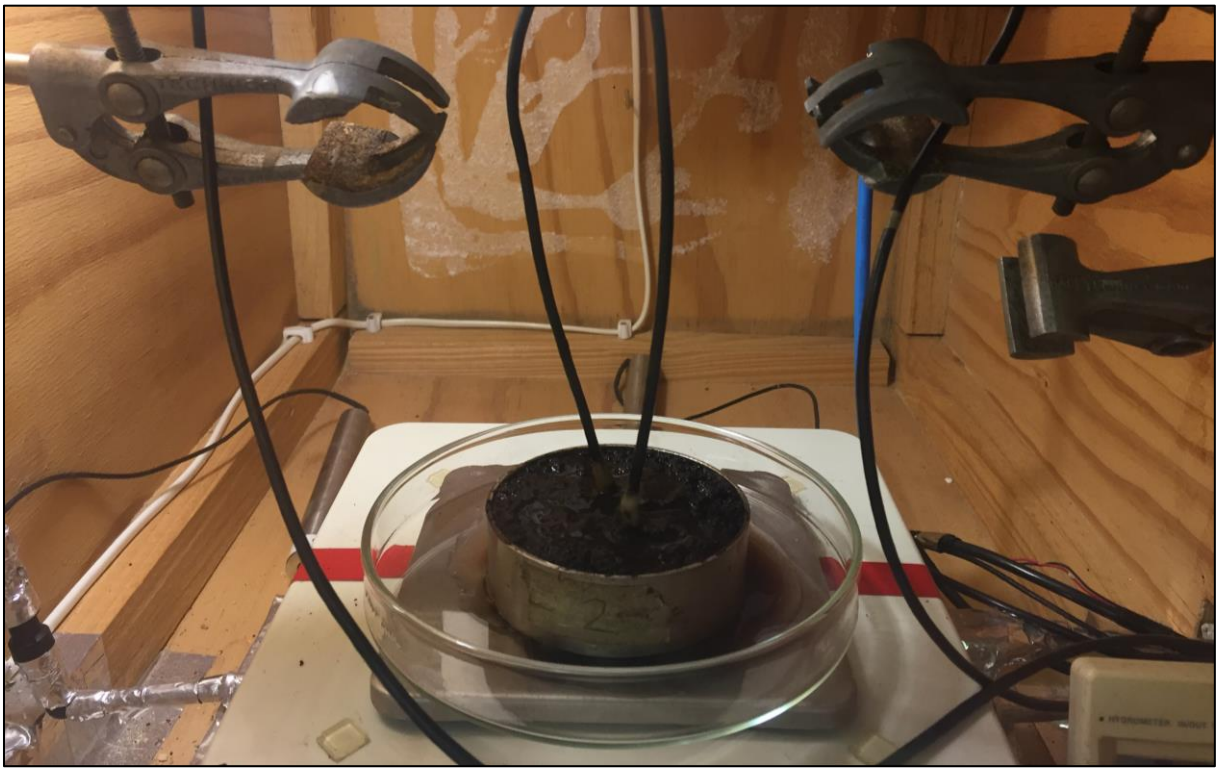

Figure 5–15: Tensiometers placed into saturated sample housed in cylinder placed in container on top of digital scale.

The suction recordings were inspected until cavitation of the PPTs occurred, as shown in Jacobsz (2018), this symbolised the end of the test. The sample was removed, weighed and placed in an oven, set at 105° C, to dry and weighed again after 12 hours. The data gathered during the test were processed and the Soil Water Retention Curve (SWRC) was produced.

The objective of the SWRCs were to determine the effect on suctions of the structured fabric compared to suctions of the same material with the structure broken down, as well as, the effect of packing the test specimens at different densities were tested. Difficulty was expected in accomplishing accurate dimension readings, and ensuring correct moisture content calculations, of the samples that would shift the curves along the x-axis. The curves were adjusted to fit the section of the curves that are known to be at full saturation (vertical line / increase in suctions with no change in saturation) to the correct position on the x-axis.

6. Results

The sampled material was handled with care during sampling, transporting and preparation procedures before testing. However, disturbance of the samples may have occurred to some extent, leading to variations of the results. This chapter will provide results and limited interpretation of the individual tests successfully conducted on the sample material. The raw and interpreted data not shown in this chapter is attached as **Appendix A**.

6.1. Triaxial test

Triaxial consolidation and triaxial permeability tests were conducted on the Doornhoek wad and Bokkraal road-cut wad samples. The Mooiplaas samples were successfully extruded, placed into the cell and underwent CU triaxial testing, each at different confining pressures as previously stated, as well as triaxial permeability tests. The samples' stress-strain relationships follow the idealised elastic-strain softening plastic model, which indicates a reduction in strength after failure as strain increases, as shown in **Figure 6–1** (Knappett and Craig, 2012). **Figure 6-2** demonstrates that the Mooiplaas samples behaved as normally consolidated fine-grained soil and **Figure 6-3** gives the effective stress path of the material that contracted during shearing. The triaxial test results are summarised in **Table 6–1**. The consolidation and stress-strain graphs and Mohr Circle of the Mooiplaas wad are in **Appendix A**.

Stress-strain relationship of Mooiplaas-A

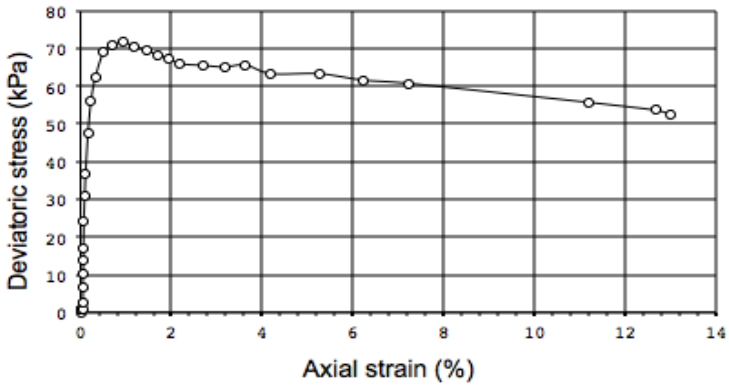

Figure 6–1: Stress-strain graph of Mooiplaas-A shows sample underwent strain softening post failure.

Excess pore pressure vs. axial strain plot of Mooiplaas-A

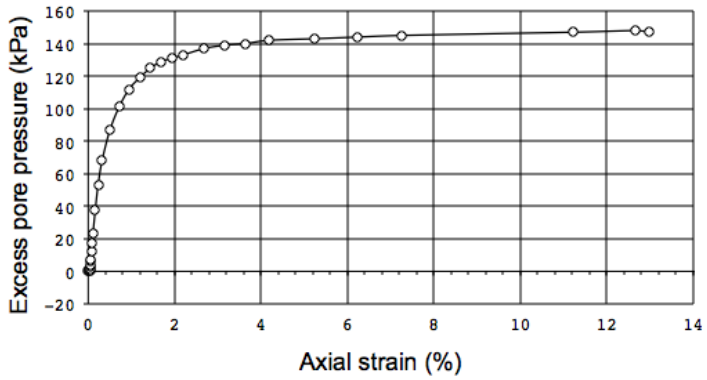

Figure 6–2: Pore pressure – strain relation shows the material contracted and behaved as normally consolidated clay.

Effective stress path of Mooiplaas sample

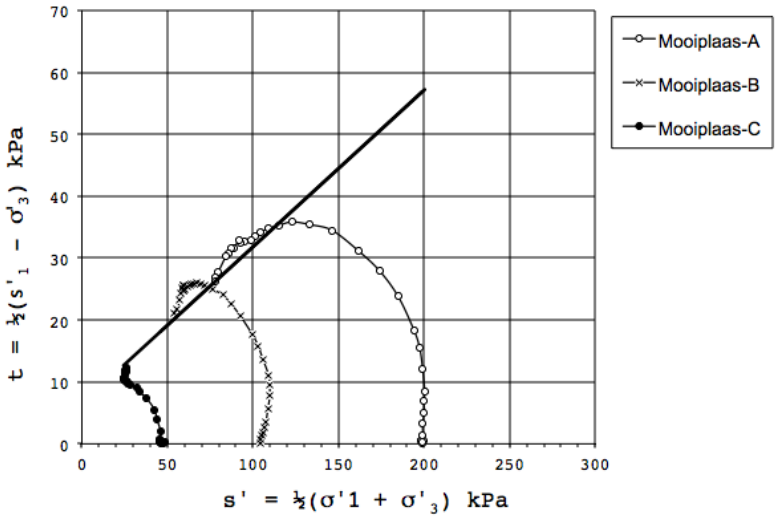

Figure 6–3 The effective stress path of the material in an s'- t space reveals the material contracted during shearing.

Table 6–1: Summary of triaxial test results.

Samples	Dry density (kg/m^3)	E-moduli (Mpa)	Shear Strength	Permeability (m/s)
Mooiplaas	1034 - 1751	3 - 28	c' = 6.5kPa ϕ' = 14.2	$9{,}00 \times 10^{-7}$
Bokkraal	1237	-	-	$2{,}80 \times 10^{-6}$
Doornhoek	539	-	-	$2{,}70 \times 10^{-6}$

6.2. Crumb test

The crumb test performed on the sample material rendered the samples from the eight localities to be non-dispersive. Photos taken of the samples at the various evaluation times during the test can be found in **Appendix A**.

6.3. XRF and XRD

The XRF and XRD analyses conducted on the eight (8) sample materials were successfully completely at the respected labs and summaries of the results are shown in **Table 6–2** and **Table 6–3.** The full results are presented in **Appendix A.**

Table 6–2: Summary of XRF analyses conducted on sample materials.

	Carleton-ville (%)	South Downs (%)	Bokkraal (%)	Mooiplaas (%)	Sudwala Caves (%)	Doornhoek (%)	R533 (%)	Highveld (%)
SiO_2	68.6	72.0	62.0	82.0	35.7	45.9	24.4	5.78
Al_2O_3	4.24	3.15	3.57	5.09	12.4	2.67	6.57	0.76
Fe_2O_3	10.2	12.3	16.5	5.61	13.3	25.5	23.8	33.9
MnO_2	10.1	8.06	10.8	3.19	27.9	11.5	36.0	45.8
MgO	0.69	0.29	0.35	0.28	0.73	0.73	0.49	0.52
CaO	0.76	0.13	0.13	0.20	0.07	0.08	0.08	2.13
PbO	-	-	-	-	-	6.43	-	-

Table 6–3: Summary of XRD analyses conducted on sample materials.

	Carleton-ville (%)	South Downs (%)	Bokkraal (%)	Mooiplaas (%)	Sudwala Caves (%)	Doornhoek (%)	R533 (%)	Highveld (%)
Goethite	1.11	2.40	11.8	1.90	3.36	12.8	6.63	19.0
Kaolinite	-	0.11	2.48	6.99	6.49	4.40	4.11	11.9
Muscovite	5.89	5.38	5.20	-	36.2	2.46	29.4	29.3
Quartz	91.3	91.8	80.5	86.2	53.3	80.3	59.9	36.9
Dolomite	1.65	0.30	-	-	0.65	-	-	2.71
Talc	-	-	-	4.90	-	-	-	-

6.4. Foundation indicators

The grading and Atterberg limits were successfully analysed on the sampled material and a summary of the results are presented in **Table 6–4**. The grading curves are presented in **Figure 6–2** and the full results are attached as **Appendix A.**

Table 6–4: Summary of results of the foundation indicator tests.

Sample	Grading				PI (%)	LL (%)	USCS
	Clay (%)	Silt (%)	Sand (%)	Gravel (%)			
Highveld	9	89	2	0	8	229	MH
R533	28	53	11	8	33	145	MH
Doornhoek	4	68	23	5	33	121	MH
Sudwala Caves	19	56	4	21	20	67	MH
Carletonville	11	39	27	23	17	94	MH
South Downs	18	46	26	10	17	65	MH
Bokkraal	11	33	45	11	16	49	SL
Mooiplaas	12	50	20	18	12	29	SC
PI - Plastic Index; LL - Liquid Limit; USCS - Unified Soil Classification System							

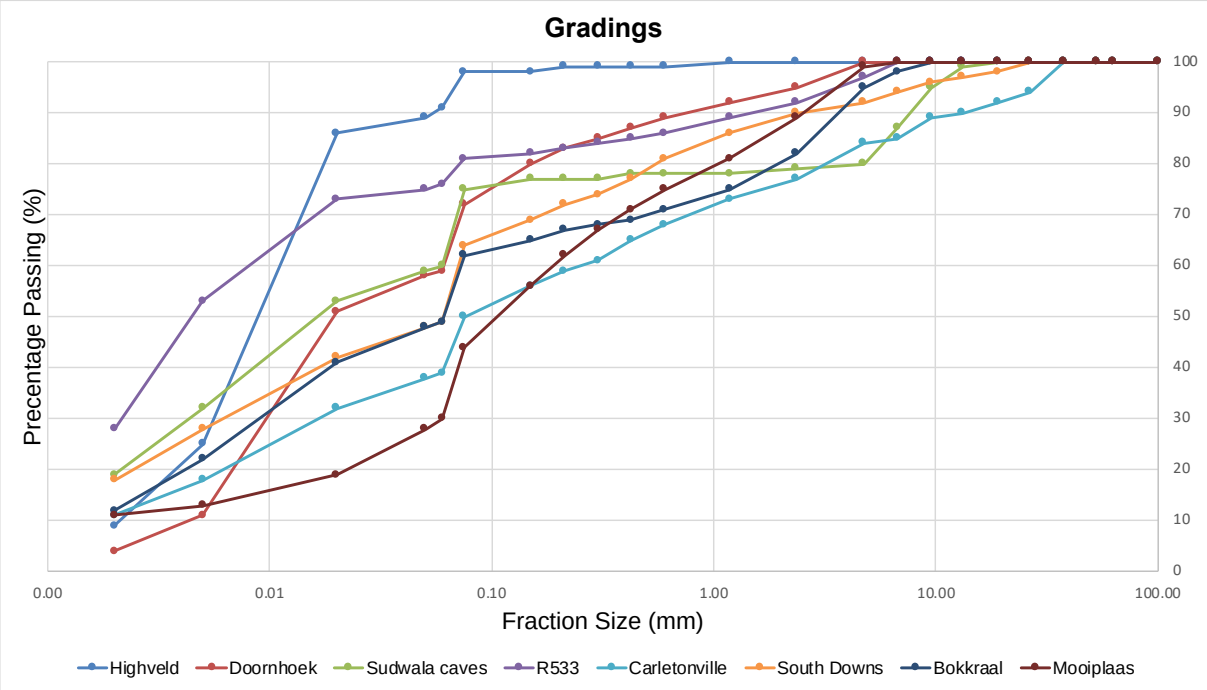

Figure 6–2: Grading curves of the sampled material.

6.5. Stereomicroscope

The stereomicroscope photographs of the samples were successfully taken at various magnifications, the photographs are shown from **Figure 6–3** to **Figure 6–10**. The photos were taken of undisturbed samples and post triaxial consolidation and shearing samples.

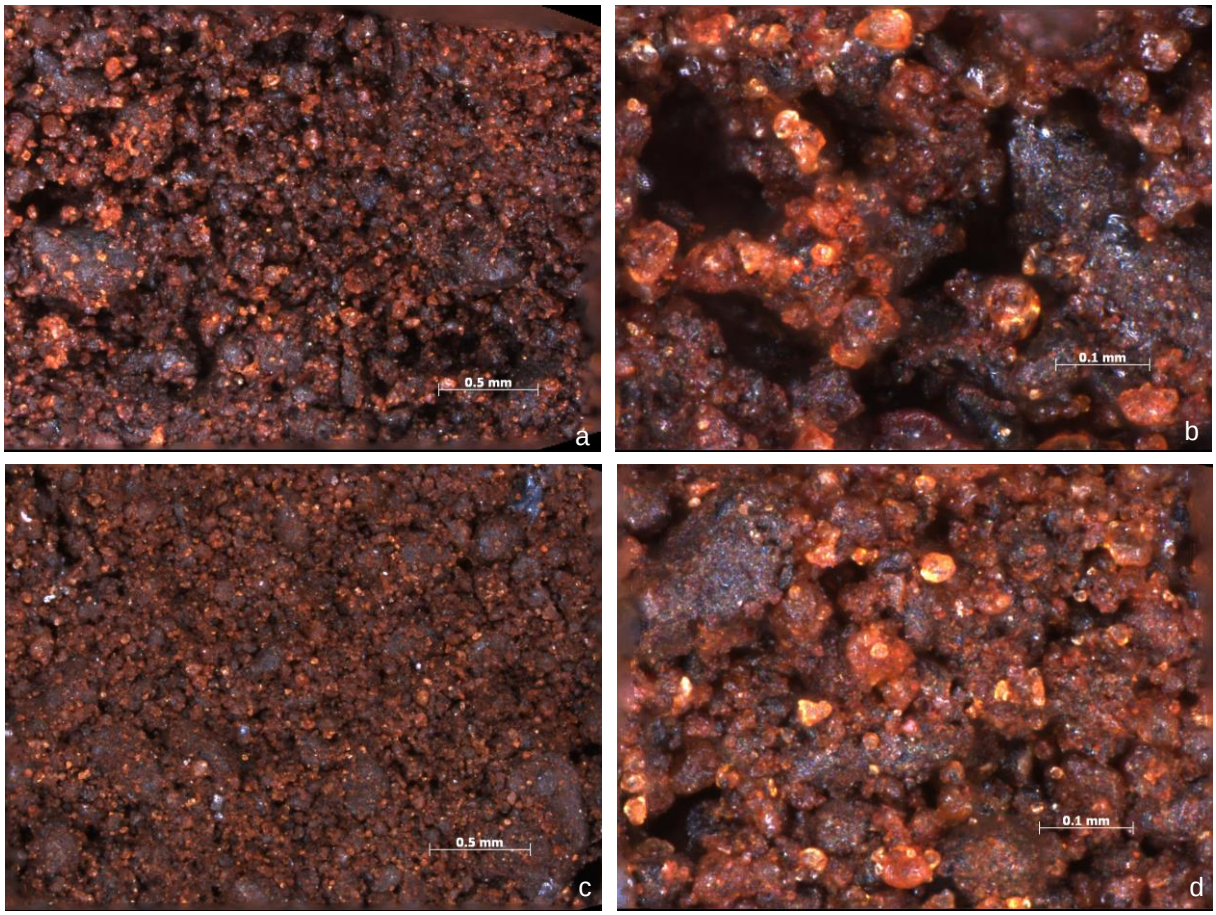

Figure 6–3: Photographs taken of the Mooiplaas samples pre- and post-triaxial undrained shear testing. (a) Photograph taken of undisturbed sample at x20 magnification. (b) Photograph taken of undisturbed sample at x94 magnification. (c) Photograph taken post testing at x20 magnification. (d) Photograph taken post testing at x94 magnification.

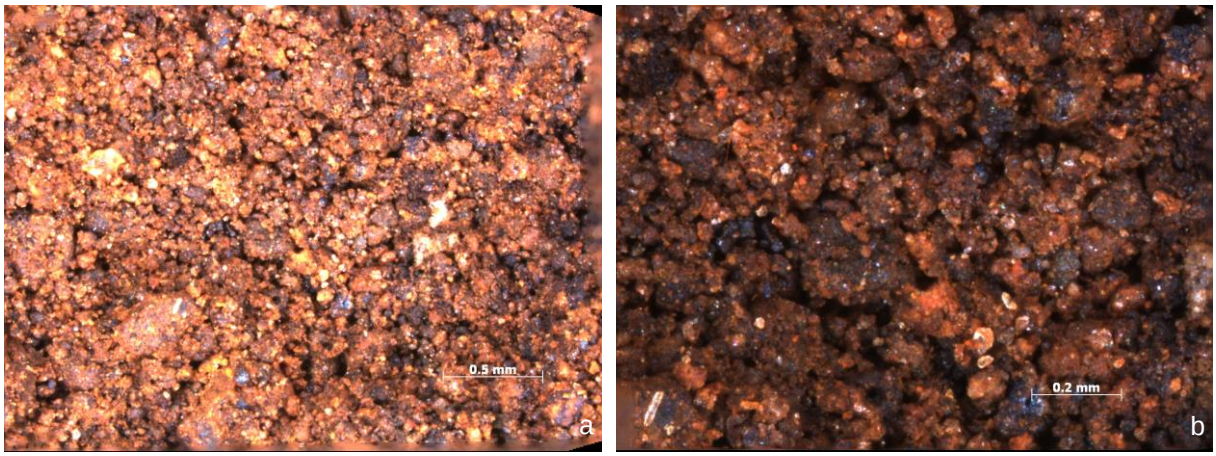

Figure 6–4: Photographs of the Bokkraal samples post-triaxial consolidation. (a) Photograph taken at x20 magnification. (b) Photograph taken at x94 magnification.

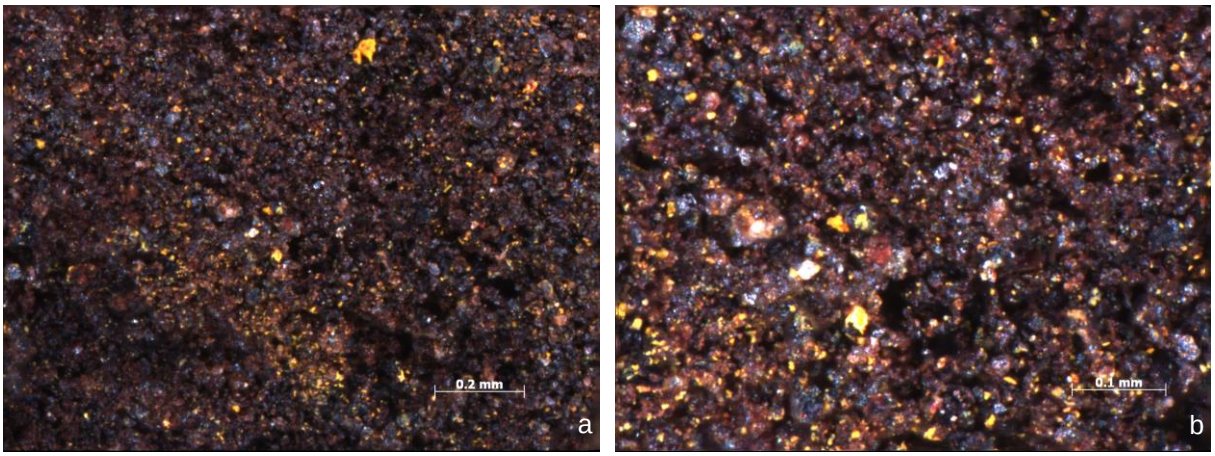

Figure 6–3: Photographs taken of Doornhoek sample post-triaxial consolidation. (a) Photograph taken at x45 magnification. (b) Photograph taken at x94 magnification.

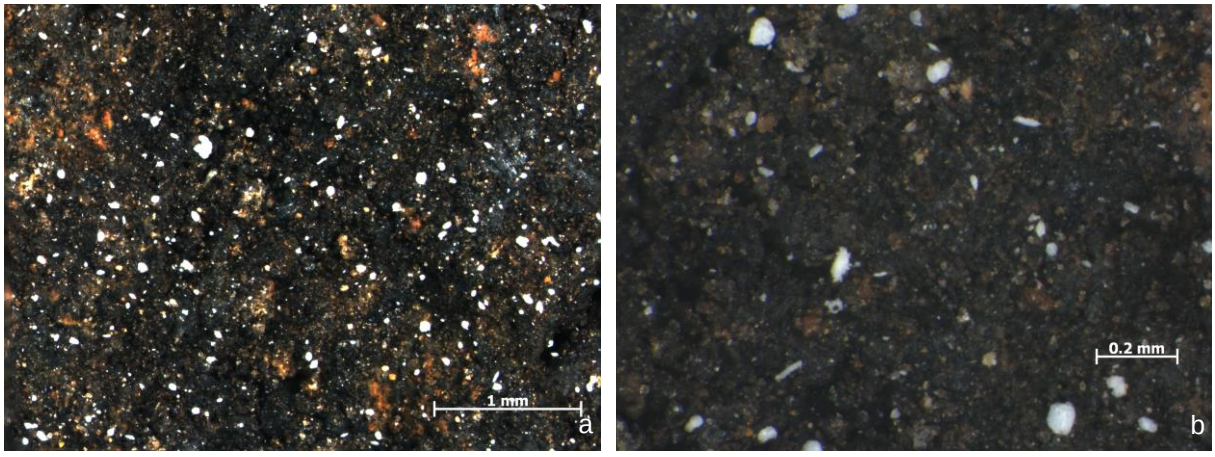

Figure 6–4: Photographs taken of Sudwala Cave undisturbed sample. (a) Photograph taken at x34 magnification. (b) Photograph taken at x94 magnification.

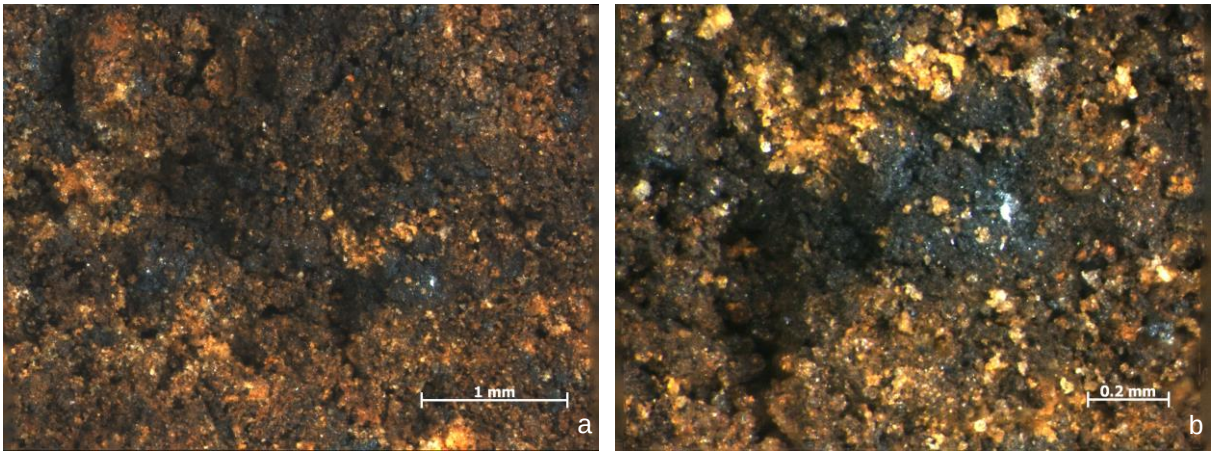

Figure 6–5: Photographs taken of South Downs undisturbed sample. (a) Photograph taken at x34 magnification. (b) Photograph taken at x94 magnification.

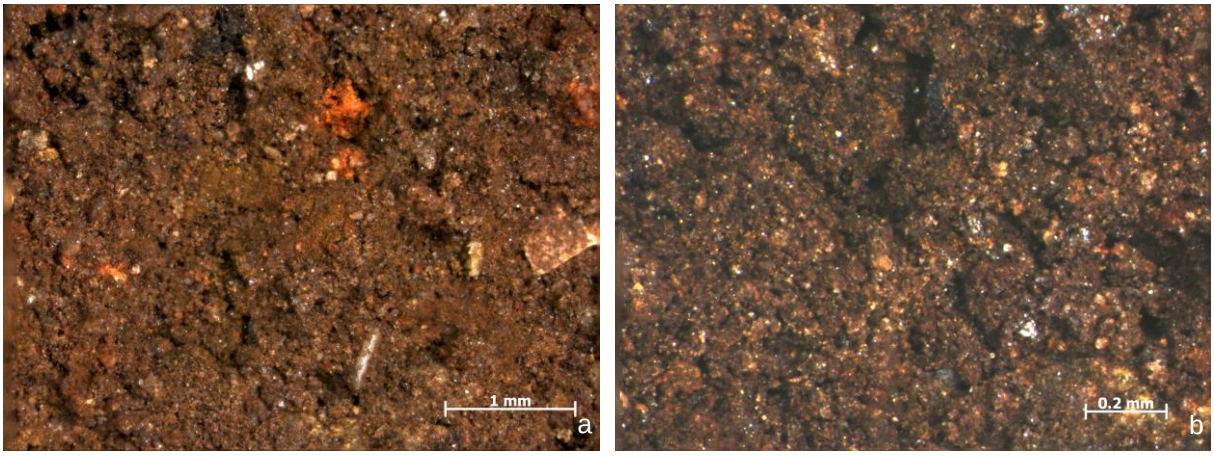

Figure 6–6: Photographs taken of Carletonville undisturbed sample. (a) Photograph taken at x34 magnification. (b) Photograph taken at x94 magnification.

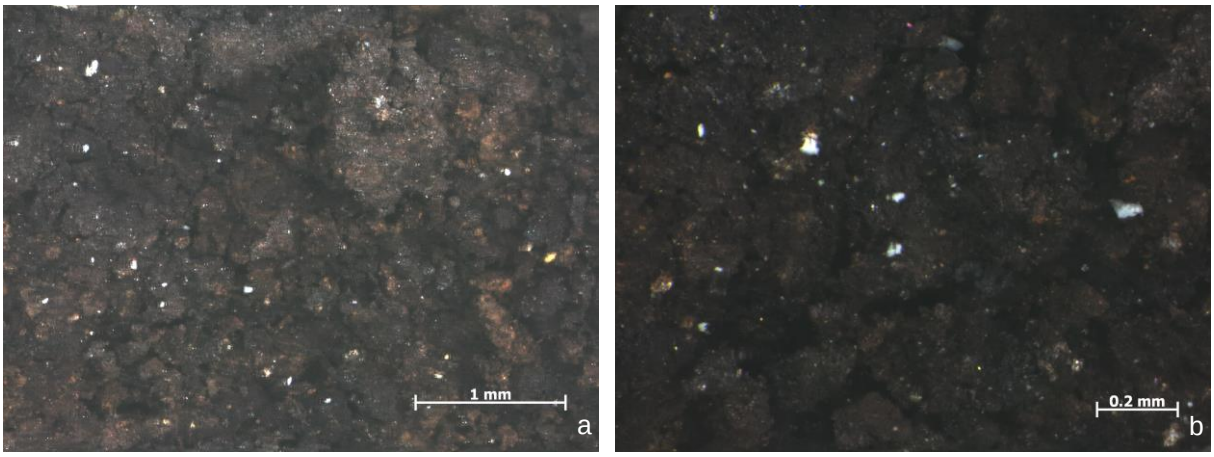

Figure 6–7: Photographs taken of R533 undisturbed sample. (a) Photograph taken at x34 magnification. (b) Photograph taken at x94 magnification.

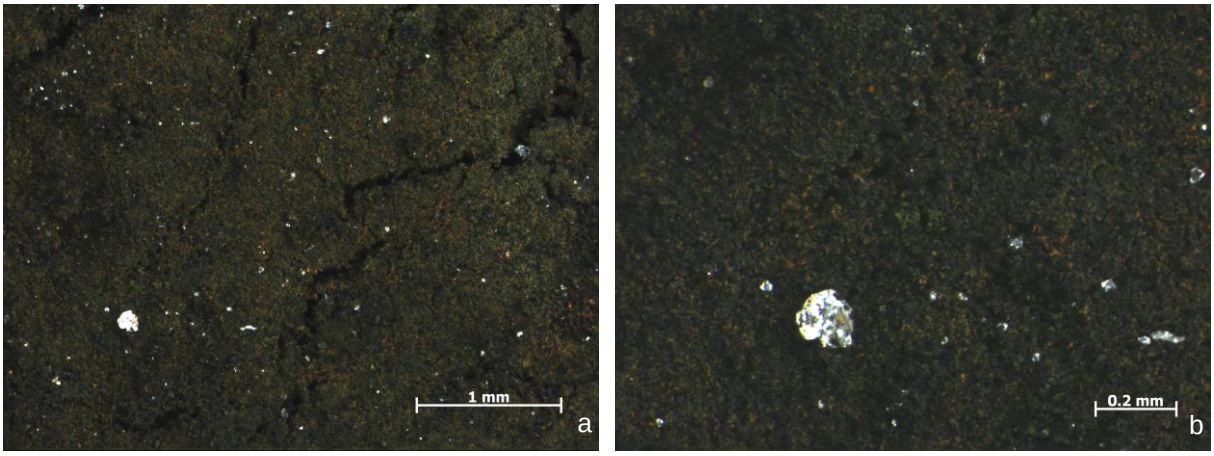

Figure 6–8: Photographs taken of Highveld undisturbed sample. (a) Photograph taken at x34 magnification. (b) Photograph taken at x94 magnification.

6.6. Scanning Electron Microscope

The SEM was successfully used to gather information at significantly high magnifications. The SEM produced images of the surface topography of the sample material at various magnifications as shown from **Figure 6–11** to **Figure 6–17**.

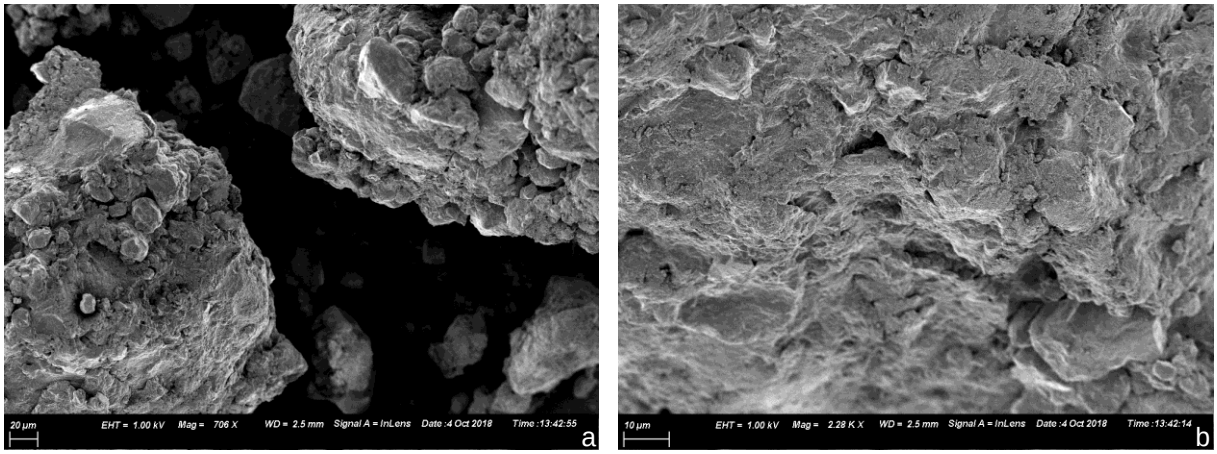

Figure 6–9: Images from the SEM of the Mooiplaas sample. (a) Image taken at x706 magnification. (b) Image taken at x2 000 magnification.

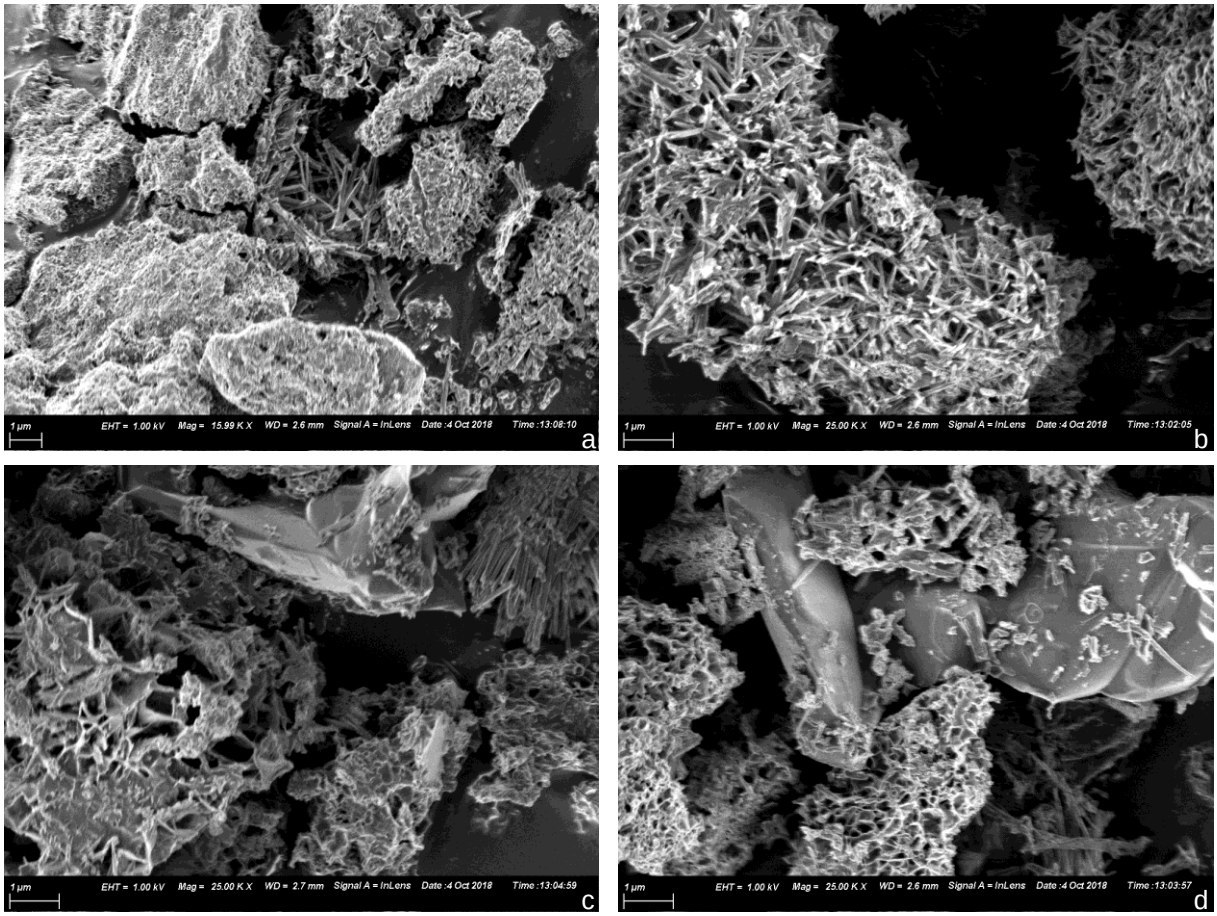

Figure 6–10: Images from the SEM of the Bokkraal sample. (a) Image taken at x10 000 magnification. (b) Image taken at x25 000 magnification. (c) Image take at x25 000 magnification. (d) Image taken at x25 000 magnification.

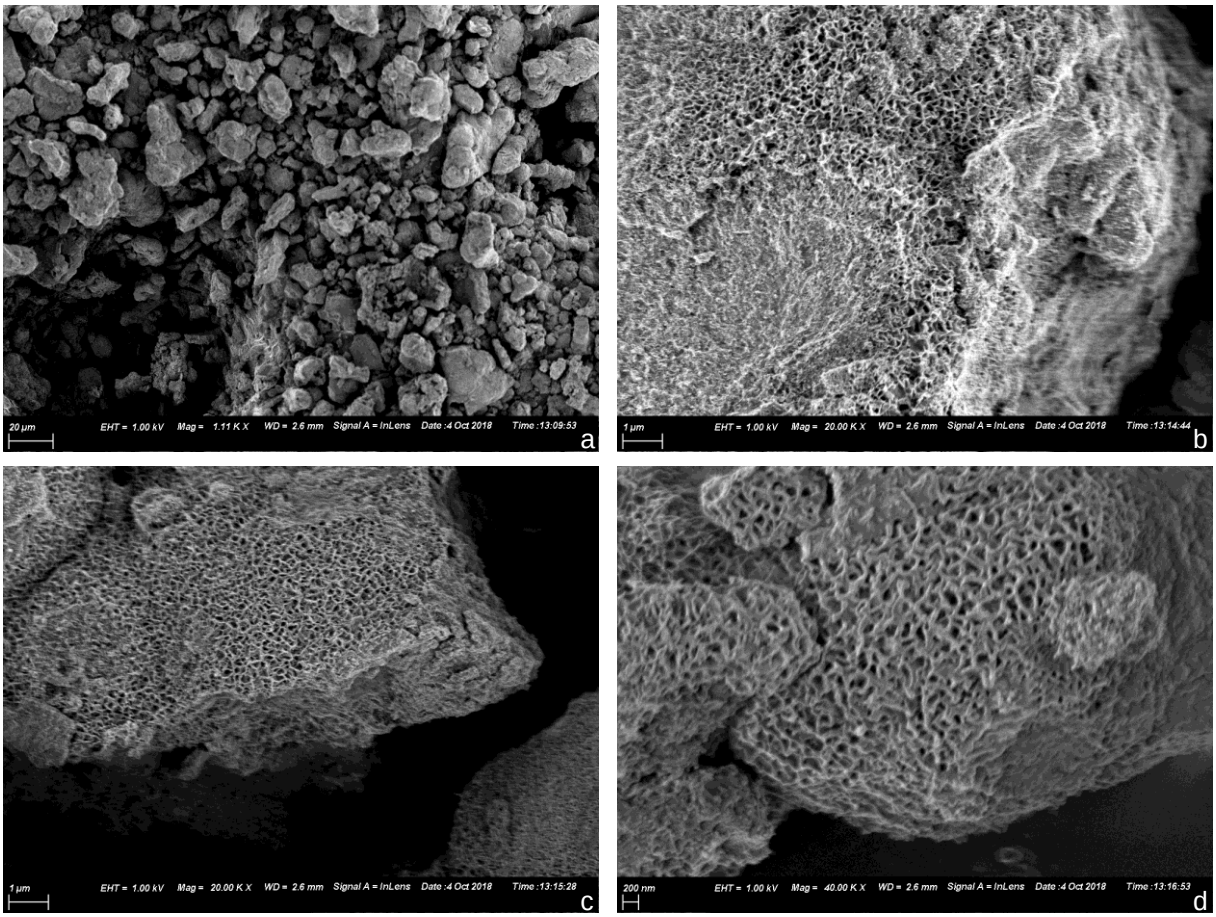

Figure 6–11: Images from the SEM of the Doornhoek sample. (a) Image taken at x1 000 magnification. (b) Image taken at x20 000 magnification. (c) Image take at x20 000 magnification. (d) Image taken at x40 000 magnification.

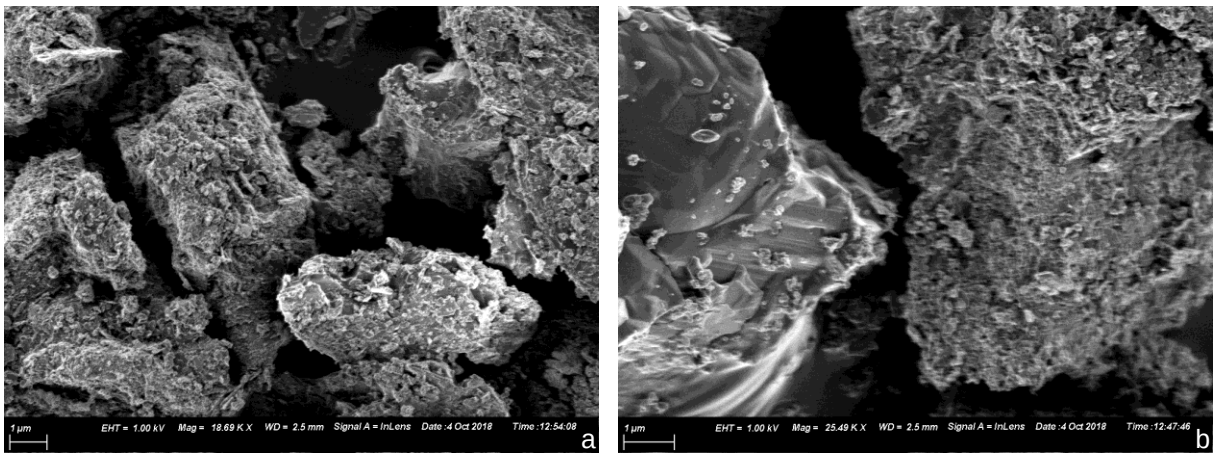

Figure 6–12: Images from the SEM of the Sudwala Cave sample. (a) Image taken at x18 000 magnification. (b) Image taken at x25 000 magnification.

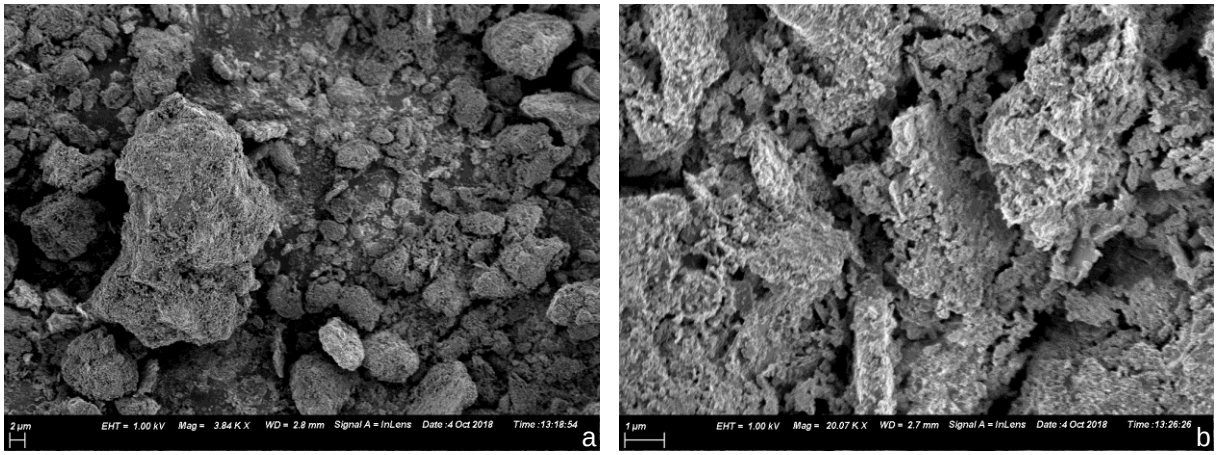

Figure 6–13: Images from the SEM of the South Downs sample. (a) Image taken at x3 800 magnification. (b) Image taken at x20 000 magnification.

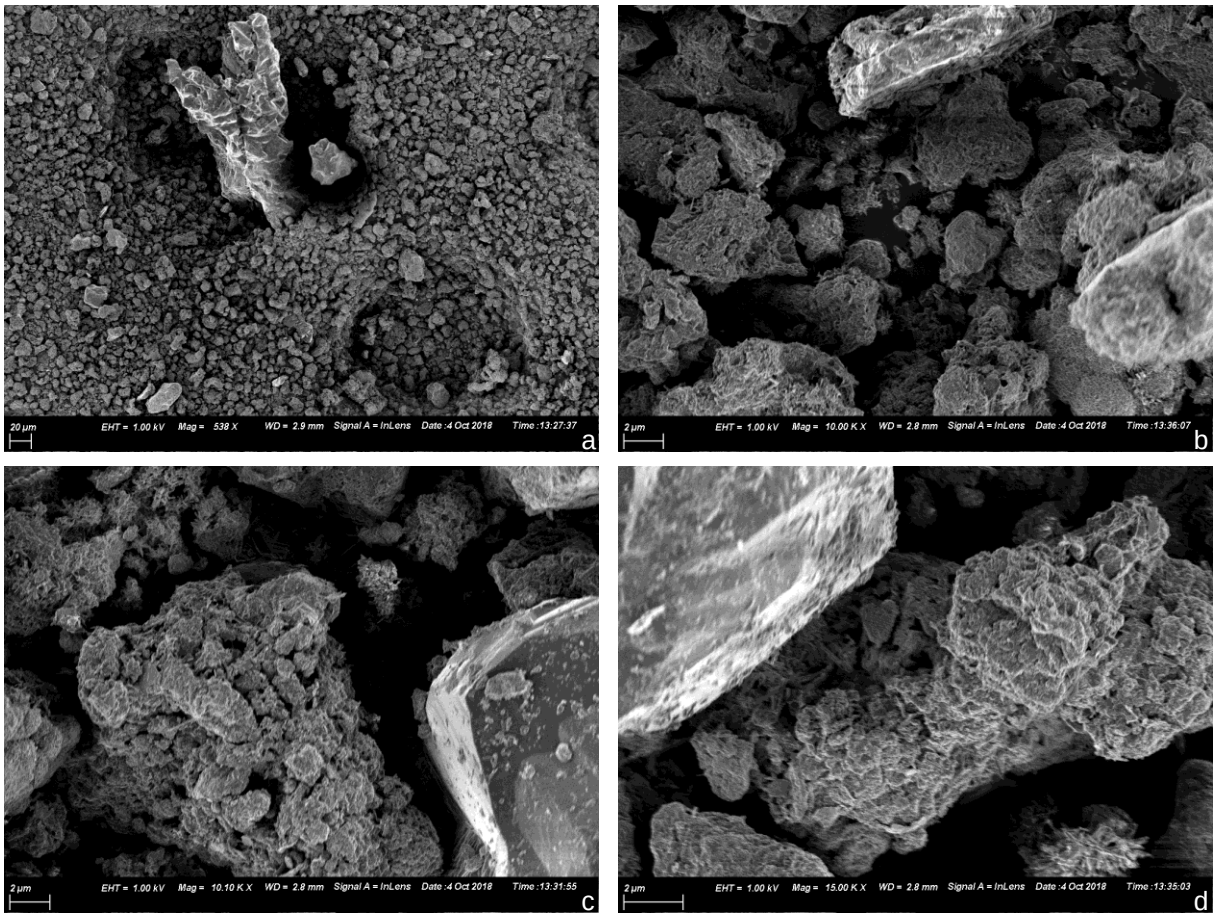

Figure 6–14: Images from the SEM of the Highveld sample. (a) Image taken at x500 magnification. (b) Image taken at x10 000 magnification. (c) Image take at x10 000 magnification. (d) Image taken at x15 000 magnification.

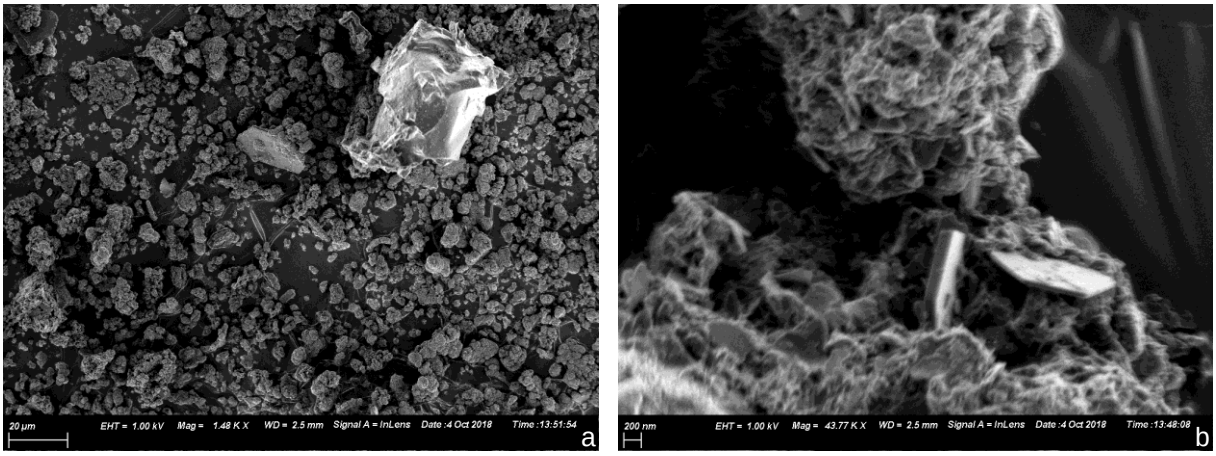

Figure 6–15: Images from the SEM of the R533 sample. (a) Image taken at x1 000 magnification. (b) Image taken at x43 000 magnification.

6.7. Columns

Eight samples successfully underwent permeability tests using Perspex columns. The hydraulic conductivities (K) are summarized in **Table 6–5**. The table includes the triaxial permeability test results and falling head infiltration and percolation field test results conducted at the Mooiplaas sample locality by Heuer (2017) for ease of comparison.

Table 6–5: Hydraulic conductivities results from field, triaxial and column tests

Sample	Fabric	Hydraulic conductivity (m/s)		
		Undisturbed		Remolded
		Field (Heuer, 2017)	Triaxial	Columns
Highveld	Structured	-	-	$3{,}0 \times 10^{-5}$
R533	Non-structured	-	-	$2{,}3 \times 10^{-5}$
Doornhoek		-	$2{,}7 \times 10^{-6}$	$4{,}0 \times 10^{-6}$
Sudwala caves	Reworked	-	-	$3{,}0 \times 10^{-5}$
Mooiplaas		$2{,}81 \times 10^{-4}$ - $9{,}52 \times 10^{-4}$	$9{,}0 \times 10^{-7}$	$2{,}0 \times 10^{-5}$
Bokkraal		-	$2{,}8 \times 10^{-6}$	$8{,}0 \times 10^{-6}$
Carletonville		-	-	$2{,}0 \times 10^{-5}$
South downs		-	-	$2{,}0 \times 10^{-5}$

Erosion tests were successfully conducted on four (4) samples using the Perspex columns. The results retrieved from the experiments are summarised in **Chart 6–1.** Photographs of the 'dirty' water samples from each scenario and summary of results are attached in **Appendix A.**

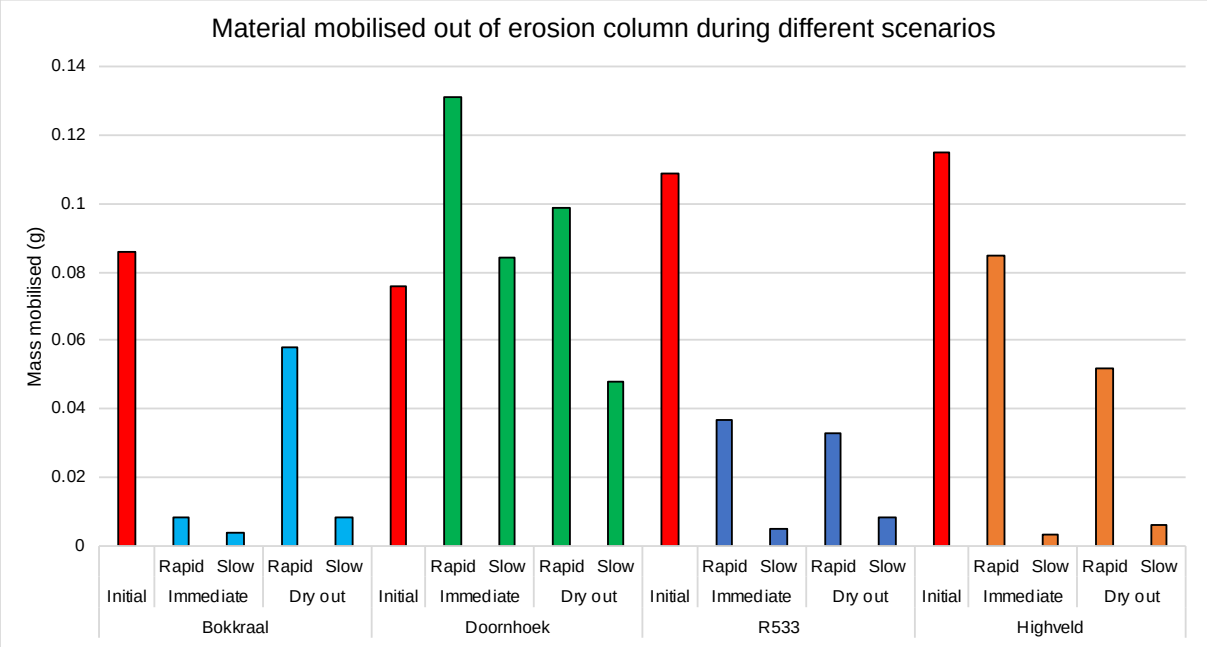

Chart 6–1: Graph presenting mass of material eroded out of the columns during different scenarios.

6.8. Specific gravity, Density and Void Ratio

Table 6–6 summaries results from the specific gravity tests and includes values of dry density and void ratio, determined from weighing saturated and dried undisturbed samples at a constant volume.

Table 6–6: Summary of dry density, void ratio and specific gravity tests conducted on the sample material

Sample	Fabric	Dry density (kg/m^3)	Void ratio	Specific gravity (kg/m^3)
Highveld	Structured	309	8,32	2886
Doornhoek	Non-structured	593	3,87	2896
R533		-	-	2050
Sudwala Caves	Reworked	-	-	2860
Mooiplaas		1034 - 1751	0,55	2727
Bokkraal		1237	1,34	2897
Carletonville		898	2,07	2760
South Downs		-	-	2934

6.9. SWRC

Seven SWRCs were successfully produced using the PPTs described by Jacobsz (2018) (**Chart 6–2**). Summary of results are shown in **Table 6–7** The initial moisture content is the moisture content at the start of the drying cycle.

The SWRCs produced included comparing structured and remoulded (structured broken down) Highveld (**Chart 6-3**), comparing remoulded Doornhoek sample at three different densities (**Chart 6–4)** and curves for samples R533 and Sudwala Cave (**Chart 6–5**).

Table 6–7: Summary of SWRC test results

Sample	Dry Density (kg/m^3)	Initial moisture content (w) (%)	AEV (kPa)	Suction pressure values: (kPa)		
				At 40% saturation	At 60% saturation	At 80% saturation
Highveld Structured	309	300	20	146	62	44
Highveld Remolded	746	87.6	0.8	146	32	5.5
Sudwala Cave	894	77.0	~0.3	-	113	7
Doornhoek Loose	702	108	20	310	46	32
Doornhoek Medium	753	103	20	124	46	34
Doornhoek Dense	809	86.4	20	-	67	34
R533	464	160	~1	161	43	7

AEV - Air Entry Value

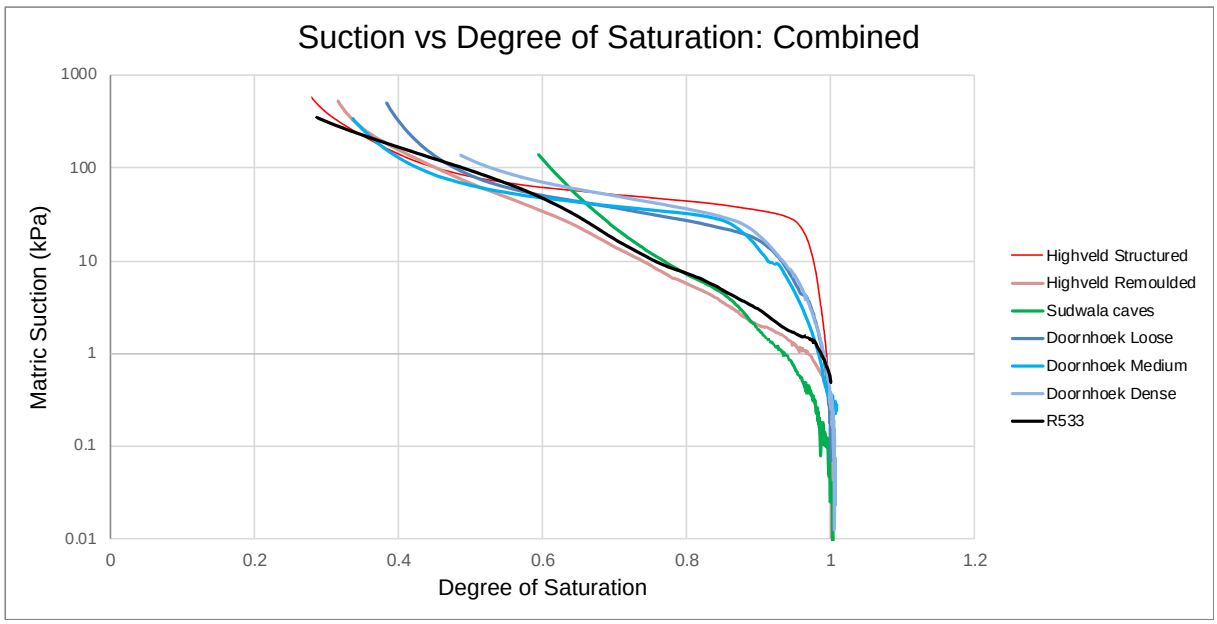

Chart 6–2: SWRCs of all tested samples

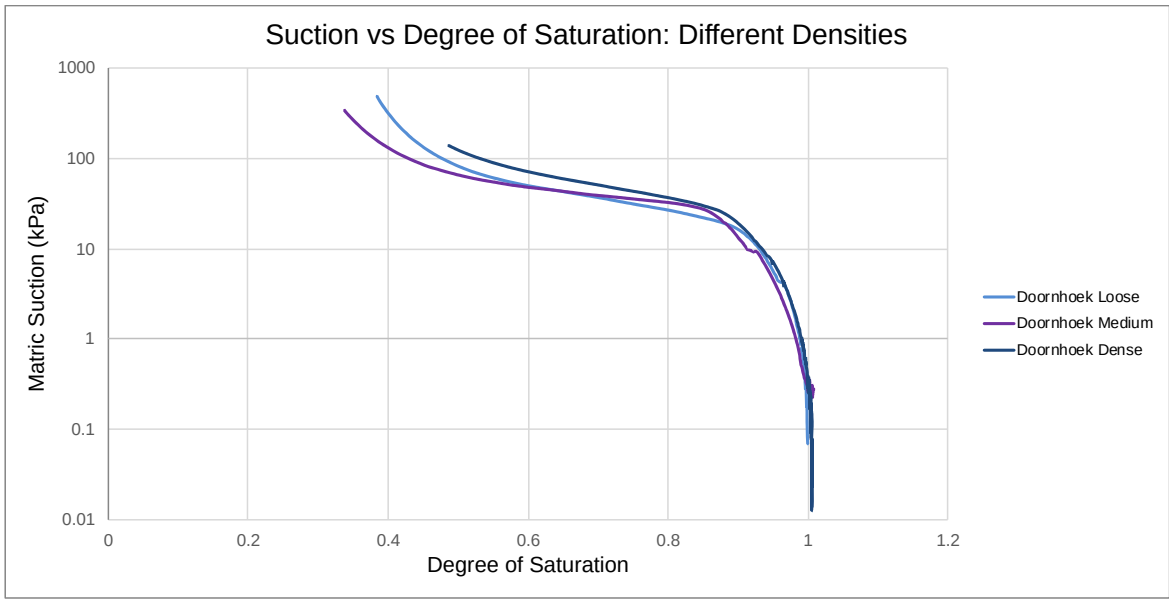

Chart 6–4: SWRC of Doornhoek sample at different densities

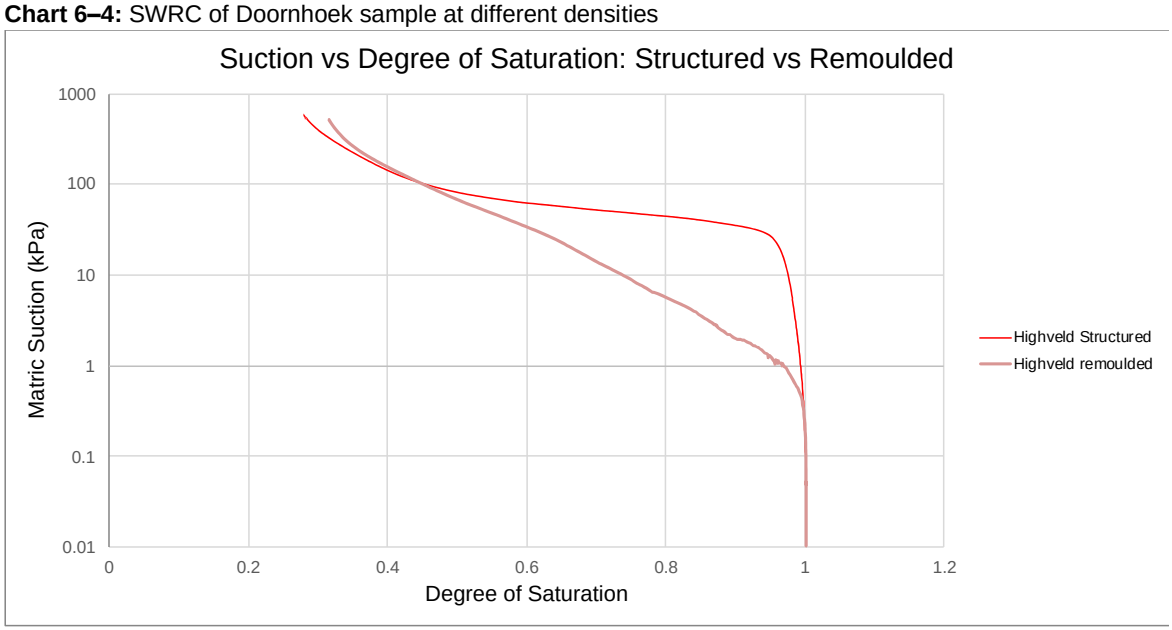

Chart 6–3: SWRC of Highveld sample with and without structured fabric

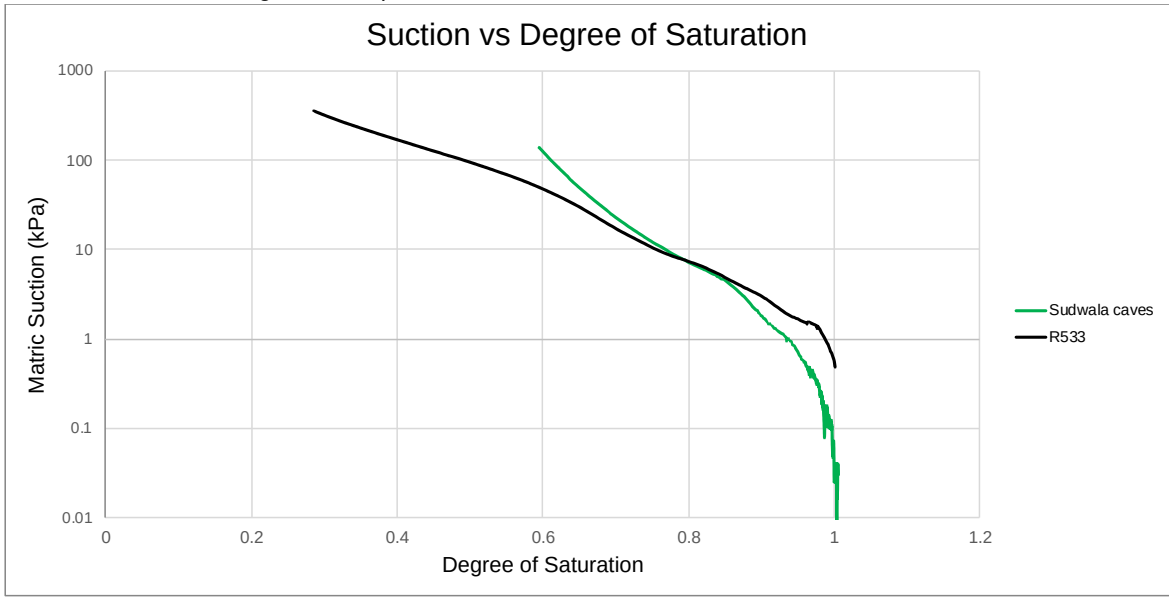

Chart 6–5: SWRC of Sudwala Cave and R533 samples

7. Discussion of Results

7.1. Triaxial Tests

The Bokkraal Shelby samples obtained from the underground mine shaft were successfully extruded; however, when the sample was being prepared for the triaxial cell, problems were encountered when attempting to cut the sample. The Bokkraal sample from within the underground mine was highly laminated with galena (PbS) being present in the fissures (**Figure 7–1**). Therefore, the soil is not a representative sample, as the lead sulphide mineral would have taken up the load during the triaxial shear testing and would have acted as a preferred pathway for water to travel. Thus, the sample was not used for triaxial shear testing or permeability testing. The samples taken from the road cut at Bokkraal was sampled at a very shallow depth (+/- 50cm) to surface. It was observed when extruding the three Shelby samples that the soil was desiccated and highly reworked. Consequently, a sample with insufficient height for shearing was successfully extruded out of the Shelby tubes.

Figure 7–1: Bokkraal material laminated with lead ore galena

The soil excavation face at Doornhoek was slightly moist and stiff to very stiff in some places due to the fabric of the wad and presence of lead ore (6,43%), though the ore was not present as laminations as in the Bokkraal samples. Thus, a Shelby tube could not be pushed in by hand any further than a few centimetres. The soil sample extruded out of the Shelby

tube was of insufficient height for triaxial shear testing, however a large enough sample was successfully gained for permeability testing.

The Mooiplaas, Bokkraal and Doornhoek samples underwent isotropic consolidation at 100 kPa confining pressure and experienced full primary consolidation under 2 minutes, verifying that the sufficient permeability makes the side drains placed on Mooiplaas-A sample unnecessary for the material. The material severely contracted during shearing due to the high initial void ratio. However, **Figure 6–** suggests voids are still present post shearing.

7.2. Dispersivity

Majority of samples completely disintegrated when placed into the distilled water, suggesting all strength and cohesion lost when saturated. The Doornhoek sample only partly crumbled with a few pieces staying intact at the beginning of the test. However, most of the sample disintegrated after an hour of being placed in the water. The photographs taken of the samples at various inspection times at presented in **Appendix A**.

7.3. Mineralogy and Foundation Indicators

The grading of the reworked wad samples is dependent on the parent rock composition but more importantly on the mechanical processes experienced by the wad material, if any. The Mooiplaas and Bokkraal samples have been highly reworked, consequently losing the inherent parent structure as well as an increase the amount of sand and gravel size chert or quartz grains, therefore affecting the grading and the chemical composition of the material. The XRF results show the Bokkraal and Mooiplaas samples have very high SiO_2 contents, 62% and 82%, respectively. These reworking processes have affected the Atterberg limits of the material, in this case lowering the liquid limit, which is expected of soil that contains more inert, coarse material. The grading of the Bokkraal sample is slightly coarser than the Mooiplaas material, however the Bokkraal sample has a higher liquid limit percentage compared to the latter. The ability for the Bokkraal sample to retain a relatively higher liquid limit than the Mooiplaas sample may be due to the difference in metal oxide contain, ~27% and ~9,0% respectively, as was elaborated in **Section 3.3**.

The Carletonville and South Downs samples were retrieved several meters below the ground surface in an existing open sinkhole. The samples seem to be reworked to a lesser degree than the Bokkraal and Mooiplaas samples and consequentially have higher liquid limits, 94% and 65% compared to 49% to 29%, respectively. Sudwala Cave material is gap-graded due to reworking of much coarser material into the fine matrix, resulting in a gravelly silty

material. The material is expected to have a slightly greater liquid limit than the other lesser reworked samples due to the greater fines and metal oxides percentages. However, it exhibits a liquid limit of 67%. The material has the highest Al_2O_3 % (12,4%), nearly double the amount of the second highest constituent (6,57%) and is expected to contain the most kaolinite of all the samples. This presence of kaolinite and the gap-graded nature of the material, due to certain processes of reworking, may affect the water holding capacity. This variation in 'degree' of reworking leads to problems in classifying the wad material and building the geological model of the material.

The R533 sample was retrieved in the greater area of Pilgrim's Rest. This material is very similar to the soils studied by Dowding (2007). The higher clay content of this soil is expected due to the relatively wetter climate of the area. The material possesses large amounts of metal-oxides (59,7%) and a significantly high liquid limit (145%). The material is expected to contain kaolinite and an arrangement of other clay particles and metal oxides that contribute to the high liquid limit.

The Doornhoek and Highveld samples have not been reworked, consequently, preserving the fabric inherent to the parent rock and maintaining the fine grading with no added impurities. The Doornhoek and Highveld samples contain only 4% and 9% clay, respectively. These two samples represent the lowest clay content of all the samples tested but exhibit some of the highest liquid limits 121% and 229%, respectively. The Doornhoek and Highveld samples have significant amounts of Fe and Mn oxides at 36,96% and 79,64%, respectively. As elucidated in **Section 3.3**, Mn-oxides commonly form coatings on other minerals and form reactive surfaces (Post, 1999), such as on inert chert or quartz grains. The high liquid limits may result from adsorption of water onto metal (Fe and Mn) oxide surfaces rather than the adsorption of the clay structure (Bear Geoconsultants, 2016). Post (1999) found that Mn-oxides could readily take up water molecules, the amount of which is dependent on the structure of the Mn-oxide. McKenzie (1972) found that a fine-grained birnessite could have a surface area of up to $300m^2/g$, allowing for the material to carry 15% to 25% of its weight in water (Post, 1999). Jenne (1968) stated that the chemical influences that Mn-oxides have on the surrounding environment and aqueous solutions far outweighs their concentrations. Dowding (2007) studied the Mn-rich soils in the Graskop, Mpumalanga, area and identified lithiophorite, birnessite and todorokite and goethite, hematite and maghemite as the common Mn and Fe minerals found in wad, respectively. Mn-oxides are typically poorly crystalline (i.e. amorphous) and generally no attempt is made to distinguish the exact Mn mineral (Post, 1999). When a large quantity of Fe-ions are present in the soil, an extensive amount of substitution with the Mn-oxides will occur, resulting in the crystal structure to morph and the

infrared (IR) spectra, or XRD ‘peaks’ used to identify the minerals, to broaden and shift (Hawkins & Thompson, 1988). This change in morphology may result in an alteration of the large surface area that may affect the water holding capacity of the oxides. Further difficulty is experienced as many of the common Mn-oxides found in wad share similar IR spectra to other common minerals found in soil. Referring to the XRD results (**Table 6–3**), none of the samples contain any aforementioned Mn-oxide minerals. Birnessite, the most common mineral in wad, has the same IR peak as kaolinite, a common clay mineral. This is the same for Mn-oxides manganite and todorokite with respect to goethite and mica or gibbsite. Therefore, the minerals identified in **Table 6–3** may not be the only constituents of the soil and a more detailed approach to identifying the minerals is needed.

7.4. Microscopy

The use of microscopy is an important tool when identifying the mineral constituents and have divulge some significant information regarding the behaviour of material in this study.

The Mooiplaas samples, when looking at the microstructure, are mainly made up of fine to medium sand size chert grains and very fine to sand size clumps of wad with Fe-oxides on the surface of the chert grains and wad. The undisturbed sample (**Figure 6–**) is highly reworked, thus has no structure and is highly voided, some voids are 0,1 millimetres across. The post shear testing sample has a reduced void ratio; however many voids are still present after consolidation and shearing. The voids are still present due to the load applied being insufficient to overcome the clay bridges and inter-granular shear strength.

The Mooiplaas and Bokkraal sample materials have very similar qualitative characteristics when observed through a microscope as can be seen in **Figure 6–** and **Figure 6–**. As mentioned in **Section 7.3**, the gradings differ slightly with the Mooiplaas sample containing more fines, yet the liquid limit of the material is much lower than the Bokkraal material. Referring to **Figure 6–11**, the Mooiplaas sample exhibits a mass of amorphous clumps, with very small scattered voids present, roughly 2 to 10 μm in size, coating a smooth inert surface. **Figure 6–12** reveals that the Bokkraal material possesses an arrangement of smooth surface particles set in between abundantly present, highly voided, individual particles with needle and rod to coral and sponge type structures, roughly 0,1 to 2 μm in size. This structure is typical of physico-chemically formed birnessite (Jiang et al., 2010; Bruins, 2016), and other Mn-oxides (Gotić, et al., 2012), and allows for a much larger available surface area for water molecules to attach onto. The greater Mn-oxide percentages in the

Bokkraal material explains why these structures are more prevalent than in the Mooiplaas material and also gives reason for the higher liquid limits exhibited by the Bokkraal material.

The South downs and Carletonville samples are both reworked with black to brown and red colours. The material is generally fine with voids present and scattered coarse material, however lesser coarse material than the Bokkraal and Mooiplaas sample. The coarse material is seemingly composed of sub-angular quartz and angular chert slabs as can be seen in **Figure 6–7** and **Figure 6–8.**

Examining the Doornhoek sample through the stereomicroscope and SEM reveals explanations for the extremely high liquid limit of a material with only 4% clay. Referring to **Figure 6–5**, the material exhibits relatively large voids between the indefinable individual grains that make up the soil. At x1000 magnification, **Figure 6–13a**, the individual grains are defined with open voids visible between the various grains. **Figure 6–13 b**, **c** and **d**, magnification at x20 000, x20 000 and x40 000, respectively, divulges some key aspects of the material. The single grain appears to be highly voided and exhibits a coral or sponge type structure. Referring to **Figure 7–2** below, the appearance of black birnessite at x9000 and x25000, from Cheney et al., (2008), is very similar to the material in **Figure 6–13**. Day (1981), Wagener (1982) and Buttrick (1986) discovered a similar material, as in **Figure 6–13** and **Figure 7–2**, in massive or non-structured wad and it was famously described by Wagener to have the appearance of “Rice Crispies”. As previously mentioned, this structure is typical of birnessite (Jiang et al., 2010; Bruins, 2016). The presence of this highly voided metal oxide birnessite that can carry up to 25% of its weight as water, will have a major influence on the high liquid limit (125%) of this clay-poor material.

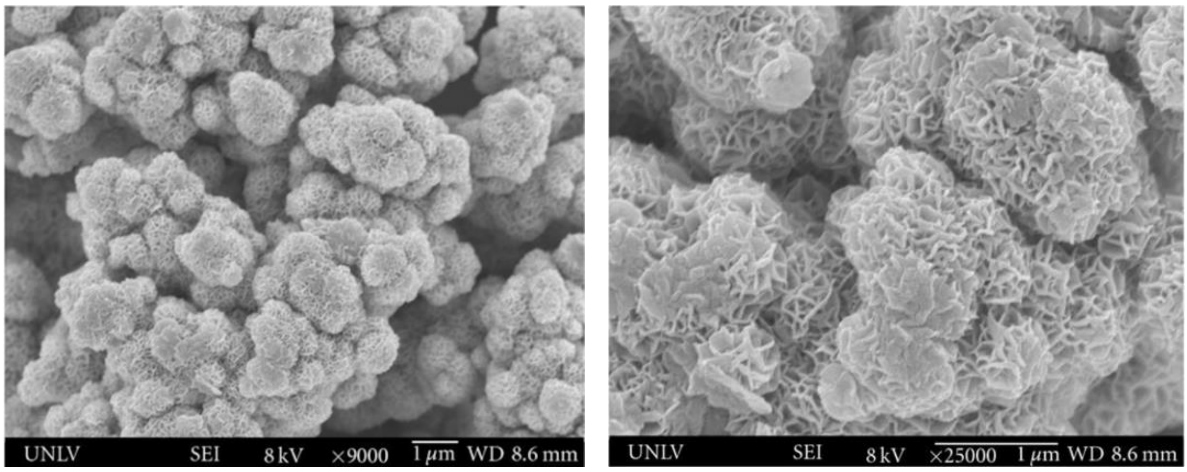

Figure 7–2: SEM images of black birnessite at (a) x9 000 and (b) x25 000 magnifications (Taken from Cheney, et al., 2008).

The Highveld, R533 and Sudwala samples comprise of very fine, dark in colour matrix with scattered coarse quartz or chert material (**Figure 6–6**, **Figure 6–9** and **Figure 6–10**). The Sudwala cave material has been slightly reworked and exhibits more orange to red colours and more abundant coarse material and voids compared to the Highveld and R533 samples. The Highveld and R533 samples reveal very few undefinable, microscopic voids with speckles of orange on a few particles. The desiccation cracks in these samples are due to the drying out of the material under the stereomicroscope's intense light, which is needed during the observation process. Referring to **Figure 6–16a**, the Highveld material is similar to the Doornhoek material and comprises of amorphous, silt size particles and coarser, smooth surfaced quartz or chert grains set in the matrix. Highly voided coral and needle type structure, as well as coating of the smooth surface, inert material can be seen in **Figure 6–16b** and **Figure 6–16c**. On closer inspection of **Figure 6–16d**, needle structurers of approximately 1 μm in length and 0,1 μm in width can be seen**.** The R533 material contains perfectly formed kaolinite, roughly 0,8 μm in size, with some of the clay particles being coated with amorphous particles assumed to be metal oxides.

The stereomicroscope reveals that the study material generally comprises of black to dark brown, very-fine grained with very few scattered coarse quartz or chert particles when not reworked. As the material becomes more reworked, the colour transgresses into brown to red-brown and the coarse component increases. The SEM reveals that well-formed to amorphous metal-oxides occur in the sample material. The metal oxides are generally voided and can be present as coatings on clay and quartz or chert particles.

7.5. Columns Conductivity and Erodibility

Very limited permeability field-testing has been conducted on material associated with residual dolomite, with expectation to Heuer (2017). Heuer (2017) preformed falling head infiltration and percolation tests at Mooiplaas mine in Laudium, in close proximity to the Mooiplaas sample location. An undisturbed Mooiplaas sample underwent a triaxial permeability test post 100kPa consolidation. Referring to **Table 6–5**, the triaxial results have a much lower permeability value than the field tests. Heuer (2017) states this may be due to lateral dispersion and the soil not being fully saturated at the time of measurement readings. Other possible reasons may be sample disturbance when retrieving, transporting and cutting of the sample, the isotropic consolidation caused a much more denser packing of grains or the sample tested had greater clay content. When the samples were cut for triaxial, many samples disintegrated due to the friable nature of the soil. The samples that maintained

structure, and ultimately used for testing, may have been from pockets of the reworked material that contained a greater clay content than the ones that disintegrated.

Majority of the other samples tested had unsaturated hydraulic conductivity (unsaturated K) values in the order of $x10^{-5}$ m/s, typical of a silty soil. The Doornhoek sample had undisturbed triaxial and remoulded column K values in the same order of magnitude ($x10^{-6}$). The fabric didn't influence the unsaturated K value for this particular sample and suggests the grading, and added impurities when reworked, influences the change in permeability for non-structured wad.

The erosion tests were successfully conducted on the Highveld, R533, Doornhoek and Bokkraal samples. The initial influx of water caused a uniformed wetting front to descend through the material all of the tested samples. A capillary barrier perching formed in the samples at the bottom opening of the column, similar to the findings of Brouwers & Dippenaar (2018). The capillary barrier held the soil and water in place until a sufficient increase in saturation caused the water to flow, and mobilise material due to dissipation of surface tension, out the bottom of the column. The material within the column underwent very little to no rearrangement of grains during the test for all samples.

The amount of material that mobilised out of the column during an increase in hydraulic head above the opening is dependent on the degree of change of moisture in the system, before and after the influx of water, and the rate of hydraulic head increase. The majority of the material that mobilised out of the column, irrespective of type of scenario, did so during the initial stages after the hydraulic head increase occurred, followed by an extensive period of clear water flow and zero material erosion. The cause of this intense initial erosion period may be explained using a theory explained by Tharp (1999; 2003). During the initial influx of water, an even wetting front slowly moves down the column and forms a capillary barrier at the opening and no material erodes. The wetting front moves slowly as the material has a low degree of saturation, therefore a low unsaturated hydraulic conductivity (K) value. During the subsequent hydraulic head increases, the material throughout the column has a greater degree of saturation and a greater unsaturated K value is expected. The greater unsaturated K value allows the new wetting front to move down faster than previously. Applying Tharp's (1999; 2003) theory of high pore pressure gradients across the wetting front, the majority of the pressure head drop occurs just behind the wetting front. As the wetting front reaches the column opening, the pressures behind the wetting front will be sufficient to cause the material to loss cohesion, due to dissipation of the surface tension, and results in mobilisation of the material. After a short period of time, the high pore pressure at the bottom opening diminish

due to the material drying out as air enters the column through the slot. The reduction in saturation causes the surface tensions to increase and a capillary barrier reforms, holding the soil in place until the next water influx. The speed at which the wetting front moves down the column and intensity of the head drop behind the wetting front is believed to increase as the rate of increase in hydraulic head increases.

The amount of material that mobilises is greater as the disparity in degree of saturation below and above the wetting front increases. This is indicated in the results as larger amounts of material eroded out of the column during the initial water influx when the material was initial air dried. The same conclusion was made by Tharp (1999; 2003) and this theory is observable in nature, as sinkhole formation is associated with modest rain after a long drought period (Gertje & Jeremais, 1989; Sower, 1975). The mobilisation potential increases as the grading tends to a well-sorted silty soil, especially if the inherent structure has been destroyed, as noted by Buttrick (1986), by mechanical means with no added impurities.

The low mass mobilised out of the Highveld sample for scenarios 4 and 5 may be due to the 12-hour dry out period not being sufficient, as the material is expected to retain moisture more than the other samples, and the difference in moisture above and below the column may not have been so great. Furthermore, the material dried out enough as to not allow the wetting front to reach the opening before the pore pressure difference above and below the wetting front dissipated.

7.6. SWRC

The tested sample material exhibited curves that are typical of fine-grained clayey to silty material and all the curves tend to the same values between 40% and 60% saturation. Referring to **Chart 6–2**, curves show well-defined Capillary Regime where the material is saturated with negative pore pressures (vertical line). The Doornhoek and structured Highveld samples developed well define AEV before entering the Funicular Regime. During all of the tests, the PTPs cavitated before entering the Pendular Regime.

Three (3) Doornhoek samples were tested at different packed densities, all expressing similar curves typical of a fine material (**Chart 6–4**). The difference in densities of the material was not significant (Loose = 702 kg/m^3; Medium = 753 kg/m^3; Dense= 809 kg/m^3) due to the inability to achieve denser packing with a small sample, resulting in nearly identical curves. The material has an AEV of approximately 20kPa and generally loses 234 kPa of suction between 40% and 80% degrees of saturation. The curves are typical of a clay

material; however, the material only possesses 4% clay. The influence of the extremely large surfaces area of the metal oxides present in the material, as discussed in **Section 3.3.**, may cause the material to follow such a curve.

A big variation of the curves occurs between the structured and remoulded Highveld curves, as shown in **Chart 6–3.** The Highveld sample with the in-situ fabric still intake has a well-defined, vertical, Capillary Regime and AEV that flattens out in the Funicular Regime. The inherent fabric material was able to achieve a moisture content value of 300% during saturation (**Table 6–7**). The remoulded sample does not have a well-defined AEV and does not exhibit a distinct vertical curve. The remoulded material, with no inherent structure present, was only able to achieve a moisture content value of 87,6%. The AEV of the curves are approximately 20 kPa and 0,8 kPa for structured and remoulded, respectively. The curves do tend to the same shape and value at lower degrees of saturation (~40%). The significant difference between the two curves is the change in suction pressure across the same change in degree of saturation. A change in the degree of saturation from 40% to 90% results in a 146 kPa and 113 kPa lose for the remoulded and structured sample respectively. The difference between the suction pressures at 90% degree of saturation is approximately 33 kPa, with the remoulded sample only obtaining roughly 2 kPa of suction. This indicates that the structured fabric of wad greatly influences the suction pressure in the material at variable saturations. The variation of suctions and the implications thereof, namely the material strength and material mobilisation potential at variable saturations, may divulge insight as to why material found in sinkholes are generally powdery to highly reworked.

8. General Discussion

Wad and residual dolomite are regarded as complex materials to identify and work with when attempting to develop a geological model from its geotechnical properties. Firstly, retrieving a representative sample is difficult due to the variability of the sample material and the random weathering patterns of the parent rock. The residual material is extremely old and vast areas have undergone different degrees of alteration throughout the millions of years of it being present. This results in wide disparities and varying chemical and physical make-ups that has led to challenges when identifying the various material constituents, especially the individual minerals. As shown in this study, the XRD method to identify the mineral constituents proved difficult when working a unique material such as residual dolomite and wad. The use of XRD combined with SEM proved to be sufficient analysing techniques to identify the minerals, especially the metal oxides.

Secondly, preparing an undisturbed sample for testing, be it cutting a block sample or extruding sample from a Shelby tube, the material, especially wad, is friable and tends to disintegrate and crumble along primary and secondary features. The Galena present in the fissures of the Bokkraal sample caused difficulties during the preparation of the sample for the triaxial cell. Lead deposits found in dolomite series of the Transvaal system can be divided into four main groups: *Southern lead-zinc belt* in the south-western Groot Marico lead deposit (Bokkraal and Doornhoek mines belong to this group), *Hennops-Crocodile River Area* southwest of Pretoria, *Northern lead belt* and *Crocodile river fragment* (Hammerbeck, 1976). It should be noted when sampling in these locations that the wad may be highly fissured with galena, and possibly other ore, therefore special care must be taken to avoid the ore stringers and inclusions.

Thirdly, the material behaviour is highly dependent on the entirety of the reworking process and environment. The Mooiplaas sample's dry density values are higher, and void ratio being the lowest, than any other material in this study (**Table 6–6**). The material was retrieved from a narrow gryke, about 1,5 metres wide, and is highly reworked, determined to be the most reworked sample. This is evidential in the microstructure photos, **Figure 6–** and the composition of the sample as it contains a high amount of chert and quartz grains that contribute to the higher density and the highest SiO_2 weight% and lowest liquid limit. The Sudwala cave sample is gap-graded and contains the highest Al_2O_3 weight%. The humid weather and position, near the crest of a hill, of the sample location resulted in the material undergoing more chemical reworking and addition of mainly gravel sized particles. This resulted in the material having lower than expected liquid limit even though it has relatively

high metal-oxide and fines percentages. The Doornhoek sample exhibits non-structured wad fabric and the Highveld sample is characterised as structured wad, therefore has not been thoroughly reworked, and both represent low dry densities and SiO_2 weight% values and high Fe- and Mn-oxide contents and the highest void ratios. The microscopy images reveal that the material retained the original fine grading and nanoscopic needle and coral type structure of the metal oxides. The reworking process and environment clearly plays a major role in the mechanical properties and geochemical content of the sample material.

Referring to **Chart 8–1**, a general trend is evident between the metal oxide content and the liquid limit of the same material. The scatter along the trend line is due to the liquid limit being dependent on other factors, namely the grading. Referring to **Chart 8–2**, the liquid limit is significantly more influenced by the silt-sized particle content than the presence of finer clay-sized particles. As previously stated, the metal oxides, namely Mn-oxides, generally occur as silt-sized aggregates in nature and results in the two trends, in **Chart 8–1** and **Chart 8–2**, being very similar. The presence of the large surface area of the silt-sized metal oxide aggregates allows the material to take up vast amounts of water before a behavioural change occurs.

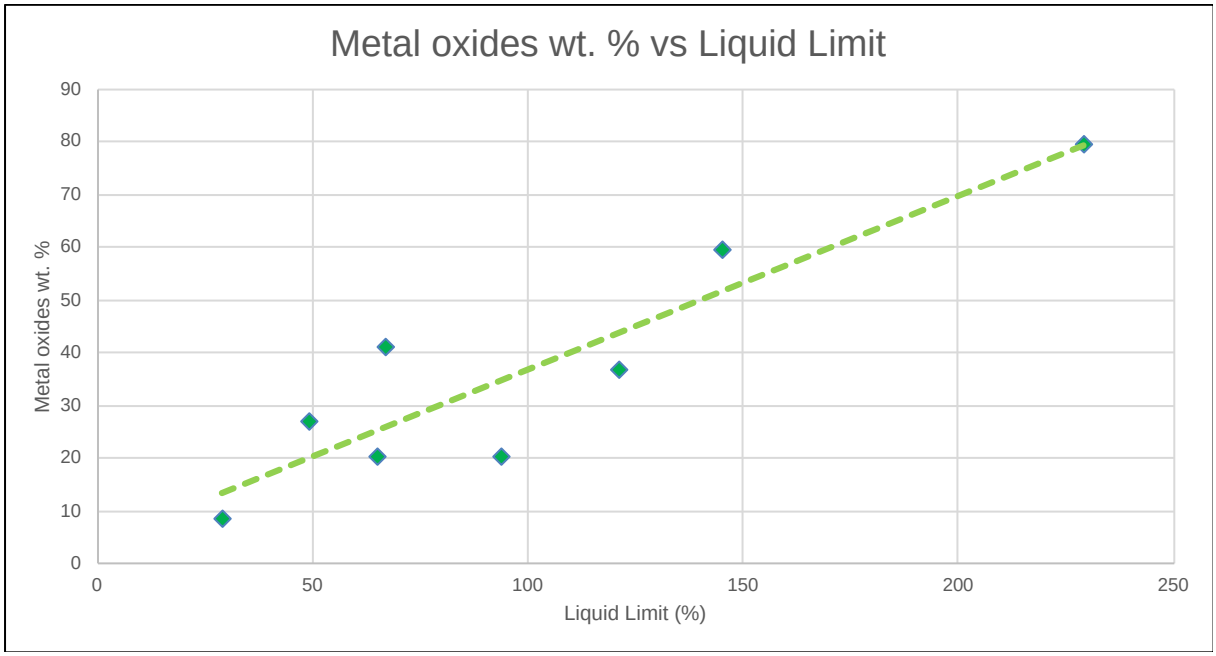

Chart 8–1: Metal oxide content of tested material plotted against the liquid limits of the researched material with trendline added.

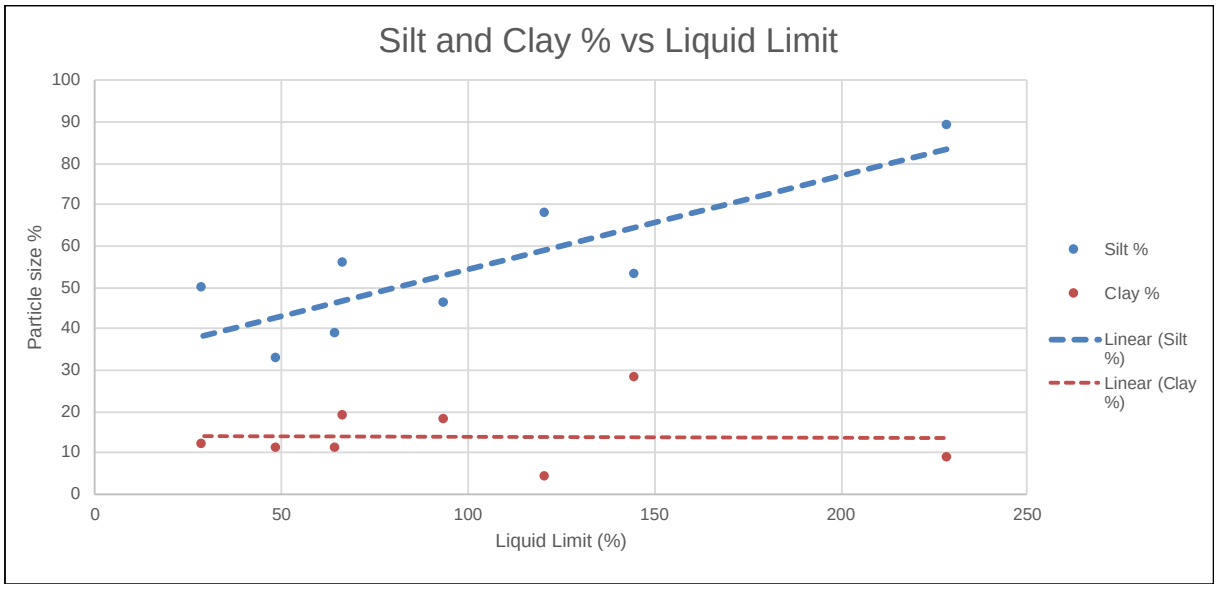

Chart 8–2: The percentages of silt and clay particle sizes plotted against the liquid limit of the researched material.

Another important factor of typical wad material is the inherent parent fabric of the material, as discussed by Day (1981) and Buttrick (1986). In this study, it can be seen that the fabric plays an important role in the water holding capacity and unsaturated behaviour of the material. The Highveld sample, with its highly voided, low density, structure intact, was able to take up a greater mass of water compared to the same material after the inherent structure was mechanically broken down. The structure allows the material to sustain higher suction pressures at high degrees of saturation, compared to the same material at a higher density packing after being remoulded. Breaking down of the structure will therefore cause inadequacies in particle to particle friction and suction strength and increase the material's mobilisation potential.

The consequences from the process of reworking the material of interest in this study can be stated as follows. The mechanically reworking process causes the material fabric to break down or compress over time. The breaking down of the initially highly voided material will cause a reduction in the overall volume, resulting in a relative decrease of the void ratio. The fines percentage and metal oxide content of the material undergoes a relative decrease as the space taken up by the original volume is occupied by foreign material, usually chemically stable, coarse-grained, SiO_2 particles and common clay minerals. Other additions into the soil, such as dissolved ions in water flowing through the primary or secondary structures or interstitial pore spaces, during the reworking process also chemically alters the material, whereby morphing the original metal oxide's and other constituent's crystal structure towards an amorphous or transformed state, consequentially changing the material colour towards a

reddish-brown appearance. The reworking process results in a relative decrease in the reactive surface area available for water molecules and increases the relative surface area of inert material, resulting in generally lower liquid limits. The addition of material is dependent on the surrounding environment; therefore, the reworking environment is important to note when describing wad or residual dolomite as the behaviour of the material will be influenced by it. It is evident that the entirety of the reworking process, such as the degree, type and environment of reworking, needs to be clarified to fully understand the behavioural characteristics of the material. The reworking process is especially important when evaluating risk of sinkhole formation as the material around these surface openings are generally reworked.

Mobilisation potential of material is dependent on the difference in the degree of saturation below and above the approaching wetting front towards a soil cavity arch or column opening. As found in this study, and suggested by previous authors, this may elucidate the triggering mechanism of sinkhole formation after long drought periods or when water flow has been recently rerouted to congregate to previously dry area. The rate in which the head increases was a factor in the mobilisation of the material in the column. This may demonstrate the triggering mechanism for sinkhole formation once a large pipe bursts, causing a relatively large hydraulic head to form above the soil cavity.

The high liquid limits exhibited in certain wad materials are dependent on the nanoscopic particle structure, the fine-grained nature of the material, and the presence of large reactive surface areas exhibited by the metal oxides, whereas the in-situ water holding capacity and the unsaturated soil behaviour of the material is partly influenced by the aforementioned factors, but mainly depends on the fabric of the material.

Table 8–1 and **Table 8–2** summaries results from this and previous studies for quick reference and comparison of material properties.

Table 8-1: Summary of properties of wad and residual dolomite

Author / Report	Fabric	Grading (%)				Dry density (kg/m^3)	Dispersiveness	PI (%)	LL (%)	e	SG (g/cm^3)	Permeability (m/s)
		Clay	Silt	Sand	Gravel							
Brink (1979)	-	<29	-	-	-	285 - 722	-	5-28	47-96	2,7-9,6	1,63-3,47	-
Day (1981)	Structured or Intact and; non-structured or Reworked	30	50	22	-	225 - 1327	-	14-27	61-125	-	-	-
		Clayey silt to silty clay										
Jones and Wagener (1981)	-	29	49	21	1	225 - 1327	-	10-29	61-125	1,1-11,2	2,9	-
		Clayey silt										
Jones and Wagener (1982)	-	Clayey silt to sandy silt				253 - 1481	-	15-23	40-135	-	-	-
Wagener (1982)	Intact (structured)	Clayey silt				225 - 1481	Not dispersive	-	-	0,9-11,2	-	High
	Powdery (non-structured)											
De Beer (1985)	-	11-60	-	-	-	273 - 1558	-	5-27	49-126	0,3-8,9	-	-
		Clayey silt										
Hawkins et al. (1986)	Laminated	-				500 - 600	-	18	71	-	-	-
Buttrick (1986)	Laminated or Structured	48	-	-	-	220 - 1221	Not to slightly dispersive	3-26	28-113	1,3-16,6	2,2-3,1	Very low to intermediate
		Clayey silt to sandy silty clay										
	Massive or Non-Structured	Sandy clayey silt				406 - 1516		11-27	27-136	0,9- 6,2	1,94-3,0	Very low to low
Bear Geoconsultants (2016)	"pure" wad (Non-structured or Structured)	-				576 - 1075	Not dispersive	10-40	57-93	2-12	-	$1,5x10^{-6}$ - $1,2x10^{-8}$
Swart	Structured	9	89	2	0	309	Not dispersive (but erodible)	8	229	8,32	2,28-2,86	-
	Non-Structured	4-28	53-68	11-23	5-8	593		33	121-145	3,87	1,79-2,89	$2,7x10^{-6}$
	Reworked wad	11-12	33-50	20-45	11-18	898 - 1751		12-17	29-94	0,55-2,07	2,72-2,93	$9,0x10^{-7}$ - $2,0x10^{-5}$
		Dependent on origin, type and degree of reworking, and environment										
PI - Plasticity Index; LL - Liquid Limit; e - void ratio; SG - specific gravity												

Table 8-2: Summary of properties of wad and residual dolomite

Author / Report	Fabric	Grading (%)				Dry density (kg/m^3)	Triaxial			
		Clay	Silt	Sand	Gravel		Structured	Non-Structured	Reworked	Not Specified
Brink (1979)	-	<29	-	-	-	285 - 722	-	-	-	-
Day (1981)	Structured or Intact and; non-structured or Reworked	30	50	22	-	225 - 1327	ϕ' = 22° c' = 55 kPa ϕ = 18° c = 59 kPa	-	-	-
		Clayey silt to silty clay								
Jones and Wagener (1981)	-	29	49	21	1	225 - 1327	ϕ' = 24,1° - 25,4° c' = 23 - 51 kPa ϕ = 17,1 - 18,6° c = 30 - 48 kPa	-	ϕ' = 20,9° c' = 63 kPa ϕ = 14,7° c = 74 kPa	ϕ' = 17,1° c' = 40 kPa ϕ = 17,1° c = 48 kPa
		Clayey silt								
Jones and Wagener (1982)	-	Clayey silt to sandy silt				253 - 1481	-	-	-	-
Wagener (1982)	Intact (structured)	Clayey silt				225 - 1481	-	-	-	-
	Powdery (non-structured)									
De Beer (1985)	-	11 - 59,6	-	-	-	273 - 1558	-	-	-	ϕ = 26° c = 40 kPa
		Clayey silt								
Hawkins et al. (1986)	Laminated	-				500 - 600	-	-	-	-
Buttrick (1986)	Laminated or Structured	48	-	-	-	220 - 1221	ϕ' = 21° - 25° c' = 23 - 63 kPa ϕ = 15° - 19,3° c = 26 - 74 kPa	ϕ' = 23° - 29° c' = 4,0 - 53 kPa ϕ = 21,5° - 33,3° c = 1,0 - 65 kPa	-	-
		Clayey silt to sandy silty clay								
	Massive or Non-Structured	Sandy clayey silt				406 - 1516				
Bear Geoconsultants (2016)	"pure" wad (Non-structured or Structured)	-				576 - 1075	-	-	-	ϕ = 16,9° - 28° c = 20 - 61 kPa
Swart	Structured	9	89	2	0	309	-	-	ϕ' = 14,2° c' = 6,5 kPa	-
	Non-Structured	4 -28	53 - 68	11 - 23	5 - 8	593				
	Reworked wad	11 - 12	33 - 50	20 - 45	11 - 18	898 - 1751				
		Dependent on origin, type and degree of reworking, and environment								

9. Conclusion

The fabric of wad is inherent to the structure of the parent rock, which is determined by the stress history of the rock. The fabric influences the unsaturated behavioural characteristics and water holding capacity of the material. The high and variable liquid limits is dependent on the overall fine grading and the nanoparticle structure and large reactive surfaces exhibited by the metal oxides in the material. The material of interest in this study is considered reworked when mechanical processes destroy the structured or non-structured inherent fabric and foreign material is introduced into the soil matrix. The factors influencing the consequential broad potential behavioural and characteristic properties of the material, due to the reworking processes, are the type and degree of reworking and the environment of reworking. The presence of ore metal and the variable nature of the material further complicates representative sampling and modelling of the material.

9.1. Main findings

The major findings of interest in this study are as follows:

1) Identifying mineral constitutes in residual dolomite is not possible using the XRD method alone. The need for XRF analysis, coupled with SEM, are required to identify the presence of Mn- and Fe-oxides.

2) The presence of metal ores present in residual dolomite fabric increases variability, geological modelling and testing of the material.

3) The residuum is not typically dispersive, has low density that can be below that of water, mostly grades in the silt fraction and has hydraulic conductivities in the order of $1x10^{-6}$ m/s.

4) The inherent fabric present in the residual dolomite is the major influencer of the water holding capacity and unsaturated soil behaviour.

5) The high and variable liquid limits found in residual dolomite is dependent on the overall fine grading of the material, and the nanoparticle structure and large reactive surfaces exhibited by the metal oxides constituents. The main factor controlling the extremely high liquid limits are the presence of the metal oxides. The material usually possesses high plasticity indices.

6) The reworking of the material effects the colour, the unsaturated soil behaviour, lowers the water holding capacity and lowers the initially high liquid limits. The process increases the density by destroying the initially highly voided inherent fabric, by introduction of usually high density inert SiO_2 material and causes the metal oxides' crystal structure to tend towards an amorphous state reducing the reactive, originally large, surface area.

7) The mobilisation potential is dependent on the presence of the fabric and variance of sorting of the material's grain sizes. The breaking down of the inherent structure of typical wad, and as the grading tends to a well-sorted silt, the mobilisation potential of the material will increase. The material will undergo more erosion if the disparity of the degree of saturation above and below the wetting front increases and the presence of a rapidly increasing hydraulic head from which the wetting front formed.

8) The term 'wad' which was original used to describe an earthy, black, manganese ore, is misused in most cases within, but not limited to, South Africa. The misuse of the term 'wad' is due to the qualitative attributes given in the definition, being dark gun blue, stains fingers black, fine-grained material. The material is known to be enriched in manganese though Buttrick (1986) found the iron content is generally double the manganese content in a typical non- to slightly reworked wad. This ambiguous definition may result in material being misinterpreted or incorrectly described. The following definitions are proposed:

Wad:

Dark, gun blue to purple, stains fingers purple to black, clayey silt with minor sand or gravel, enriched in metal oxides with Fe (w%) ≤ Mn (w%) and Fe2O3 (w%) ≤ MnO_2 (w%) and SiO2 < 50 w%, insoluble material formed from leaching of manganese-rich dolomite and is divided into two groups assessed on the fabric, being structured or non-structured wad, partly powdery to partly indurated, with a spongy to brittle behaviour, a low density and a high void ratio, and a nearly unnoticeable weight in hand specimen when sample is free of ore metals. The material mobilisation potential is lower if the structure is present.

Residual dolomite:

Dark reddish brown, stains fingers dark brown, intact or massive, sandy silt to silty sand with minor gravel or clay that is enriched in SiO_2 (>50 w%), in the form of chert and/or quartz particles, with Fe (w%) ≥ Mn (w%) and Fe_2O_3 (w%) ≥ MnO_2 (w%); insoluble material formed from weathering of chert-rich dolomite, or formed from the mechanical reworking of wad through the addition of impurities and break down of the original fabric to a degree where the open and relict structure and brittle to spongy behaviour is lost, and the density increases to a noticeable weight in hand specimen.

9.2. Limitations and assumptions

The study included samples across a large area of research to factor in weather, topography and formation differences, however the variability of residual dolomite across small distances remains an implausible obstacle to overcome and the future geological model will always include basic understanding, as present in this study, coupled with certain assumptions of the material and the surround environment. The difficulty in gaining material with desired properties, such as structure intact and completely non-reworked samples, resulted in this study having limited testing material, though the author believes sufficient testing and research from previous studies justifies the interpreted conclusions made.

9.3. Way forward

The effect of variability of the material on the mobilisation potential is to be looked at on a large-scale testing rig, such as a centrifuge. The model should include different degrees of reworked material with defined boundaries between a non-reworked structured and highly reworked material, to assess the mobilisation potential on the plane of the structure material, similar to scenarios of saturation increases along a dolomite pinnacle surface.

10. Acknowledgments

The completion of this undertaking could not have been possible without the participation and assistance of so many people whose names may not all be enumerated. Their contributions are sincerely appreciated and gratefully acknowledged.

The author would like to express his deep appreciation and indebtedness particularly to the following:

The Water Research Commission for funding the entirety of this Masters.

Ilse Kleinhans for her deep knowledge and enthusiasm shared and for allowing me to sample material from and study various invaluable sinkhole sites.

Bronwen Klaas for taking time out of her day to discuss and share her knowledge of dolomite sites.

Deon Bester and Tony A'Bear for samples and knowledge they provided throughout the duration of the masters.

Prof. SW Jacobsz for opening up time in his busy schedule, allowing me to use the tensiometers in this study and sharing with me his deep understanding of unsaturated soil mechanics and dolomite residuum.

My co-supervisor, Dr. Matthys Dippenaar, for his incredible knowledge and his support, keenness and motivation from my undergrad studies up and till the very last week of my Dissertation write up. The trips to Dinokana, late nights in Tallies and the Kalahari, to nearly getting lost in a dolomite cave will always be cherished in my memories.

My supervisor, Prof. Louis van Rooy, for his unwavering support and numerous opportunities to learn and grow as an Engineering Geologist and for the knowledge and tools instilled in me that go far beyond the scope of this Masters. I will forever be grateful for the Botswana, Sabie and Clarens trips and the for the always appropriate 'grappies', be it early morning site visits or late night camp fires.

My family, friends and loved ones, for their undying support and motivation to undertake and finish this Dissertation.

11. Bibliography

Barbour, S., & Fredlund, D. (1989). Mechanics of osmotic flow and volume change in clay soils. *Canadian Geotechnical Journal, 26*, 551-562.

Bear Geoconsultants. (2016). *Report on dolomite stability and geotechnical investigation for the proposed township of Monavoni Extension 11.* Report J15-132/3. Prepared for M&T Development.

Bester, D., A'Bear, A., & Day, P. (2017). A Review of the Geotechnical Properties of Wad from the Oaktree Formation in Centurion, South Africa. *9th South African Geotechnical Engineers Conference* (pp. 375 - 383). Salt Rock: SAYGE.

Beukes, N., Niekerk, H., & Gutzmer, J. (1999). Post Godwana African land surfaces and pedogenic ferromanganese deposits on the Witwatersrand at the West Wits Gold Mine, South Africa. *S. Afr. J. Geol., 102*(1), 65-82.

Bishop, A. W. (1959). The principle of effective stress. *Teknisk Ukeblad*, 859-863.

Borggaard, O. (1983). Effect of surafce area and mineralogy of iron oxides on thier surface charge and anion-adsorption properties. *Clays and Clay Minerals, 31*(3), 230-232.

Brink, A. (1979). *Engineering Geology of Southern Africa* (Vol. 1). South Africa: Building Publications.

Brink, A. (1996). Mechanism of Sinkhole and Doline Formation. *Dolomite Seminar.* University of Pretoria.

Brouwers, L., & Dippenaar, M. (2018). Partially saturated flow from sand into discrete smooth open vertical fracture at the soil-rock interface: experimental studies. *Bull. Eng. Geol. Environ.*

Bruins, J. (2016). Manganese removal from groundwater: Role of biological and physico-chemical autocatalytic processes. *Dissertation at Delft University of Technology*.

Burland, J. (1965). Some Aspects of the Mechnical Behaviour of Partly Saturated Soils. In G. Aitchison (Ed.), *Moisture Equilibria and Moisture Changes in Soils Beneath Covered Areas: A Symposium in Print* (pp. 270-278). London: Butterworths.

Burns, R., & Burns, V. (1977). Mineralogy. In G. Galsby (Ed.), *Marine Manganese Deposits* (pp. 185-248). Amsterdam: Elsevier .

Buser, W., & Graf, P. (1955). Differenzierung von Mangan(II)-manganite und S-Mn02 durch Oberflächenmessung nach. *Brunauer-Emmet-Teller. Helv. Chim. Acta, 38*, 830-834.

Buttrick, D. B. (1986). Wad and Ferroan Soil Developed in the Dolomitic Area South of Pretoria. *MSc (University of Pretoria)*.

Buttrick, D., Van Schalkwyk, A., & Kleywegt, R. (2001). Proposed method for dolomite land and hazard and risk assessment in South Africa. *Journal of SAICE, 42*(2), 27-36.

Chen, H., Chu, P., He, J., Hu, T., & Yang, M. (2011). Porous magnetic manganese oxide nanostructures: Synthesis and their appplication in water treatment. *Journal of Colloid and Interface Science, 359*, 68-74.

Cheney, M., Bhowmik, P., Moriuchi, S., Villalobos, M., Qian, S., & Joo, S. (2008). The Effect of Stirring on the Morphology of Birnessite Nanoparticles. *Journal of Nanomaterials*.

Cho, G., & Santamarina, J. (2001). Unsaturated particulate materials - Particle-level studies. *Jounral of Geotechnical and Geoenvironmental Engineering, 127*(1), 84-96.

Constantinou, S., & van Rooy, J. (2017). *Sinkhole and subsidence size distribution across dolomitic land in Gauteng.* University of Pretoria.

Day, P. W. (1981). Properties of Wad. *Seminar on Engineering Geology of Dolomite Areas* (pp. 135-147). Pretoria: University of Pretoria.

De Beer, J. (1985). Investigation of a Site with Extensive Occurrences of Wad. *Proceedings of Problem soils in South Africa*.

De Villiers, J. (1960). *The manganese Deposits of the Union of South Africa.* Pretoria: Goverment Printer.

Dippenaar, M. (2012). How we lose ground when earth scientists become territorial: defining "soil". *Nat. Resource. Res., 21*(1), 137-142.

Dippenaar, M. (2014a). Towards hydrological and geochemical understanding of an ephemeral palustrine perched water table "wetland" (Lanseria Gneiss, Midrand, South Africa). *Environ. Earth Sci., 72*(7), 2447-2456.

Dippenaar, M. (2014b). Towards a multi-faceted Vadose Zone Assessment Protocol: cemetery guidelines and application to a burial site located near a seasonal wetland (Pretoria, South Africa). *Bull. Eng. Geol. Environ., 73*(4), 1105-1115.

Dippenaar, M., & van Rooy, J. (2014). Review of engineering, hydrogeological and vadose zone hydrological aspects of the Lanseria Gneiss, Goudplaats-Hout River Gneiss and Nelspruit Suite Granite (South Africa). *J. Afr. Earth Sci., 91*, 12-31.

Dippenaar, M., & van Rooy, J. (2018). Vadose Zone Characteristics for Hydrogeological and Geotechnical Applications. *IAGE/AEG Annual Meeting Proceedings, San Francisco, California, 2*, pp. 63-67.

Dippenaar, M., van Rooy, J., & Diamond, R. (2018). Engineering, hydrological and vadose zone hydrological aspects of Proterozoic dolomites (South Africa). *African Earth Sciences*.

Dippenaar, M., van Rooy, J., Breedt, N., Huisamen, A., Muravha, S., Mahlangu, S., & Mulders, J. (2014c). *Vadose Zone Hydrology: Concepts and Techniques* (Vol. TT 584/13). Water Research Commision.

Dixon, J. (1988). Todorokite, birnessite and lithiophorite as indicator minerals in soils. *Manganese Symposium.* Adelaide.

Dowding, C., & Fey, M. (2007). Morphology, mineralogy and surface chemistry of mangaiferous oxisols near Graskop, Mpumalanga Province, South Africa. *Geoderma, 141*, 23-33.

Eriksson, P., & Altermann, W. (1998). An overview of the geology of the Transvaal Supergroup dolomites (South Africa). *Environmental Geology , 36*, 179-188.

Eriksson, P., Altermann, W., & Hartzer, F. (2006). The Transvaal Supergroup and Its Precursors. In *Geology of South Africa* (pp. 237 - 260). Pretoria: Geological Society of South Africa.

Fitts, C. (2002). *Groundwater Science.* London: Academic Press.

Fredlund, D. (2017). Role of the Soil-water Characteristic Curve in Unsaturated Soil Mechanics. *Proceedings of the 19th International Confernce on Soil Mechanics and Geotechnical Engineering*, (pp. 57-80). Seoul.

Fredlund, D. G., & Rahardjo, H. (1993). *Soil Mechanics for Unsaturated Soils.* John Wiley & Sons, Inc.

Fredlund, D. G., Rahardjo, H., & Gan, J. (1978). Non-linearity of strength envelope for unsaturated soils. New Delhi; Rotterdam; Balkema: Proceedings, 6th International Conference of Expansive Soils.

Fredlund, D., & Morgenstern, N. (1977). Stress state variables for unsaturated soils. *Journal of Geotechnical Engineering Division, 103*(GT5), 447-466.

Fredlund, D., Rehardjo, H., & Fredlund, M. (2012). *Unsaturated Soil Mechanics in Engineering Practice.* John Wiley & Sons, Inc.

Gaspar, T. (2017). *INVESTIGATING THE TENSILE BEHAVIOUR OF UNSATURATED SOILS USING THE BRAZILIAN DISC TEST .* University of Pretoria. Unpublished.

Geologists, C. f. (2003). *Guideline for engineering geological characterisation and development of dolomitic land.* Council of Geoscience Publication.

Gertje, H., & Jeremais, A. (1989). "Building construction over an erosive sinkhole site: A case study in Lancaster County, Pennsylvania, USA.". *Proc. 3rd Multidisciplinary Conf. On Sinkholes and the Engineering and Environmental Impacts of Karst.*, 311-318.

Golden , D., Dixon, J., & Kanehiro, Y. (1993). The manganese oxide mineral, lithiophorite, in an oxisol from Hawaii. *Australian Journal of Soil Research, 31*, 51-66.

Gotić, M., Jurkin, T., Musić, S., Unfried, K., Sydlik, U., & Bauer-Šegvić, A. (2012). Microstructural charaterizations of different Mn-oxide nanoparticles used as models in toxicity studies. *Journal of Molecular Structure, 1004*, 248-254.

Greathouse, J., Johnson, K., & Greenwell, H. (2014). Interaction of Natural Organic Matter with Layered Minerals: Recent Developments in Computational Methods at the Nanoscale. *Minerals, 4*, 519-540.

Hammerbeck, E. (1976). Lead. In C. Coetzee (Ed.), *Mineral Resources of the Republic of South Africa* (5th ed., pp. 159 - 164). Pretoria: Geological Survey.

Hawkins, Hawkins, & Osborn. (1986). *A Geological Investigation and Geotechnical Appraisal of Subsurface Conditions in Tokoza.*

Hawkins, L., & Thompson, J. (1988). Weathering Sequence and Alteration Products in Genesis of the Graskop Manganese Residua, Republic of South Africa. *Clays and Clay Minerals, 36*(5), 448-454.

Herman, J. (2012). Water Chemistry in Caves. In W. White, & D. Culver (Eds.), *Encyclopedia of Caves* (2nd Edition ed., pp. 881-887). Elsevier.

Heuer, S. (2017). Vadose Zone hydrological characterisation of resdiual dolomite (Malmani Subgroup, Gauteng). *(Unpublished Honours Project at the University of Pretoria)*.

Hunter, R. (2001). *Foundations of colloid science.* Oxford. Oxford Univ Press.

Imam, S., Maghvan, S., & Saaly, M. (2016). Parameters affecting soil-water characteristics curves of unsaturated soils. *5th International Conference on Geotechnical Engineering and Soil Mechanics.* Tehran: Iranian Geotechnical Society.

Jacobsz, S. (2016). Trapdoor experiments studying cavity propagation. Pretoria: Proceedings of the first Southern African Geotechnical Conference.

Jacobsz, S. (2018). Low cost tenisometers for geotechnical applicators. *Proc of 9th International Conference on Physical modelling in Geotechnics* (pp. 305-310). CRC Press.

Janssen, D., & Dempsey, B. (1980). Soil-moisture properties of subgrade soils. *Sixtieth Annual Transportation Research Board Meeting*.

Jenne, E. (1968). Trace Inorganics in Water. *ACS Advances in Chemistry Series, 73*, 337-387.

Jennings, J. E., & Burland, J. (1962). Limitations to the use of effective stresses in partly saturated soils. *Géotechnique, 12*(2), 125-144.

Jiang, S., Kim, D., Kim, J., & Ko, S. (2010). Characterization of the Biogenic Manganese Oxides Produced by Pseudomonas Putida strain MnB1. *Environmental Engineering Research, 15*(4), 183-190.

Jindal, P. (2016). *Effect of pore-water surface tension on tensile strength of unsaturated sand.* Thesis, York University , Earth and Space Science , Toronto.

Jones and Wagener. (1981). *Geotechnical Assessment of Proposed Township on Dolomite. Rooihuiskraal Extension, Verwoerdburg.*

Jones and Wagener. (1982). *Geotechnical Investigation for Township Development North of Krugersdorp/Pretoria Freeway on Farm Brakfontein.*

Kim, T., & Hwang, C. (2003). Modeling of tensile strength on moist granular earth material at low water content. *Engineering Geology, 69*(3), 233-244.

Kleinhans, I., & van Rooy, J. (2016). Guidelines for sinkhole and subsidence rehabilitation based on generic geological models of dolomite environment on the East Rand, South Africa. *Journal of Earth Sciences, 177*, 86-101.

Knappett, J. A., & Craig, R. F. (2012). *Craig's Soil Mechanics* (8th Edition ed.). New York: Spon Press.

Lu, N., & Likos, W. (2004). *Unsaturated Soil Mechanics .* Hoboken, New Jersey: John Wiley & Sons, Inc.

Lu, N., Kim, T.-H., Sture, S., & Likos, W. (2009). Tensile stregnth of unsaturated Sand. *Journal of Engineering Mechanics, 12*(135), 1410-1419.

Maharaj, A. (2013, May). The Evaulation of Test Protocols for Dispersive Soil Identification in Southern Africa. *Master Dissertation, University of Pretoria*.

McKenzie, R. (1972). The Manganese Oxides in Soils - A Review. *Journal of Plant Nutrition and Soil Science, 131*(3), 221 - 242 .

McQueen, I., & Miller, R. (1974). Approximating soil moisture characteristics from limited data: empirical evidence and tentative model. . *Water Resource Research*(10), 521-527.

Myre, E., & Shaw, R. (2006). *The Turbidity Tube: Simple and Accurate Measuement of Turbidity in the Field.* Michigan Technological University, Department of Civil and Environment Engineering. Michigan Technological University.

Ng, C., & Menzies, B. (2007). *Advanced Unsaturated Soil Mechanics and Engineering.* London: Taylor & Francis.

Nguyen, D., Tran, Q., Trinh, X., Hoang, T., Nguyen, H., & Nguyen, H. (2012). Crystallization and magnetic properties of amorphous iron-chromium oxide nanoparticles synthesized by sonochemisty. *Adv. Nat Sci.: Nanosci. Nanotechnol., 3*.

Obbes, A. (1995). The Structure, Stratigraphy and Sedimentology of the Black Reef-Malmani-Rooihoogte Succession of the Transvaal Supergroup South-West of Pretroia. *Master Thesis, Rand Afrikaans University*.

Oosthuizen, A., & Richardson, S. (2011). *Sinkhole and Subsidence in South Africa.* Council for Geoscience. Council for Geoscience.

Perdial, J., Thompson, A., & Chorover, J. (2015). Chapter 6 -Soil Geochemistry in the Critical Zone: Influence on atmosphere, surface- and groundwater composition. *Developmetns in Earth Surface Processes, 19*, 173-201.

Post, J. (1999). Manganese oxide minerals: Crystal structures and economic and environmental significance. *Proc. Natl. Acad. Sci. , 96*, 3447-3454.

Post, J., & Bish, D. (1988). Reitveld refinement of the todorokite structure. *American Mineralogists, 78*, 861-869.

Reed, B., Smith, M., & Shaw, R. (2017). *Measureing the turbidity of water supplies.* Loughborough University, School of Civil and Building Engineering. Leicestershire: WEDC Publications.

Richardson, S. (2013). *Sinkhole and subsidence record in the chuniespoort group dolomite, Gauteng, South Africa.* MSc Thesis. University of Pretoria.

Ross, S., Franzmier, D., & Roth, C. (1976). Mineralogy and chemistry of manganse oxides in some Indiana soils. *Soil Science Society of America Journal, 40*, 137-143.

Shepard, F. (1954). Nomenclature based on sand-silt-clay ratios. *Journal of Sedimentary Petrology, 24*, 151 -158.

Snyman, C. (1981). Economic Potential. *Seminar on the Engineering Geology of Dolomitic Areas.* Pretoria: University of Pretoria.

Sophocleous, M. (2010, January 15). Understanding and explaining surface tension and capillarity: an introduction to fundamental physics for water professionals. *Hydrogeology Journal, 18*, 811-821.

Sower, G. (1975). Failure in limestones in humid subtropics. *J. Geotech. Engng. Div.*(101), 771-787.

Taylor, R., McKenzie, R., & Norrish, K. (1964). The mineralogy and chemistry of manganse in some Australian soils. *Australian Journal of Soil Research , 2*, 235-248.

Terzaghi, K. (1943). *Theoretical Soil Mechanics.* New York: Wiley.

Tharp, T. (2003). Cover-collapse sinkhole formation and soil plasticity. *Sinkholes and Engineering / Environmental Impacts of Karst*, 110 - 123.

Tharp, T. M. (1999). Mechanics of upward propagation of cover-collapse sinkholes. *Engineering Geology, 52*, 22-33.

Toker, N., Germaine, J., Sjoblom, K., & Culligan, P. (2004). A new technique for rapid measurments of continuous soil moisture characteristic curves. *Géotechnique, 54*(3), 179-186.

Toll, D. (2012). The behaviour of unsaturated soils. In B. Haut, D. Toll, & A. Prasad (Eds.), *Handbook of Tropical Residual Soils* (pp. 119-145). London: Taylor & Francis.

Trollip, N. (2006). The geology of an area south of Pretoria with specific reference to dolomite stability. *Master dissertation, University of Pretoria*.

Turner, S. (1982). *A structual study of tunnel manganese oxides by high resolution transmission electron microscopy.* Arizona State University.

van Tonder, W., & Jacobsz, S. (2017). Swwpage column hydraulic condictivity tests in the geotechnical centrifuge. *Journal of the South African Institution of Civil Engineering*, 16-24.

Wagener, F. (1982, November). Engineering Construction on Dolomite.

Warren, J. (2000). Dolomite: occurrence, evolution and economically important associations. *Earth Science Reviews*(52), 1-81.

Weinert, H. (1980). The natural road construction materials of southern Africa. *Academica*.

Weiss, J. (n.d.). *Stress-Strain behaviour of Concrete.* Retrieved October 21, 2017, from The Concrete Portal: http://www.theconcreteportal.com/cons_rel.html

Yong, R., Mohamed, A., & Wang, B. (1992). Influnce of amorphous silica and iron hydroxide on interparticle action and soil surface properties. *Canadian Geotechnical Journal, 29*, 803-818.

APPENDIX A:

Raw Data

Triaxial

Mooiplaas

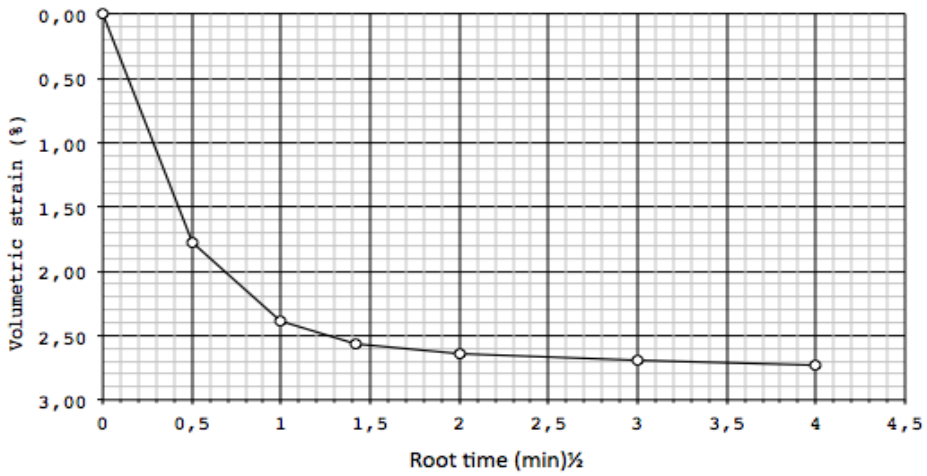

Figure A-1: Consolidation curve of Mooiplaas A sample at 100kPa isotropic confinement.

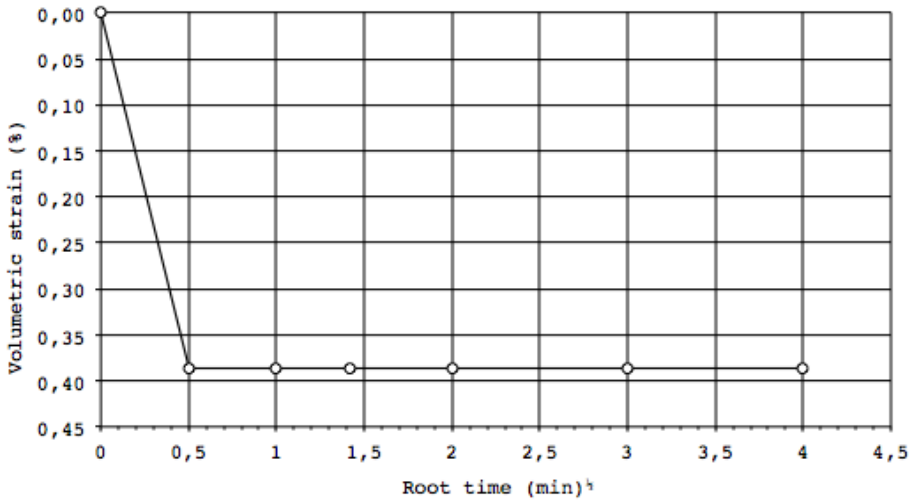

Figure A-2: Consolidation curve of Mooiplaas C sample at 100kPa isotropic confinement.

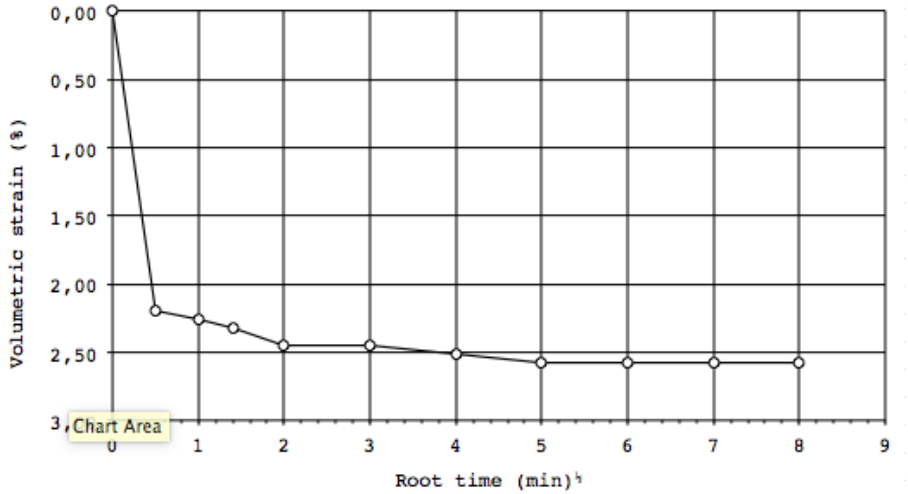

Figure A-3: Consolidation curve of Mooiplaas D sample at 100kPa isotropic confinement

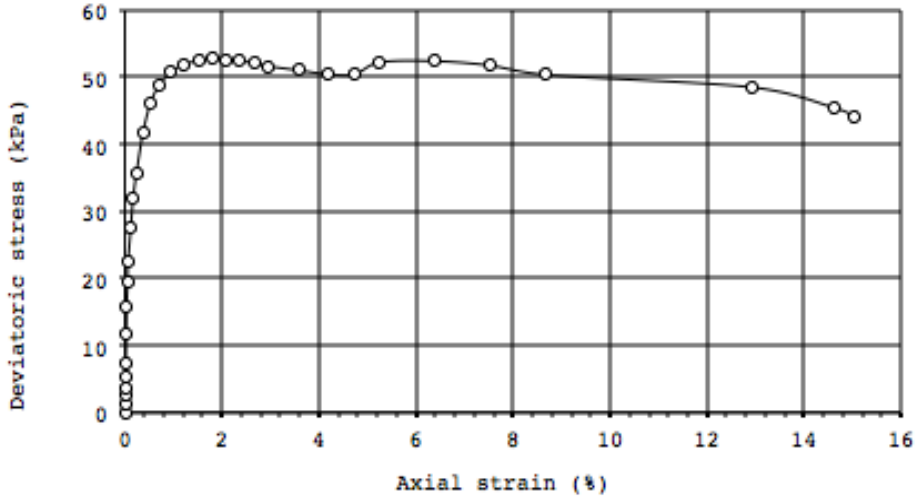

Figure A-4: Stress-strain relationship of Mooiplaas B sample.

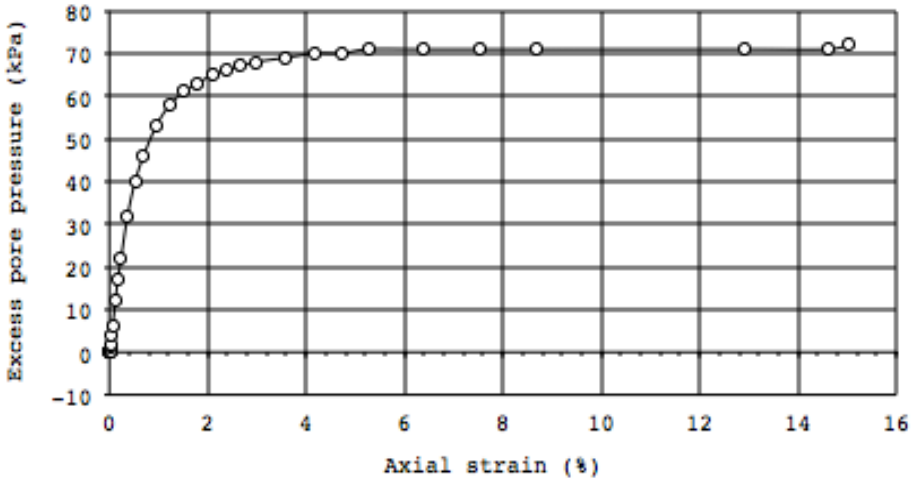

Figure A-5: Pore pressure – strain relation of Mooiplaas B shows the material contracted and behaved as normally consolidated clay.

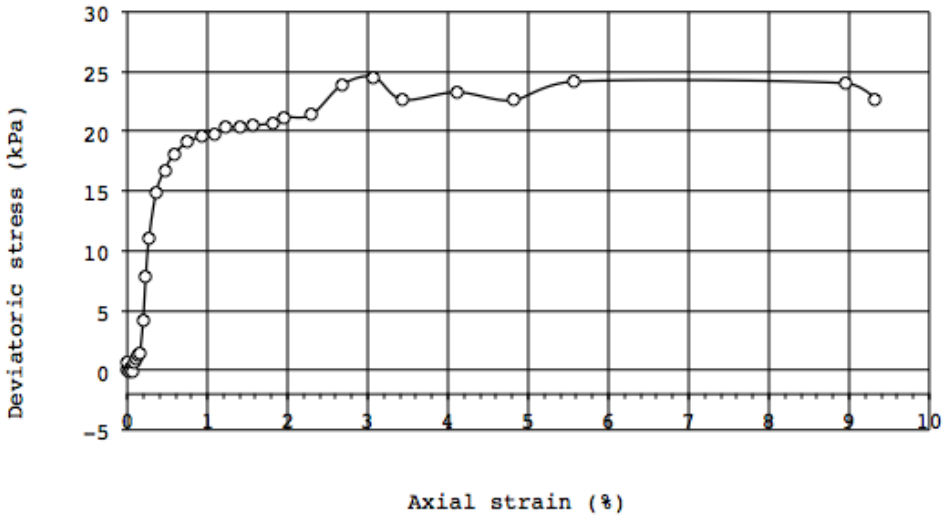

Figure A-6: Stress-strain relationship of Mooiplaas C sample.

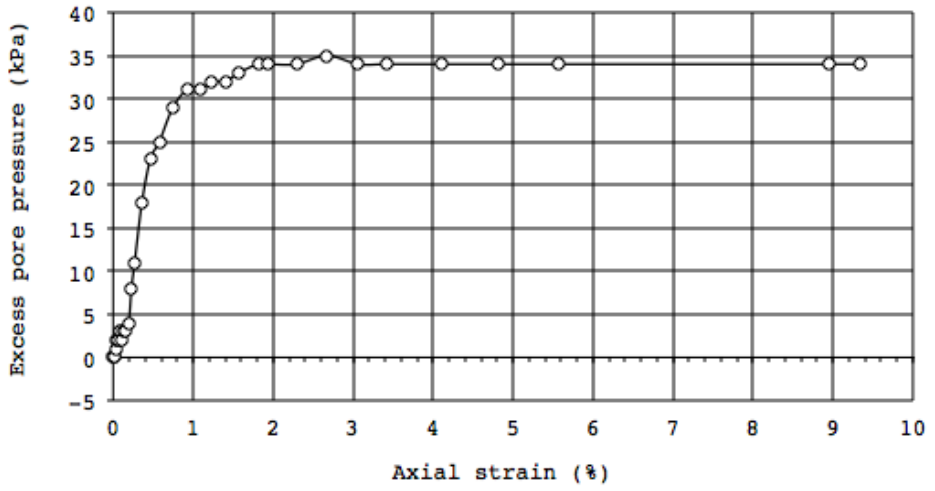

Figure A-7: Pore pressure – strain relation of Mooiplaas C shows the material contracted and behaved as normally consolidated clay.

Bokkraal

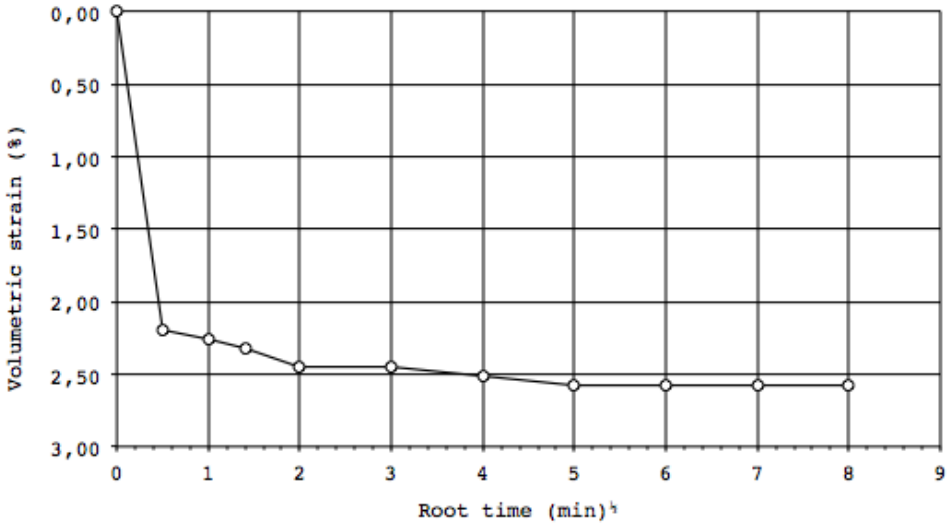

Figure A-8: Consolidation curve of Bokkraal sample at 100kPa isotropic confinement.

Doornhoek

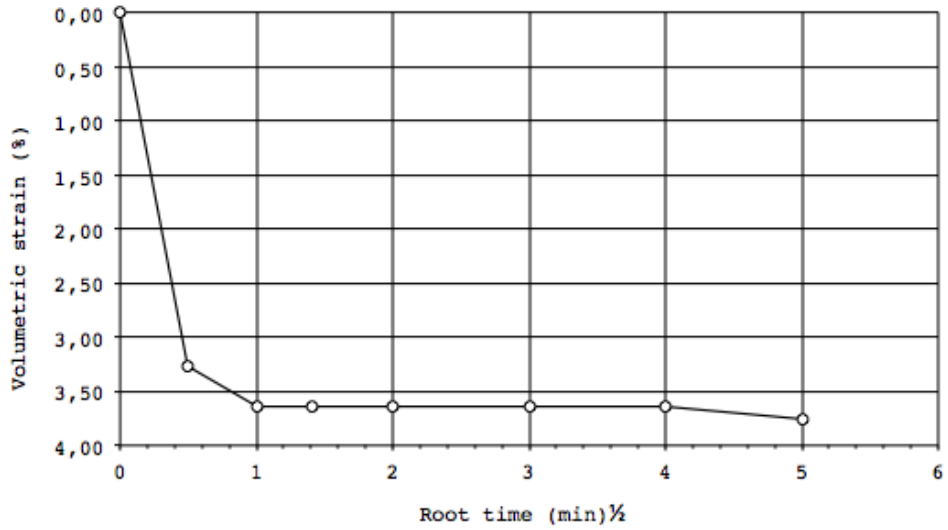

Figure A-9: Consolidation curve of Doornhoek sample at 100kPa isotropic confinement.

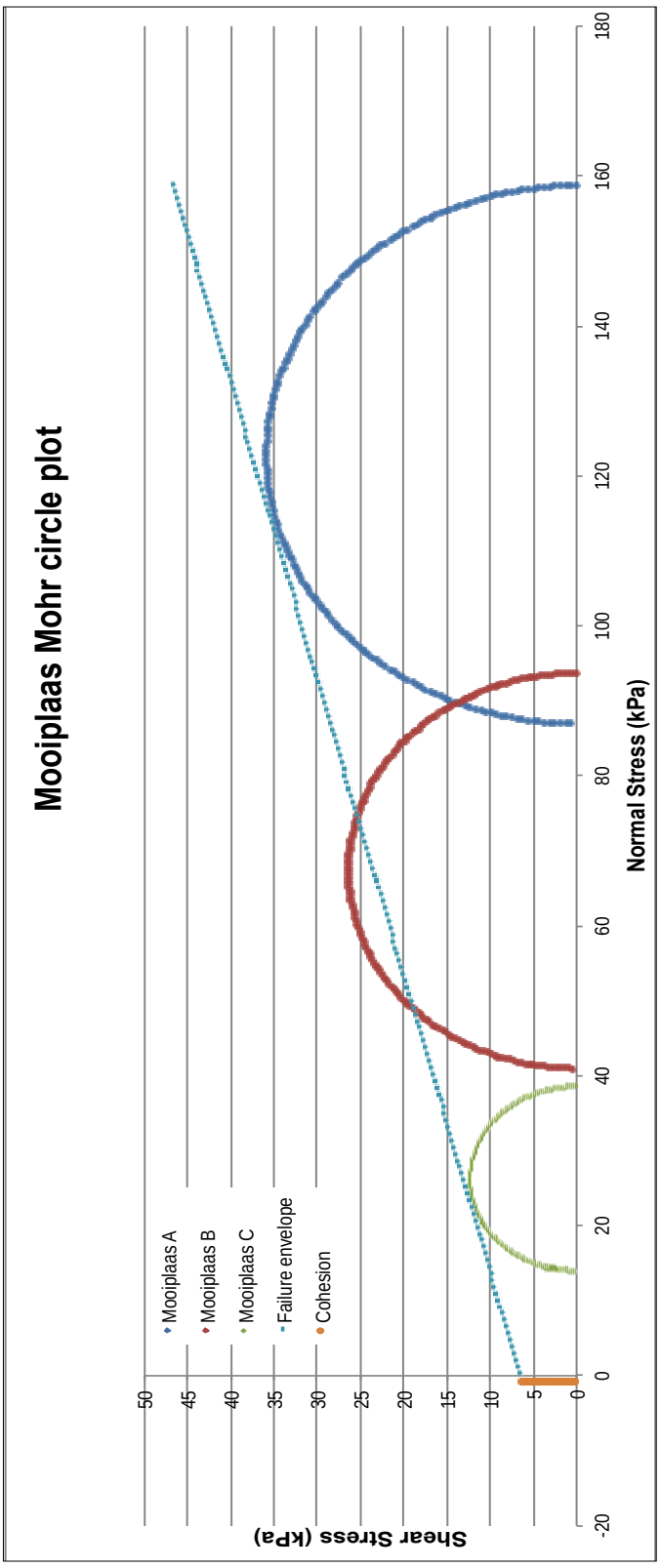

Figure A-9: Mohr circle plot for Mooiplaas triaxial tests

Crumb test

Figure A-10: Photos taken at 10 minutes, 1 hour and 2 hours during the crumb test conducted on the Bokkraal sample.

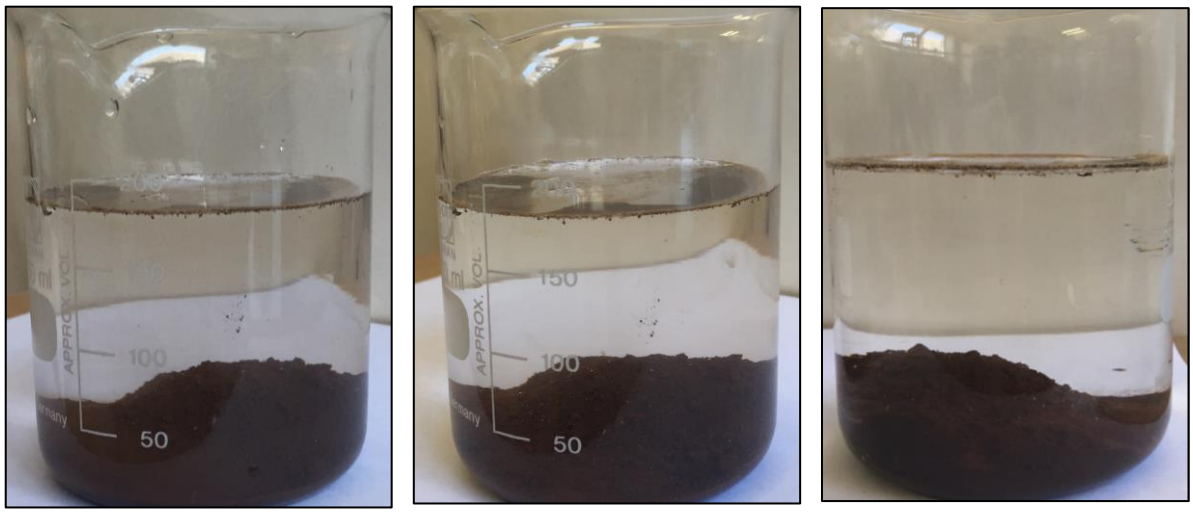

Figure A-11: Photos taken at 10 minutes, 1 hour and 2 hours during the crumb test conducted on the Mooiplaas sample.

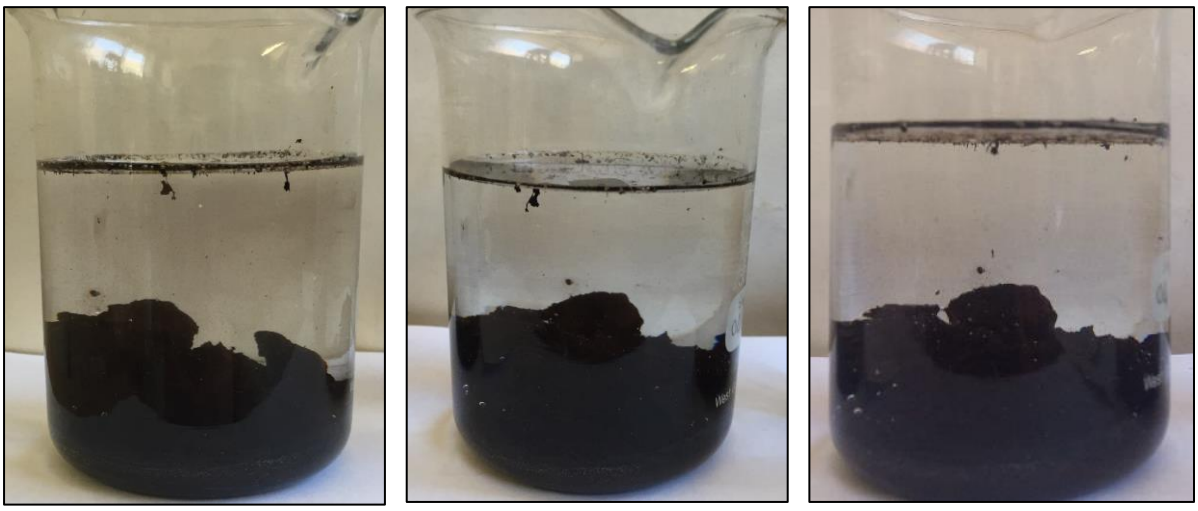

Figure A-12: Photos taken at 10 minutes, 1 hour and 2 hours during the crumb test conducted on the Doornhoek sample.

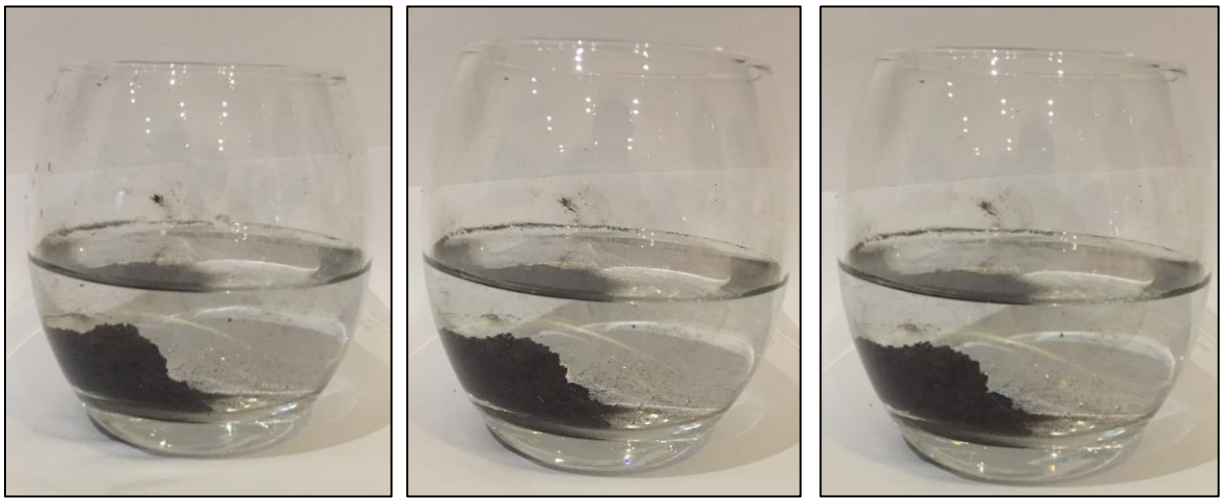

Figure A-13: Photos taken at 10 minutes, 1 hour and 2 hours during the crumb test conducted on the Carletonville sample.

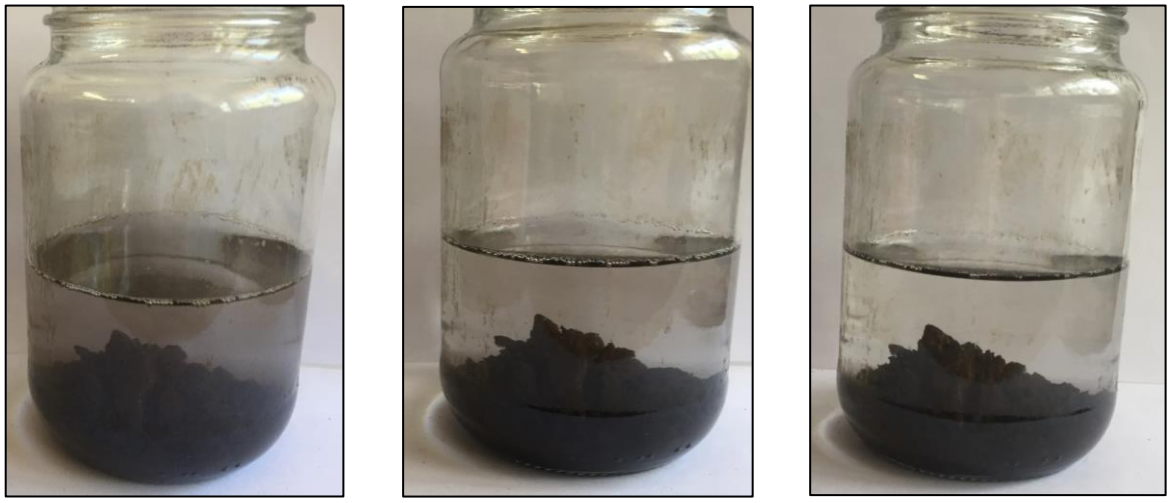

Figure A-14: Photos taken at 10 minutes, 1 hour and 2 hours during the crumb test conducted on the South Downs sample.

Figure A-15: Photos taken at 10 minutes, 1 hour and 2 hours during the crumb test conducted on the Highveld sample.

du Plessis Civil Engineering
Reg. No: cc 200004833323

250 ORION Ave
Monument Park
0181

PO Box 26272
Monument Park
0105

Tel/Fax 012 346 7586
Cell: 082 375 3003
bennie@geotesting.co.za

Project: Wad
Test: GRADINGS, PARTICLE DENSITY & ATTERBERGS
Date: 24-Oct-17 Set 1 of 1 Rev 0

Lab Sample No.		17/594	17/595	17/596	-	-	-	-
Client Sample No.		Doornhoek	Bokkraal	Mooiplaas	-	-	-	-
Depth / Position		-	-	-	-	-	-	-
Description / Notes (ASTM USCS)		Dusky Blue Elastic Silt with Sand (MH)	Dark Brown Sandy Lean Clay (CL)	Dark Brown Clayey Sand (SC)	-	-	-	-
Percentage Passing Size (mm)	200	100	100	100	-	-	-	-
	100	100	100	100	-	-	-	-
	63	100	100	100	-	-	-	-
	53	100	100	100	-	-	-	-
	37.5	100	100	100	-	-	-	-
	26.5	100	100	100	-	-	-	-
	19.0	100	100	100	-	-	-	-
	13.2	100	100	100	-	-	-	-
	9.5	100	100	100	-	-	-	-
	6.7	100	98	100	-	-	-	-
	4.75	100	95	99	-	-	-	-
	2.36	95	82	89	-	-	-	-
	1.18	92	75	81	-	-	-	-
	0.600	89	71	75	-	-	-	-
	0.425	87	69	71	-	-	-	-
	0.300	85	68	67	-	-	-	-
	0.212	83	67	62	-	-	-	-
	0.150	80	65	56	-	-	-	-
	0.075	72	62	44	-	-	-	-
	0.060	59	49	30	-	-	-	-
	0.050	58	48	28	-	-	-	-
	0.020	51	41	19	-	-	-	-
	0.005	11	22	13	-	-	-	-
	0.002	4	12	11	-	-	-	-
Particle Density		2.93	2.90	2.72	-	-	-	-
Atterberg Limits	Liquid Limit	121	49	29	-	-	-	-
	Plastic Limit	88	33	17	-	-	-	-
	Linear Shrinkage	7.2	5.8	4.4	-	-	-	-
	Plasticity Index	33	16	12	-	-	-	-
Moisture Content (%)		-	-	-	-	-	-	-
Notes:								

BM du Plessis
Civil Engineering
Reg. No: cc 200004833323

250 ORION Ave
Monument Park
0181

PO Box 26272
Monument Park
0105

Tel/Fax 012 346 7586
Cell: 082 375 3003
bennie@geotesting.co.za

Project: Wadd
Test: GRADINGS, PARTICLE DENSITY & ATTERBERGS
Date: 03-Dec-18 Set 1 of 1 Rev 0

	Lab Sample No.	18/385	18/386	18/387	18/388	18/389	-	-
	Client Sample No.	Highveld	SC02	R533-6	CV	SDSH	-	-
	Depth / Position	-	-	-	-	-	-	-
	Description / Notes (ASTM USCS)	Dusky Blue Elastic Silt (MH)	Dusky Blue Elastic Silt with Gravel (MH)	Dark Brown Elastic Silt with Sand (MH)	Dark Brown Sandy Elastic Silt with Gravel (MH)	Dark Brown Sandy Elastic Silt (MH)	-	-
Percentage Passing Size (mm)	200	100	100	100	100	100	-	-
	100	100	100	100	100	100	-	-
	63	100	100	100	100	100	-	-
	53	100	100	100	100	100	-	-
	37.5	100	100	100	100	100	-	-
	26.5	100	100	100	94	100	-	-
	19.0	100	100	100	92	98	-	-
	13.2	100	99	100	90	97	-	-
	9.5	100	95	100	89	96	-	-
	6.7	100	87	100	85	94	-	-
	4.75	100	80	97	84	92	-	-
	2.36	100	79	92	77	90	-	-
	1.18	100	78	89	73	86	-	-
	0.600	99	78	86	68	81	-	-
	0.425	99	78	85	65	77	-	-
	0.300	99	77	84	61	74	-	-
	0.212	99	77	83	59	72	-	-
	0.150	98	77	82	56	69	-	-
	0.075	98	75	81	50	64	-	-
	0.060	91	60	76	39	49	-	-
	0.050	89	59	75	38	48	-	-
	0.020	86	53	73	32	42	-	-
	0.005	25	32	53	18	28	-	-
	0.002	9	19	28	11	18	-	-
	Particle Density	2.82	3.18	2.05	2.86	3.03	-	-
Atterberg Limits	Liquid Limit	229	67	145	94	65	-	-
	Plastic Limit	221	47	112	77	48	-	-
	Linear Shrinkage	9.3	8.8	7.5	5.0	6.4	-	-
	Plasticity Index	8	20	33	17	17	-	-
	Moisture Content (%)	-	-	-	-	-	-	-
	Notes:							

Figure A-16: 'Dirty' water flowed out of Bokkraal erosion column with insoluble material entrained. Scenarios 1 to 5 are arranged from left to right.

Figure A-17: 'Dirty' water flowed out of Doornhoek erosion column with insoluble material entrained. Scenarios 1 to 5 are arranged from left to right.

Figure A-18: 'Dirty' water flowed out of R533 erosion column with insoluble material entrained. Scenarios 1 to 5 are arranged from left to right.

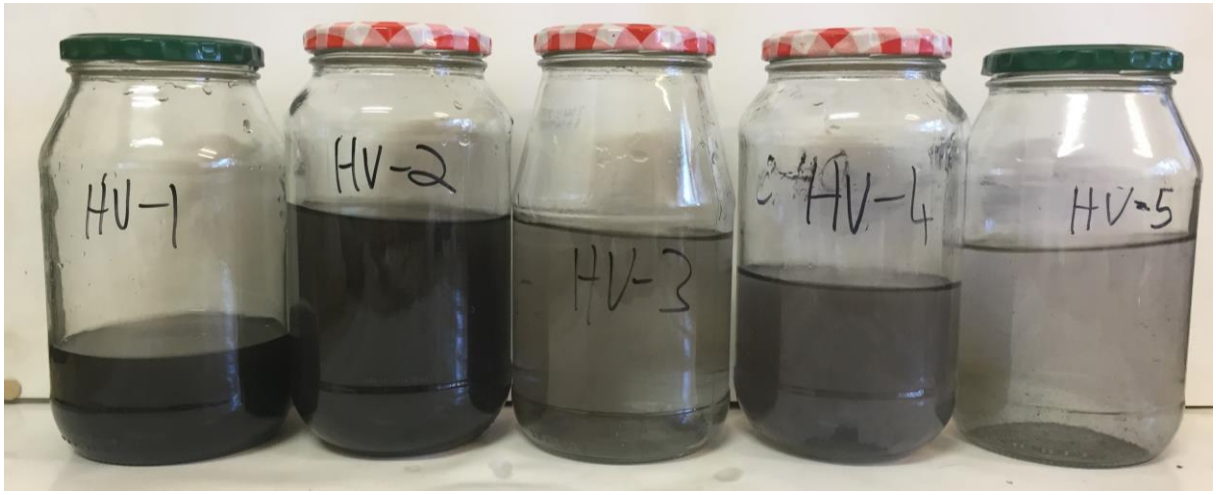

Figure A-19: 'Dirty' water flowed out of Highveld erosion column with insoluble material entrained. Scenarios 1 to 5 are arranged from left to right.

Table A-1: Summary of results from erosion column testing

Sample	Head increase scenario		Water flowed out (ml)	Mass mobilised (g)
Bokkraal	Initial		200	0.086
	Immediate	Rapid	500	0.008
		Slow	500	0.004
	Dry out	Rapid	500	0.058
		Slow	500	0.008
Doornhoek	Initial		200	0.076
	Immediate	Rapid	500	0.131
		Slow	500	0.084
	Dry out	Rapid	500	0.099
		Slow	500	0.048
R533	Initial		180	0.109
	Immediate	Rapid	500	0.037
		Slow	500	0.005
	Dry out	Rapid	500	0.033
		Slow	500	0.008
Highveld	Initial		200	0.115
	Immediate	Rapid	500	0.085
		Slow	500	0.003
	Dry out	Rapid	500	0.052
		Slow	500	0.006